University of Alberta

Development and Application of Analytical Methodologies to Study Carbohydrate-Modifying and Carbohydrate-Binding Proteins

by

Glen Shoemaker

A thesis submitted to the Faculty of Graduate Studies and Research in partial fulfillment of the requirements for the degree of Doctor of Philosophy

Department of Chemistry

Edmonton, Alberta

Spring 2007

Library and Archives Canada

Published Heritage Branch

395 Wellington Street
Ottawa ON K1A 0N4
Canada

Bibliothèque et Archives Canada

Direction du Patrimoine de l'édition

395, rue Wellington
Ottawa ON K1A 0N4
Canada

Your file Votre référence
ISBN: 978-0-494-29744-5
Our file Notre référence
ISBN: 978-0-494-29744-5

NOTICE:
The author has granted a non-exclusive license allowing Library and Archives Canada to reproduce, publish, archive, preserve, conserve, communicate to the public by telecommunication or on the Internet, loan, distribute and sell theses worldwide, for commercial or non-commercial purposes, in microform, paper, electronic and/or any other formats.

The author retains copyright ownership and moral rights in this thesis. Neither the thesis nor substantial extracts from it may be printed or otherwise reproduced without the author's permission.

AVIS:
L'auteur a accordé une licence non exclusive permettant à la Bibliothèque et Archives Canada de reproduire, publier, archiver, sauvegarder, conserver, transmettre au public par télécommunication ou par l'Internet, prêter, distribuer et vendre des thèses partout dans le monde, à des fins commerciales ou autres, sur support microforme, papier, électronique et/ou autres formats.

L'auteur conserve la propriété du droit d'auteur et des droits moraux qui protège cette thèse. Ni la thèse ni des extraits substantiels de celle-ci ne doivent être imprimés ou autrement reproduits sans son autorisation.

In compliance with the Canadian Privacy Act some supporting forms may have been removed from this thesis.

While these forms may be included in the document page count, their removal does not represent any loss of content from the thesis.

Conformément à la loi canadienne sur la protection de la vie privée, quelques formulaires secondaires ont été enlevés de cette thèse.

Bien que ces formulaires aient inclus dans la pagination, il n'y aura aucun contenu manquant.

Canada

Abstract

This work describes the development and application of analytical techniques to study protein function and characterize interactions in protein-ligand complexes. The first part of this work describes the development of small-scale enzyme assays. Using a novel nanopipettor, which was shown capable of tunable and reproducible nanolitre sampling, combined with cell manipulation and the ultrasensitivity of capillary electrophoresis with laser-induced fluorescence detection (CE-LIF), a single cell enzyme assay was developed. Individual Sf9 cells were assayed for the enzyme α-glucosidase II and were found to be very heterogeneous with respect to their levels of α-glucosidase II activity. The most important benefit afforded by this technique is that a single cell lysate can be repeatedly sampled, which was demonstrated in the time-course study of α-glucosidase II activity in a single Sf9 cell.

Nanoflow electrospray (nanoES), Fourier transform ion cyclotron resonance mass spectrometry (FT-ICR/MS) was used to determine the association thermochemistry of two protein-ligand systems. The ligand specificity of the monoclonal antibody (mAb) CS-35 towards a polysaccharide cell wall component in *Mycobacterium tuberculosis* was investigated. Determination of the association thermochemistry for a series of ligands allowed the key residues in the interaction to be identified. A nanoES-MS study was also performed on the blood group enzyme, GTB, representing the first direct thermodynamic study of this enzyme. It was shown that GTB exists exclusively as a dimer in aqueous solutions (pH 7) with two equivalent acceptor binding sites. A study of GTB_2 interacting with donor and donor fragments, both alone and in the presence of a divalent metal cofactor, concluded that GTB_2 possesses a weak binding affinity for its native donor in

the absence of cofactor. The metal cofactor also exhibited a drastic effect on catalysis and it was suggested that the biologically relevant cofactor is Mn^{+2}. Using a novel gas-phase assay, based on time-resolved tandem MS, the two GTB_2 acceptor sites were found to maintain their equivalency in the gas-phase. The gas-phase assay was used to confirm that the binding site equivalency in the homotetramer of streptavidin was also maintained upon transfer to the gas-phase. This suggests that time-resolved tandem MS can be used to evaluate binding-site equivalency for protein-ligand complexes in solution.

Acknowledgements

There are many people to whom I owe a great deal of thanks over the course of my Ph.D. for either helping me scientifically or for helping me keep whatever sanity I had when I began this journey. I would like to thank my family first and foremost, as they have always been there for me and have taught me the most valuable lessons. Mom, Dad, Grandma and Grandpa thank you so much and no matter where I go the "farm" will always be home. Thanks to my sisters, Lori and Trace, for being such good friends. And how could I forget Jake and Caleigh, for helping me stay young (okay, maybe even childish at times). As for keeping me sane over the past 5 years, I owe the most to Sarah. Thanks for always being there to help me in the toughest times.

I have also been extremely lucky to have had several excellent mentors during my time at the Ú of A. I definitely would not have made it without the help of my supervisors, John and Monica, for inspiring me and keeping me moving in a forward direction. I would also like to thank all of the past and current members of both the Klassen and Palcic research groups, particularly Rob, to whom I owe a great debt for helping me through my 502, candidacy, and various research obstacles. Thanks to Tish, Sandra, Elena and Igor as well for putting up with my frequent questions regarding everything from proteins to computers and to Rambod and Justin for showing me the ropes in the Klassen and Palcic labs. I have also been very fortunate to have had rewarding collaborations with many people, especially Dr. Todd Lowary and other members of the Alberta Ingenuity Centre for Carbohydrate Science and I would like to thank them. I also thank the support staff at the U of A in the machine shops (Dieter), electronic shops (Al), and the office staff for all of their help.

My most fond memories of the U of A will no doubt be the friends I've met and the times we've shared. Thanks for all the memorable mountain excursions to Sarah, Rob, Wiggy, Stevie and Ebbing. The Burnd's day crew helped me getting through those tougher weeks, particularly D-lo, who rarely says no to a pint. Husky, I wish you could be here to celebrate with us, you may be gone but shall never be forgotten. I will miss the soccer, hockey, and baseball friends and thank you all for many great times!

Table of Contents

Chapter 1 1

Development and Application of Analytical Methodologies to Study Carbohydrate-Modifying and Carbohydrate-Binding Proteins

1.1 Introduction 1

1.2 Small-Scale Enzyme Assays Using CE-LIF 3

1.2.1 Capillary Electrophoresis with Laser-Induced Fluorescence 4

1.2.2 Separation and Detection of Carbohydrates by CE-LIF 5

1.2.3 Single Cell Analysis using CE-LIF 8

1.3 Studying Protein-Carbohydrate Complexes using NanoES-MS 11

1.3.1 Mass Spectrometry 13

1.3.2 NanoES-FT-ICR/MS 14

1.3.3 Blackbody Infrared Radiative Dissociation 19

1.4 Literature Cited 23

Chapter 2 28

Development of a Quantitative Nanopipettor for Miniaturized Chemical and Biochemical Reaction Sampling

2.1 Introduction 28

2.2 Experimental 29

2.2.1 Materials and Reagents 29

2.2.2 Nanopipettor Construction 30

2.2.3 Nanopipettor Procedure for Aliquot Transfer 33

2.2.4 Capillary Electrophoresis with Laser-Induced Fluorescence 33

2.3 Results and Discussion 34

2.3.1 Linearity and Precision of Volume Delivery 34

2.3.2 Experimental Challenges: Differential Elution 39

2.3.3 Monitoring β-galactosidase Activity using the Nanopipettor 40

2.4 Conclusions 41
2.5 Literature Cited 43

Chapter 3 45
Multiple Sampling in Single Cell Enzymes Assays using Capillary Electrophoresis with Laser-Induced Fluorescence Detection
3.1 Introduction 45
3.2 Experimental 48
3.2.1 Materials and Reagents 48
3.2.2 Cell Culture 48
3.2.3 Single Cell Manipulation 49
3.2.4 Single Cell Enzyme Assays 53
3.2.5 *Arabidopsis* Embryo Analysis 54
3.2.6 Capillary Electrophoresis with Laser-Induced Fluorescence 55
3.3 Results and Discussion 56
3.3.1 Optimization of Sf9 Cell Manipulation 56
3.3.2 Single Cell α-glucosidase II Assay 57
3.3.3 Single Cell α-glucosidase II Reaction Profile 61
3.3.4 Analysis of a Low Abundance Enzyme 61
3.3.5 Gene Ablation Verification 64
3.4 Conclusions 67
3.5 Literature Cited 68

Chapter 4 71
Determination of Protein-Carbohydrate Association Thermochemistry by the Direct nanoES-MS Assay
4.1 Introduction 71
4.2 Experimental 78
4.2.1 Materials and Reagents 78
4.2.2 Protein Expression and Purification 80

4.2.3 Mass Spectrometry 83
4.2.4 Determination of K_{assoc} Values by ES-MS 84
4.2.5 Experimental Challenges to the Direct NanoES-MS Binding Assay 85
4.2.6 Isothermal Titration Microcalorimetry 89
4.3 Results and Discussion –NanoES-MS Study of the mAb CS-35 90
4.3.1 Determining K_{assoc} Values for CS-35 Ligand Binding 90
4.3.2 Determining ΔH_{assoc} For CS-35 Ligand Binding 94
4.4 Results and Discussion –ES-MS Study of a Glycosyltransferase 97
4.4.1 The Native Oligomeric Form of GTB 97
4.4.2 NanoES-MS Binding Measurements of GTB_2 with Acceptor Analogues 103
4.4.3 NanoES-MS Binding Study of GTB_2 to Donor and Donor Fragments 107
4.4.4 Role of a Divalent Metal Cofactor in GTB_2 Substrate Binding and Catalysis 109
4.5 Conclusions 119
4.6 Literature Cited 121

Chapter 5 **127**
Equivalency of Binding Sites in Protein-Ligand Complexes Revealed by Time-Resolved Tandem Mass Spectrometry
5.1 Introduction 127
5.2 Experimental 128
5.2.1 Protein and Ligand Preparation 128
5.2.2 Mass Spectrometry 130
5.3 Results and Discussion 131
5.3.1 Probing Equivalency of GTB_2 Binding Sites in the Gas-Phase 131
5.3.2 NanoES-MS Gas-Phase Assay: S_4-Biotin Dissociation 137
5.4 Conclusions 142

5.5 Literature Cited 143

Chapter 6 Conclusions and Future Work 145

Literature Cited 150

List of Tables

Table 2.1	Linear volume delivery of LacNAc-TMR to Le^y-TMR using the nanopipettor and the corresponding theoretical value calculated from equation 2.6. The average relative fluorescence intensity represents the ratio in the measured fluorescence intensity of Le^y-TMR and LacNAc-TMR. The blank relative fluorescence was subtracted from all measurements.	37
Table 4.1	Binding affinities of oligosaccharides **1 – 6** for CS-35 F_{ab} determined by nanoES-MS, FAC-MS, and ITC at 25°C. K_{assoc} values obtained from FAC-MS measurements have been corrected to take into account the effect of the extra binding site possessed by the mAb compared to the F_{ab}.	92
Table 4.2	Binding affinities of carbohydrate acceptor analogues **7, 9 – 14** for GTB determined by nanoES-MS.	104
Table 4.3	Binding affinities of the native acceptor (**7**) and donor fragments **15** and **16** for GTB_2 with and without the addition of 100 μM metal cofactor determined by nanoES-MS.	112

List of Figures

Figure 1.1	Schematic of the CE-LIF instrument.	6
Figure 1.2	Illustration of the ES process.	15
Figure 1.3	Cyclotron motion of a positive ion of charge q moving at velocity **v** in the presence of a constant magnetic field, **B**, which is pointing into the page. The ion moving to the left experiences a downward force, **F** = q(**v** x **B**), resulting in a counterclockwise orbit.	18
Figure 1.4	Illustration of (a) ion excitation and (b) the generation of a mass spectrum from the measured image current for ions in an FT-ICR/MS mass analyzer cell.	20
Figure 1.5	Schematic of the nanoES-FT-ICR/MS instrument used in this study.	21
Figure 2.1	Schematic of nanopipettor design and components.	31
Figure 2.2	Representative electropherograms of solutions containing a Le^y-TMR internal standard in CE running buffer. To each solution LacNAc-TMR was added using the nanopipettor, varying the amount of time the nanopipettor was left in the LacNAc-TMR solutions from (a) 15 s, (b) 30 s, (c) 40 s, and (d) 50 s. (e) Blank measurements, in which no volume was withdrawn on the Hamilton syringe, were also carried out to account for any spontaneous injection.	36
Figure 2.3	Linear volume delivery of LacNAc-TMR to samples containing a constant concentration of Le^Y-TMR using the nanopipettor. Blank measurements were subtracted from each aliquot. Aliquots were collected using a volume displacement of 200 μL to 320 μL on the Hamilton syringe. Samples were analysed in triplicate. Regression analysis yielded a y-intercept of 0.03 ± .03 and a r^2 value of 0.99 ± 0.02.	38
Figure 2.4	Time course of LacNAc hydrolysis by β-galactosidase using a standard serial dilution (▫), the nanopipettor (•), and the nanopipettor after correcting for differential elution (○).	42

Figure 3.1	Micromanipulator schematic. (A), (B), (C) x,y,z translational stages which are attached to three stepping motors (not shown). A capillary holder (D) holds the vertically oriented capillary (E). One end of the capillary was attached to a 50 μL Hamilton syringe (F) to allow withdrawal of single cells (G) from a PHEMA coated microscope slide.	50
Figure 3.2	View through the microscope objective of the micromanipulator sampling capillary emerged in a solution of Sf9 cells.	52
Figure 3.3	Representative electropherograms obtained from the CE-LIF analysis of 5 nL aliquots removed from (a) a single Sf9 cell and (b) a control α-glucosidase II assay after 4.5 h of incubation at 37°C . The inset demonstrates the level of MG product present in the control assay as well as fluorescent impurities in the substrate.	58
Figure 3.4	Calculated percent conversion of the DG-TMR substrate for 20 individual Sf9 cells and 2 controls after 4.5 h at 37°C. For the 20 Sf9 cells the average activity was found to be 20.9 ± 9.4 %. For each sample, three aliquots were removed and analysed by CE-LIF. The error bars correspond to the standard deviation obtained from this triplicate analysis	59
Figure 3.5	Representative electropherograms of aliquots removed from a single Sf9 cell reaction incubated in a 100 mM phosphate buffer (pH 7), 0.1 % Triton X-100, protease inhibitors (Roche, 1 tablet/ 20 mL), and 50 μM DG-TMR substrate. Aliquots were removed after (a) 1h, (b) 3h, (c) 5h, and (d) 21h using the nanipipettor and added to 3.5 μL of CE running buffer containing 0.7 μM Le^Y-TMR internal standard.	62
Figure 3.6	Time course illustrating the percent conversion of DG-TMR by α-glucosidase II for a single Sf9 cell (●) and control (□). Each time point was analysed in duplicate by removing two 5 nL aliquots from the reaction mixture.	63
Figure 3.7	Sample electropherograms of the single cell GTA analysis. The blood group enzyme transfers GalNAc from a UDP-GalNAc donor to the H-antigen (H) , producing the A-antigen (A). The addition of a (a) single HT29 cell to 100 nL of reaction buffer resulted in 0.81% conversion of the H precursor after 52 hours whereas a (b) control assay without any cells did not exhibit any product formation. Electropherograms have been offset to facilitate visual comparison.	65

Figure 3.8 Single *Arabidopsis* embryo analysis of (a) mutant and (b) wildtype embryos. Both embryo samples exhibited conversion of the LN-TMR to GN-TMR by β-galactosidase. Mutant embryos, however, were not effective in hydrolyzing the TG-TMR to the TMR linker arm due to deletion of the gene corresponding to α-glucosidase I. The electropherograms have been offset to aid comparison. (c) A blank assay was also performed using reaction buffer in place of embryo lysate and resulted in no conversion of either substrate. 66

Figure 4.1 Schematic diagram of the temperature-controlled nanoES device. The sample droplets are sprayed using a nanoES tip inserted through a small aperture in the Plexiglas cover of the chamber. The temperature of the nanoES solution is controlled by regulating the air flow through the Cu tubing which is in thermal contact with the Cu sleeve that surrounds the ES chamber. The temperature of the nanoES solution is determined by a thermocouple, TC_1, attached to the nanoES tip and positioned 1-2 mm from the heated sampling inlet capillary. To satisfy the gas intake requirement of the ion source, a portion of the regulated air (~700 mL/min) is introduced into the chamber through the Plexiglas disc. The total volume inside the chamber is approximately 60 mL. 74

Figure 4.2 Oligosaccharide ligands used in the CS-35 F_{ab} nanoES-MS binding experiments: β-D-Ara*f*-(1→2)-α-D-Ara*f*-(1→5)[β-D-Ara*f*-(1→2)-α-D-Ara*f*-(1→3)]-α-D-Ara*f*-(1→5)-α-D-Ara*f*-OCH_3 (**1**), β-D-Ara*f*-(1→2)-α-D-Ara*f*-(1→5)[β-D-Ara*f*-(1→2)-α-D-Ara*f*-(1→3)]-α-D-Ara*f*-OCH_3 (**2**), β-D-Ara*f*-(1→2)-α-D-Ara*f*-(1→5)[α-D-Ara*f*-(1→3)]-α-D-Ara*f*-(1→5)-α-D-Ara*f*-OCH_3 (**3**), β-D-Ara*f*-(1→2)-α-D-Ara*f*-(1→3)[α-D-Ara*f*-(1→5)]-α-D-Ara*f*-(1→5)-α-D-Ara*f*-OCH_3 (**4**), β-D-Ara*f*-(1→2)-α-D-Ara*f*-(1→5)-α-D-Ara*f*-(1→5)-α-D-Ara*f*-OCH_3 (**5**), α-D-Ara*f*-(1→3)[α-D-Ara*f*-(1→5)]-α-D-Ara*f*-(1→5)-α-D-Ara*f*-OCH_3 (**6**). 75

Figure 4.3 The reaction catalysed by the human blood group enzyme α(1→3)galactosyltransferase (GTB). The enzyme recognizes the terminal carbohydrate structure α-L-Fuc*p*-(1→2)-β-D-Gal*p*-O-R (**7**) and transfers a monosaccharide from a nucleotide sugar donor, uridine 5'-diphosphate-Gal (UDP-Gal, **8**), to this acceptor at the 3'-O- position generating the B antigen, α-D-Gal*p*-(1→3)[α-L-Fuc*p*-(1→2)]-β-D-Gal*p*-O-R (**9**). It has been shown previously that a metal ion, possibly Mn^{+2}, is critical for enzyme activity. 77

Figure 4.4 Structures of the acceptor analogues used in the nanoES-MS study of GTB: α-L-Fuc*p*-(1→2)-β-D-3-deoxy-Gal*p*-O-R (**10**), 3-Amino-3-deoxy-β-D-Gal*p*-O-R (**11**), 2-O-carbamoylmethyl-β-D-Gal*p*-(1→4)-2-acetamido-2-deoxy-β-D-Glc*p*-O-R (**12**), 3-O-carboxymethyl-β-D-Gal*p*-(1→4)-2-Acetamido-2-deoxy-β-D-Glc*p*-O-R (**13**), 2-O-Aminoethyl-β-D-Gal*p*-(1→4)-2-Acetamido-2-deoxy-β-D-Glc*p*-O-R(**14**). 79

Figure 4.5 NanoES mass spectra obtained in positive ion mode for an aqueous solution of (a) 30-μM GTB and (b) 30-μM GTB with 50-μM **7**. After optimizing the purification of GTB the protein was analysed again using nanoES-MS at a concentration of (c) 17-μM alone and with (d) 40-μM **7**. All solutions contained 10 mM ammonium acetate (pH 7). 82

Figure 4.6 Illustrative nanoES mass spectra obtained for aqueous solution of (a) 5 μM mAb CS-35, (b) 5 μM mAb CS-35 mixed with 5 μM **1**, (c) 6.2 μM CS-35 F_{ab}, and (d) 6.2 μM CS-35 F_{AB} with 9.4 μM **1** and 5 μM Pref. Digestion of the mAb CS-35 resulted in four distinct F_{ab} species which are labeled **a**, **b**, **c**, and **d**. 91

Figure 4.7 Linear van't Hoff plots constructed from nanoES-MS-derived K_{assoc} values obtained at varying temperatures for the association of CS-35 F_{ab} with (●) **1**, (■) **3**, and (▲) **4**, and (▼) **5**. 95

Figure 4.8 Representative (a) thermogram and (b) the corresponding binding isotherm for the titration of 600 μM **1** into a solution of 37.3 μM CS-35 F_{ab} in a 50 mM Tris buffer (pH 7.2) containing 150 mM NaCl. Titrations were carried out on a MicroCal VP-ITC at a temperature of 25°C. 96

Figure 4.9 Illustrative nanoES mass spectra of an aqueous solution of GTB (12 μM) in a 10 mM ammonium acetate buffer (pH 7) and in a b) 10 mM ammonium acetate buffer containing 10% acetic acid (pH 2.6). 99

Figure 4.10 Illustrative nanoES mass spectra of solutions consisting of 10 mM ammonium acetate (pH 7), 7 μM GTB_2 and **7** at concentrations of (a) 40 μM and (b) 100 μM. A reference protein, Pref, was added to both solutions at a concentration of 5 μM to quantify the extent of nonspecific protein-ligand binding during the ES process. 101

Figure 4.11 (a) Observed intensities for $(GTB_2 + q(7))^{n+}$, q = 0 – 4, ions and for $(P_{ref} + q(7))^{n+}$, q = 0 – 2, ions taken from a nanoES mass spectrum of an aqueous solution consisting of 8.5 μM GTB, 80 μM **7**, and 5 μM Pref in a 10 mM ammonium acetate buffer (pH 7). (b) The distribution of nonspecific binding was used to correct the observed intensities by removing the nonspecific contributions to the apparent ion abundances. 102

Figure 4.12 Plot of K_{assoc} values obtained at varying hexapole accumulation times for GTB_2 binding to (•) **7** and (■) **11**. 106

Figure 4.13 Stucture and K_{assoc} values determined by nanoES-MS for GTB donor (**8**) and the donor fragments **15** and **16**. 108

Figure 4.14 Illustrative nanoES mass spectra of solutions consisting of 8 μM GTB_2, 5 μM reference protein (P_{ref}), and either (a) 150 μM Mn^{+2} or (b) 300 μM Mg^{+2} in a 10 mM ammonium acetate buffer (pH 7). 110

Figure 4.15 Illustrative nanoES mass spectrum of a solution consisting of 8 μM GTB_2, 10 μM **16**, and 10 μM Mn^{+2} in a 10 mM ammonium acetate buffer (pH 7). 113

Figure 4.16 Representative nanoES mass spectrum of a solution composed of (a) 8 μM GTB_2 and 20 μM **8**. The addition of 100 μM Mn^{+2} led to the hydrolysis of **8** forming the products **15** and **16** (b) after 5 minutes. After (c) 25 minutes no GTB_2 – **8** complex was detected in the mass spectrum. All solutions were prepared in a 10 mM ammonium acetate buffer (pH 7). 115

Figure 4.17 Representative nanoES mass spectra of solutions composed of (a) 8 μM GTB_2 and 100 μM **8** alone and (b) in the presence of 100 μM Mg^{+2}. Both solutions were prepared in a 10 mM ammonium acetate buffer (pH 7). 117

Figure 4.18 Representative nanoES mass spectrum of an aqueous solution composed of 8 μM GTB_2, 20 μM **8**, 20 μM **7**, and 100 μM Mn^{+2} in a 10 mM ammonium acetate buffer (pH 7). 118

Figure 5.1 (a) Crystal structure of the GTB dimer (GTB_2) and (b) the structure of the acceptor binding site based on the published crystal structure. (c) Crystal structure of the streptavidin tetramer bound to 4 molecules of biotin (**2**) and the key (d) hydrophobic and (e) hydrogen bonding interactions in the biotin binding pocket. 129

Figure 5.2 NanoES mass spectra of solutions consisting of 10 mM ammonium acetate (pH 7), 7 μM GTB_2 and **1** at concentrations of (a) 40 μM and (b) 100 μM. A reference protein, scFv, was added to both solutions at a concentration of 5 μM to quantify the extent of nonspecific protein-ligand binding during the ES process. 132

Figure 5.3 Illustrative BIRD mass spectra obtained for (a) $(GTB_2 + \mathbf{1})^{15+}$ ion, originating from specific interaction in solution, at a reaction temperature 145 °C and reaction time of 3 s, (b) $(GTB_2 + 2(\mathbf{1}))^{15+}$ ion, originating from specific interactions, 150 °C and 7 s, (c) $(GTB_2 + \mathbf{1})^{15+}$ ions, originating from specific and nonspecific interactions, 122 °C and 20 s. 133

Figure 5.4 Plots of natural logarithm of normalized intensity (I/I_o) of the gaseous $(GTB_2 + \mathbf{1})^{15+}$ ions, produced from the specific (GTB_2 + **1**) complex (•) and from a mixture of specific and nonspecific (GTB_2 + **1**) complexes (o), versus reaction time, at the temperatures indicated. 134

Figure 5.5 BIRD kinetic plots of the natural logarithm of normalized intensity (I/I_o) of the gaseous $(GTB_2 + 2(\mathbf{1}))^{15+}$ ions, originating from the specific (GTB_2 + 2(**1**)) complex in solution, versus reaction time at the temperatures indicated. 136

Figure 5.6 Arrhenius plots for the loss of **1** from the $(GTB_2 + q\mathbf{1})^{15+}$ ions, where q = 1 (•) or 2 (o). 138

Figure 5.7 (a) NanoES mass spectrum obtained for a solution of 10 mM ammonium acetate (pH 7), 5 μM S_4, and 25 μM **2**. (b) NanoES mass spectrum obtained for a solution of 10 mM ammonium acetate (pH 7), 5 μM S_4, 25 μM **2** and 4 mM imidazole. Three distinct complexes are detected at each charge state: $(S_4 + 4(\mathbf{2}))^{n+}$, $(S_4 + 4(\mathbf{2}) + KH_2PO_4)^{n+}$, and $(S_4 + 4(\mathbf{2}) + 2(KH_2PO_4))^{n+}$. 140

Figure 5.8 Breakdown curves for the sequential loss of **2** from the $(S_4 + 4(\mathbf{2}))^{13+}$ ion at a reaction temperature of 133 °C; The symbols (•= $(S_4 + 4(\mathbf{2}))^{13+}$), □= $(S_4 + 3(\mathbf{2}))^{13+}$), ▲= $(S_4 + 2(\mathbf{2}))^{13+}$), ∇= $(S_4 + 1(\mathbf{2}))^{13+}$), ◆ = $(S_4)^{13+}$) represent experimental BIRD data and the solid curves represent the expected breakdown curves based on four equivalent binding sites with an intrinsic dissociation rate constant of 1.4 s^{-1}. 141

List of Abbreviations

A-factor	Preexoponential factor
A antigen	α-D-GalNAc*p*-(1→3)[α-L-Fuc*p*-(1→2)]-β-D-Gal*p*-O-R
B antigen	α-D-Gal*p*-(1→3)[α-L-Fuc*p*-(1→2)]-β-D-Gal*p*-O-R
BIRD	Blackbody infrared radiative dissociation
CE-LIF	Capillary Electrophoresis with Laser Induced Fluorescence
CID	Collision induced dissociation
ΔH_{assoc}	Enthalpy of association
ΔS_{assoc}	Entropy of association
DG	α-D-Glc*p*-(1→3)-α-D-Glc*p*
DTT	Dithiothreitol
E_a	Activation energy
ECD	Electron capture dissociation
E.coli	*Escherichia coli*
EOF	Electroosmotic flow
ES	Electrospray
F_{ab}	Antigen binding fragment
FAC/MS	Frontal affinity chromatography-mass spectrometry
FT-ICR/MS	Fourier transform ion cyclotron resonance-mass spectrometry
Fuc	L-fucose
Gal	D-galactose
GalNAc	*N*-acetylgalactosamine
GlcNAc	*N*-acetylglucosamine

GTA	α(1,3)*N*-acetylgalactosaminyltransferase
GTB	α(1,3)-galactosyltransferase
HT29	Human colon adenocarcinoma
i.d.	Inner diameter
IRMPD	Infrared multiphoton dissociation
ITC	Isothermal titration microcalorimetry
K_{assoc}	Association constant
LAM	Lipoarabinomannan
LacNAc	*N*-acetyllactosamine
Le^y	α-L-Fuc*p*-(1→2)-β-D-Gal*p*-(1→4)- [α-L-Fuc*p*-(1→3)]-β-D-GlcNAc*p*
M. tuberculosis	*Mycobacterium tuberculosis*
mAb	Monoclonal antibody
MALDI	Matrix-assisted laser desorption ionization
MBS	MOPS buffered saline
MEKC	Miceller electrokinetic chromatography
MG	α-D-Glc
MOPS	3-(N-morpholino)propanesulfonic acid
MS	Mass spectrometry
MWCO	Molecular weight cutoff
m/z	Mass-to-charge ratio
nanoES	Nanoflow electrospray
NMR	Nuclear magnetic resonance
o.d.	outer diamater

PBS	Phosphate buffered saline
PHEMA	Poly(2-hydroxyethyl methacrylate)
rf	Radio frequency
S_4	Streptavidin homotetramer
scFv	Single chain variable domain fragment
SDS	Sodium dodecyl sulphate
Sf9	*Spodoptera frugiperda*
S/N	Signal-to-noise ratio
SPR	Surface plasmon resonance
TG	α-D-Glc*p*-(1→2)-α-D-Glc*p*-(1→3)-α-D-Glc*p*
TMR	Tetramethylrhodamine
TOF	Time of flight
UDP	Uridine 5'-diphosphate

Chapter 1

Development and Application of Analytical Methodologies to Study Carbohydrate-Modifying and Carbohydrate-Binding Proteins

1.1 Introduction

In today's post-genomic era, a great deal of research is now focused on the biological interpretation of the information gained from genome sequencing. This involves the large-scale study of the functional aspect of the genome: the proteins. Proteomics embraces the study of protein expression levels, modifications, networks, localizations, and functions.[1] This area of research is very diverse and requires the efforts of researchers from many disciplines from physics to biology. Discoveries within this challenging and immense field will lead to an enhanced understanding of complex biological processes. The majority of the work presented in this thesis focuses on the study of one important class of proteins: enzymes.

Enzymes act as biological catalysts, and as such are responsible for the catalysis of most biological reactions that are essential for life.[2] Without enzymes, important biochemical processes, such as metabolism, would not occur at a significant rate. Enzymes typically carry out their function with exquisite specificity and are capable of accelerating reaction rates be several orders of magnitudes while working under ambient conditions. Amino acid decarboxylases, for example, enhance reactions rates by a factor of 10^{20}.[3] There are six different classes of enzymes: oxidoreductases, transferases,

hydrolases, lyases, isomerases, and ligases. Collectively they represent the functional agents of the cell and are thus critical to maintaining cellular homeostasis.

Carbohydrate-modifying enzymes, such as glycosyltransferases and glycosidases, are an important class of enzymes that are responsible for the synthesis and metabolism of oligosaccharides. Glycosidases catalyse the hydrolysis of specific glycosidic linkages between carbohydrate residues of oligosaccharides[4,5] while glycosyltransferases[6] catalyse the transfer of a monosaccharide from an activated donor, such as a sugar nucleotide, to an acceptor substrate. Glycosyltransferases are responsible for the synthesis of the specific oligosaccharide structures that are covalently attached to proteins and lipids, forming complex glycoconjugates. These glycoconjugates represent the most structurally diverse class of molecules in nature, and the high specificity by which they are synthesized by glycosyltransferases is truly remarkable. Glycosylation of proteins is the most common form of covalent modification and it plays a role in protein solubility, structure, and its interactions with substrate.[4] When expressed on cell surfaces, these glycoconjugates moderate cell-cell and cell-matrix interactions.[7] Thus this class of enzymes play a vital role in many essential life processes.

This work focuses on the development and application of analytical methodologies to gain a better understanding of proteins, the reactions they catalyse, and their interactions with ligands and substrates. Although the analytical methodologies presented in this work can be applied to the study of other enzyme classes, this thesis focuses on carbohydrate-modifying enzymes and can be divided into two main sections. The first section involves the development of small-scale enzyme assays using capillary electrophoresis with laser induced fluorescence detection (CE-LIF), while the second

section describes the application of mass spectrometry in evaluating the association thermodynamics of protein-carbohydrate complexes.

1.2 Small-Scale Enzyme Assays using CE-LIF

Increasing the sensitivity and the miniaturization of enzyme assays has been the focus of significant bioanalytical research.[8,9] The motivation for this lies, partly, in the beneficial effect afforded by decreased sample size. This is advantageous in biomedical research or any study where the sample size is limited. Also, in the study of low abundance enzymes such as glycosyltransferases, ultrasensitive detection is required.[10] Enhancing the sensitivity of analytical methodologies also permits the development of novel biochemical assays. Single cell analysis, for example, is an emerging field of research that promises to enhance our fundamental understanding of various biological phenomena.[11,12]

A general requirement in any enzyme assay is that there must be a measurable change in a physical property of either the substrate or product for the reaction progress to be monitored. In spectroscopic based approaches, this requirement can be met by using fluorogenic substrates, in which there is a change in the substrates' fluorescent properties upon action of an enzyme. There are, however, only a limited number of fluorogenic substrates and thus the range of reactions that can be studied is somewhat limited. A second disadvantage to this approach is that it can only be used to monitor the formation of one specific product, or alternately, the depletion of a specific substrate. This is disadvantageous in metabolic studies where the action of multiple enzymes is being studied, or where a distribution of products may be formed. The addition of a

separation step before detection greatly enhances the amount of information which can be extracted as it allows the detection of the original substrate, intermediates, and products of a reaction. Owing to its high sensitivity, small sample size requirements, and excellent separation efficiency, CE has been successfully applied in a wide range of small-scale enzyme assays.[10,13,14] In this work, CE-LIF is used to analyse reaction aliquots from small-scale and single cell enzyme assays.

1.2.1 Capillary Electrophoresis with Laser Induced Fluorescence Detection

Capillary electrophoresis, which was first reported by Jorgenson and Lukacs in 1981,[15] is the movement of charged species in a narrow bore fused silica capillary (10 – 200 μM inner diameter, i.d.) under the influence of an electric field. Charged particles migrate through the capillary and are separated based upon their electrophoretic mobility, μ_{EP}, which is given in eq 1.1.[16]

$$\mu_{EP} = \frac{q}{6\pi\eta r} \qquad 1.1$$

In eq 1.1, q is the charge on the analyte, η is the solution viscosity, and r is the radius of the analyte. Due to the nature of the fused silica capillaries, a second factor exists which determines the mobility of charged species in a CE separation. This factor, called electroosmotic flow (EOF), is a result of the negatively charged capillary walls. This leads to the formation of the so called diffuse double layer of positively charged ions present in solution. The application of a positive electric potential at the injection end of the capillary causes the bulk flow of this positively charged layer towards the grounded detection end. The strength of the EOF is described in eq 1.2:[16]

$$\mu_{EOF} = \frac{\varepsilon\zeta}{4\pi\eta} \qquad 1.2$$

where ε is the dielectric constant of the buffer, ζ is the zeta potential, and η is the buffer viscosity. Since the magnitude of the EOF is greater than the electrophoretic mobility of all species, there is a net movement of positively charged, negatively charged, and neutral species towards the detector. Thus all species can be detected and are separated by their different electrophoretic mobilites.

The CE-LIF instrument used in this work was an in-house built unit with a post-column detection system using a sheath-flow cuvette. A schematic of the CE setup used in the present work is given in Figure 1.1 and has been described in detail previously.[17,18] Briefly, samples are injected electrophoretically at the injection end of the capillary. The capillary used in this study was a 10 μm i.d. and 150 μm o.d. fused-silica capillary. Analytes are then separated as they migrate towards the detection end of the capillary. The detection end of the capillary is housed within a quartz sheath flow cuvette. As the analytes exit the capillary they are washed away via this sheath flow system. A 5 mW HeNe laser (Melles Griot, Nepean, Canada) with a wavelength of 543.5 nm is focused on the eluting end of the capillary. The fluorescent light is collected at 90° with a 60 x microscope objective (Melles Griot), passed through a 580dF27 band pass filter, and focused onto a photomultiplier tube (PMT) (Hamamatsu, R1477, Osaka, Japan) for detection.

1.2.2 Separation and Detection of Carbohydrates by CE-LIF

For the small-scale enzyme assays presented here, the species being analysed by CE-LIF are carbohydrates. There are two challenges to the electrophoretic separation and

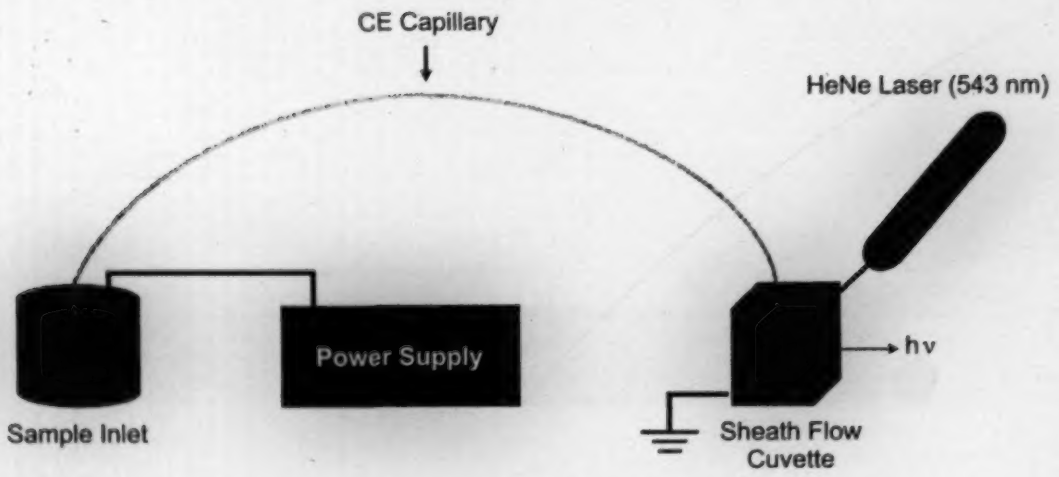

Figure 1.1 Schematic of the CE-LIF instrument.

LIF detection of carbohydrates: they are typically neutral and generally possess very lowextinction coefficients and are thus not amenable to spectroscopic detection. While the separation of neutral carbohydrates would not be possible using traditional CE techniques, various approaches have been developed to overcome this challenge. One approach is to perform the CE analysis at elevated pH, which leads to the ionization of the hydroxyl group at the anomeric position. The carbohydrates can then be separated based on their different pK_a values.[19-21] Alternatively, in the analysis of neutral species by CE, electrokinetic chromatography (EKC) can be employed.[22,23]

In this work micellar electrokinetic chromatography (MEKC) was used. MEKC is a mode of EKC in which a surfactant, such as sodium dodecyl sulfate (SDS) which was used in this work, is added to the CE buffer above the critical micelle concentration. The micelles act as a pseudo-stationary phase and analyte migration depends on the extent of partitioning within the micelles. SDS forms negatively charged micelles in solution. Since their electrophoretic mobility is in the direction opposite to the electroosmotic flow, they move very slowly towards the detector. Neutral species, such as carbohydrates, can then be separated based on their degree of partitioning within these micelles. To enhance the resolution of carbohydrates, a borate buffer is also used in the electrophoretic separation. In moderately alkaline conditions, borate forms stable anionic complexes with polyhydroxy compounds such as carbohydrates. [24,25] Complexation with borate effectively alters the degree of partitioning within the SDS micelles for each oligosaccharide, thus improving the resolution in MEKC.

The detection of carbohydrates by LIF is achieved by derivatizing the carbohydrate substrates with a tetramethyrhodamine (TMR) tag.[26,27] TMR has an

absorption maximum at 552 nm and is thus well suited to excitation using a 543 nm HeNe laser. The emission maximum for TMR is 570 nm, which is significantly different than the excitation wavelength. This large stokes shift allows selective transmission of emission light to the detector use through the use of band pass filters. This leads to a decrease in background signal caused by the excitation source and thus an increase in sensitivity.

1.2.3 Single Cell Analysis using CE-LIF

The single cell represents the basic unit of life and as such has become the focus of extensive research. Single cell analysis is advantageous over conventional bulk cell methods as it allows complex and heterogeneous biological systems to be probed at their most basic level. The minimal sample size requirements also make it well suited to cell developmental studies or in confirming deleterious gene knockouts. One area of single cell analysis is chemical cytometry, which focuses on the quantification of various analytes at the single-cell level.[8,11,12,28,29] These analytes include drugs, neurotransmitters, amino acids, ions, carbohydrates and peptides. There is also considerable interest in single-cell genomics and proteomics. Numerous techniques have been employed for single-cell analysis including flow cytometry, microfluidics and CE using electrochemical, mass spectrometry or LIF for detection. When studying enzymes, however, it is often more informative to determine enzyme activity rather than quantity by performing single-cell enzyme assays. Examining enzyme function at the single-cell level offers insights into complex and heterogeneous biochemical processes such as cell signaling pathways[9] and metabolism.[30,31]

Single-cell enzyme assays typically use CE with electrochemical or laser-induced fluorescence detection, due to the ultrasensitivity and small sample size requirements of the technique. There are many variations in single-cell enzyme assays, but in general two approaches are employed. In one approach individual cells are loaded on a CE capillary containing substrate for the enzyme of interest. The cell is lysed, releasing its enzymes, which are then free to interact with substrate. At any point after initiating the reaction, the CE voltage is applied to separate and detect the substrate and product molecules. This online approach is very sensitive since there is minimal dilution of cellular enzymes within the CE capillary. Using this approach the variation in lactate dehydrogenase activity in single erythrocytes has been determined.[32] A drawback to this method, however, is that the enzymatic reaction must occur in a CE-compatible buffer. The buffer requirements for CE are quite different than the native cellular environment and thus the measured activity may not reflect the enzymes true cellular activity.

A second approach involves incubating or culturing cells in a medium that contains a fluorescent substrate. The substrate is taken into the cells and converted to product in a natural enzyme environment. Cells are then individually loaded onto a CE capillary. After cell lysis the relative amounts of substrate and product are determined by CE-LIF analysis. Experiments such as these have the added benefit of providing information regarding the cellular uptake of substrate, but are thus also limited to analysing cell permeable substrates or involve the use of techniques such as microinjection or electroporation to introduce substrate into the cell. This approach has been used to monitor the metabolism of a fluorescently labeled carbohydrate in individual cancer cells and correlate the observed metabolism with cell cycle.[30] More recently, this

method has been employed to examine the metabolism of a Ras-mimicking peptide by three different enzymes in single cells.[33]

One limitation to both of these approaches is that the entire cell is consumed in the analysis. Thus only one measurement is performed which gives only a snapshot of enzyme activity. Multiple sampling would enhance the amount of information available from a single-cell study. For example, repeated sampling permits a single-cell enzymatic reaction to be monitored over time providing more details pertaining to the time-dependence of single-cell metabolism. For large cell types, such as the *Xenopus laevis* oocyte (diameter ≈1 mm), direct and multiple sampling of the cell cytoplasm is possible.[34] Allbritton and co-workers have employed this approach to inject RNA encoding for β-galactosidase into oocytes as well as β-galactosidase substrate. Aliquots of 100 pL were then directly removed from the oocyte cytoplasm and analysed using CE-LIF to monitor β-galactosidase activity. Since this is a non-destructive sampling method, spatial resolution regarding the distribution of enzyme activity throughout the cell is possible. This is a very powerful technique but is difficult to apply in the study of smaller cell types. Using capillaries with nanometer diameters, mammalian cells with a diameter of 10 μm have been directly sampled.[35] Each aliquot consumes a significant amount of the total cell volume however, limiting the extent of multiple sampling. An alternate approach is an off-line method by which individual cells are isolated in miniaturized reaction vessels and sampled repeatedly to monitor a single cell enzyme reaction.[36] The three main challenges to single cell assays are the isolation of individual cells from a cell population, sampling this single cell reaction, and the ability to monitor

the reaction progress. The solutions to these problems are the focus of Chapters 2 and 3 of this thesis.

1.3 Studying Protein-Carbohydrate Complexes using NanoES-MS

While monitoring the activity of enzymes can yield insights into the function and mechanism of an enzyme, it is also worthwhile to characterize their interactions with substrates. Biomolecular noncovalent complexes, such as protein-carbohydrate complexes, play a significant role in many fundamental life processes.[37-39] A better understanding of these interactions will thus provide an enhanced view into the nature of these processes at the molecular level. Two methods that have greatly enhanced our understanding of these interactions, allowing the atomic resolution of protein-ligand complexes, are x-ray crystallography and NMR spectroscopy. The first protein crystal structure, sperm whale myoglobin, was solved in 1958 by Max Ferdinand Perutz and Sir John Cowdery Kendrew. Since then protein crystallography has been used extensively in the determination of protein structure as well as the structure of protein-ligand complexes. According to the protein data bank, over 32,000 protein structures and 1500 protein-ligand structures have been determined using x-ray crystallography. NMR spectroscopy also allows the determination of protein-ligand complexes with atomic resolution and, with recent advances, can even be applied in the study of large (900 kDa) complexes, although not with atomic resolution.[40] Both of these techniques, however, are very labour intensive and in the case of x-ray crystallography, the structure is determined under conditions which are far from the native physiological conditions.

Mass spectrometry (MS) has emerged as a major tool in the field of proteomics, and is used for protein identification,[41] determining protein expression profiles,[42] and identifying post-translational modifications.[43] As well as the identification of monomeric species present in solution, structural information pertaining to proteins and protein complexes can be obtained using MS by the implementation of hydrogen-deuterium (H/D) techniques.[44-46] Using electrospray ionization (ES), which is capable of preserving noncovalent interactions present in solution, MS is also well suited to the study of protein assemblies[47,48] and protein-ligand interactions.[49,50] The work presented here describes the application of ES-MS to measure protein-carbohydrate association thermochemistry.

The first demonstrations of the preservation of noncovalent complexes during the ES process was that of the FKBP-FK506 receptor-ligand complex[51,52] and the noncovalent binding of heme to myoglobin.[53] Since then, ES-MS has become widely used in the study of noncovalent biological complexes.[50,54] ES-MS is well suited to such studies as it allows a fast and direct measure of all species, including noncovalent complexes, present in solution and requires no derivitization or immobilization of either receptor or ligand. Also, from the relative ion abundances, relative[55] and absolute binding affinities[56-59] of the complexes can be evaluated. The application of ES-MS to measure the binding affinity of protein-ligand complexes is dealt with in greater detail in Chapter 4.

In addition to the detection of noncovalent complexes and the determination of their association thermochemistry and stoichiometry, another dimension can be added to the analysis by using tandem MS (MS^n). MS^n experiments involve multiple steps of mass selection and analysis on the gaseous ions and enhance the amount of information

available from MS experiments. They also typically involve various gas-phase dissociation or fragmentation techniques. These include collision-induced dissociation (CID),[60] blackbody infrared radiative dissociation (BIRD),[61-64] electron capture dissociation (ECD),[65-67] and multiphoton dissociation (IRMPD).[68] Tandem MS has been used in a wide variety of applications to study the topology, higher order structure, and stability of protein assemblies and protein-ligand complexes. Recently, it was demonstrated that ECD-MS/MS can be used to identify what region of a protein is involved in interactions within a noncovalent complex.[69] In this study ECD was performed on a protein-ligand complex and the corresponding peptide fragments were analysed using MS/MS to determine which fragments remained bound to the ligand. Using the BIRD dissociation technique it is possible to follow dissociation kinetics as a function of temperature, which allows the construction of Arrhenius plots and the determination of activation energies and A-factors for a dissociation process. This technique has been combined with functional group replacement to map the intrinsic interactions for a protein-carbohydrate complex.[70,71] In Chapter 5 of this thesis, the BIRD dissociation technique is applied to probe the equivalency of binding sites in protein-ligand complexes.

1.3.1 Mass Spectrometry

In general, mass spectrometry involves the formation of gas-phase ions by various ionization techniques followed by their separation and detection according to their mass-to-charge ratio (*m/z*) using a mass analyzer. Many different ionization methods and mass analyzers exist and deciding which combination is best suited for any given analysis

depends on the nature of the sample and the type of information required. In the analysis of biomolecules, such as proteins, the so called "soft ionization" techniques, ES and matrix-assisted laser desorption/ionization (MALDI) are most commonly used. These techniques are capable of generating intact macromolecular ions. There are a number of different types of mass analyzers such as magnetic sector,[72] quadrupole,[73] ion trap,[74] time of flight (TOF),[79] FT-ICR,[76] and most recently, orbitrap.[77] In the present study, nanoES combined with FT-ICR/MS was used to study protein-ligand complexes.

1.3.2 NanoES-FT-ICR/MS

The ES process, as described by Kebarle and coworkers,[78,79] involves the production of charged droplets from electrolyte dissolved in a solvent; the shrinkage of the droplets by solvent evaporation accompanied with droplet fissions leads to formation of very small, highly charged droplets from which gaseous ions are produced. NanoES, a low solution flow variant of ES developed by Matthias Mann,[51,52] has a similar mechanism to that of ES. Shown in Figure 1.2 is a diagram describing the ES process in the positive ion mode.[78] A high positive voltage applied to the ES capillary induces charge separation of electrolytes in the solution. Positive charges drift towards the liquid surface, leading to the formation of a liquid cone refereed to as a Taylor cone. At a sufficiently high electric field, the liquid cone becomes unstable and emits a thin liquid filament which then breaks up into small positively charged droplets. With solvent evaporation, these droplets start to shrink into smaller droplets. As the charge density on the droplet surface increases to the Rayleigh limit, which is the point at which the Coulombic repulsion of the surface charges is equal to the surface tension of the droplets,

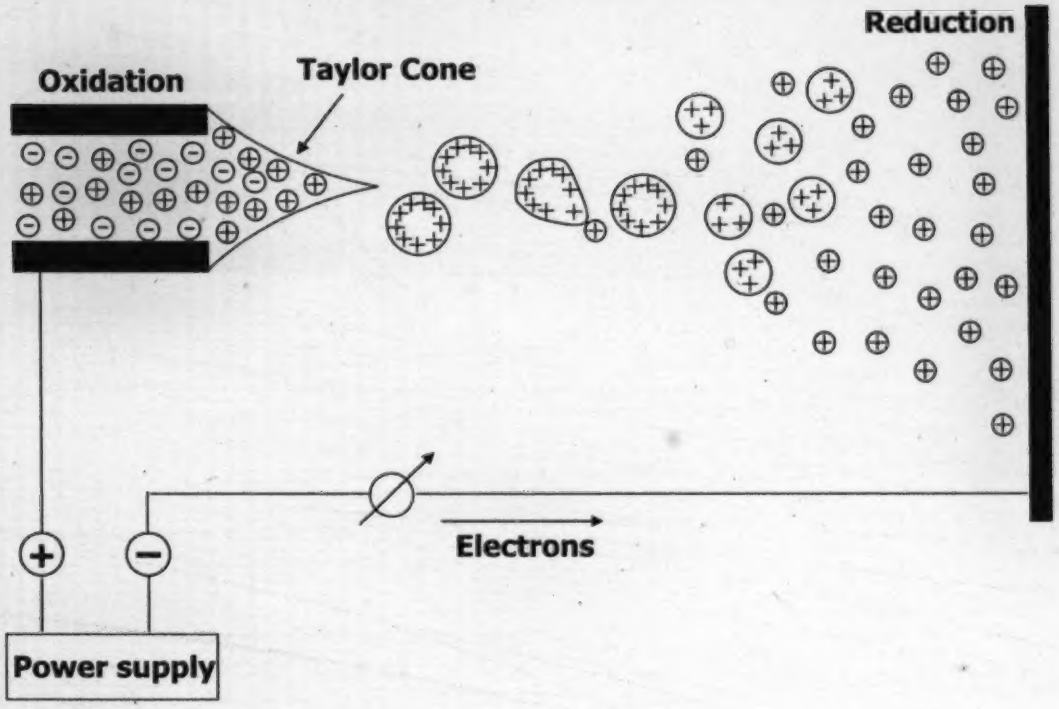

Figure 1.2 Illustration of the ES process.

the droplets undergo Rayleigh fission. This fission leads to the production of small, highly charged offspring droplets. The formation of gas-phase ions from these small, highly charged droplets follows one of two mechanisms. The first mechanism, which is based on the ion evaporation model,[80,81] assumes ion emission directly from very small and highly charged droplets and accounts for the production of gas-phase ions of small molecules. For macromolecules, however, it is believed that the charged residue model most accurately describes the formation of gaseous ions.[82] In the charge residue model, as proposed by Dole,[82] the droplets undergo many fissions, finally producing smaller droplets containing a single analyte molecule. These droplets undergo further solvent evaporation producing gaseous ions.

Due to its lower solution flow rate (10 – 50 nL/min), nanoES is better suited to the study of noncovalent complexes than conventional ES. One result of this lower flow rate is that less solution is consumed. NanoES, which typically consumes picomoles of analyte per analysis, is well suited to studies where the sample is limited. Additionally, the lower flow rate translates to smaller droplet size in the ES process which results in a shorter droplet lifetime, which should be advantageous in preserving the original solution composition throughout the formation of gaseous ions. It also allows for the transfer of noncovalent complexes from buffered aqueous solution to the gas-phase, permitting the study of these complexes under near physiological conditions.

The mass analyzer used to detect the ions generated by nanoES was FT-ICR/MS, which exhibits the highest resolving power and mass accuracy among available mass analyzers. FT-ICR/MS is a technique that converts *m/z* to an experimentally measurable ion cyclotron orbital frequency.[76,83-85] The basis for FT-ICR/MS is ion cyclotron motion,

which arises from the interaction of an ion, trapped within a cyclotron cell, with a spatially homogeneous static magnetic field. Figure 1.3 illustrates the cyclotron motion of a positive ion subjected to a static magnetic field, B, directed into the plane of the paper. The cyclotron frequency, ω_c, is described in eq 1.3:

$$\omega_c = \frac{zeB}{m} \qquad 1.3$$

where z is the charge on the ion, e is the elementary charge, B is the magnetic field strength, and m is the mass of the ion. Note that in eq 1.3 there is no velocity term and thus the ion cyclotron motion is independent of ion velocity and kinetic energy. This feature makes ICR especially amenable to MS and is responsible for the high resolution attainable by FT-ICR/MS.

Figure 1.4 illustrates how a mass spectrum is generated from this ion cyclotron motion. First, the addition of an rf pulse equal to the cyclotron (resonance) frequencies of the ions is transmitted by the excitation plates of the cell to generate a coherent ion packet. The excitation plates are an opposing pair of plates which lie parallel to the magnetic field. The trajectory of a group of excited ions of the same *m/z* ratio at their cyclotron frequency is given in Figure 1.4a. As these coherently orbiting ions pass another pair of opposing electrodes (detection plates), which are also parallel to the magnetic field, they induce an alternating current in the detection plates called an image current (Figure 1.4b). The amplitude of this transient signal is proportional to the number of ions in the cell and its frequency is the same as the cyclotron frequency of the ions. The transient signal is amplified, digitized, and stored for processing. A Fourier transform of the time domain signal is performed and then eq 1.3 is used to generate a

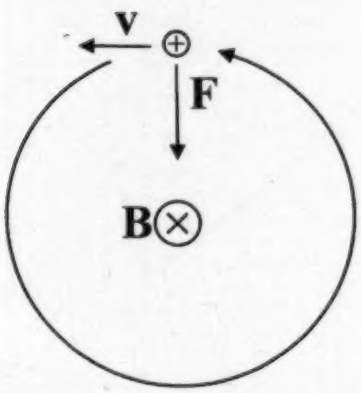

Figure 1.3 Cyclotron motion of a positive ion of charge q moving at velocity **v** in the presence of a constant magnetic field, **B**, which is pointing into the page. The ion moving to the left experiences a downward force, $\mathbf{F} = q(\mathbf{v} \times \mathbf{B})$, resulting in a counterclockwise orbit.

mass spectrum from the resultant frequency components of the signal. This process is summarized in Figure 1.4.

A schematic diagram of the nanoES-FT-ICR/MS instrument used in the present work is given in Figure 1.5. A solution containing the analyte of interest, typically mixed in a 10 mM ammonium acetate buffer, is placed in a aluminosilicate capillary (1.0 mm o.d., 0.68 mm i.d.), pulled to 4–7 μm o.d. at one end, forming the nanoES tip. A platinum wire is inserted into the distal end of the nanoES tip and a voltage (± 800-1000 V) is applied. Droplets and gaseous ions produced by nanoES are sampled into the mass spectrometer through a heated metal capillary. Gaseous ions are then transmitted through the skimmer and accumulated in the hexapole for a certain period of time to enhance the signal-to-noise (S/N) ratio. The accumulated ions are ejected from the hexapole and accelerated into a 9.4 T superconducting magnet. Here the ions are decelerated and eventually trapped by a combination of electric and magnetic fields in the FT-ICR cell for detection. The pressure for the instrument is typically maintained at 5 x 10^{-10} mbar by the differential pumping system.

1.3.3 Blackbody Infrared Radiative Dissociation (BIRD)

BIRD is a dissociation technique which allows ions to undergo unimolecular dissociation at essentially zero pressure by the exchange of energy with an ambient blackbody radiation field. Consequently, BIRD experiments can be performed in the ultra-low pressure, heated ion cell of the FT-ICR/MS instrument. Molecular activation by blackbody photons was originally suggested by Perrin.[86] The unimolecular dissociation reaction of a hypothetical molecular ion, AB^+, can be envisioned as a two

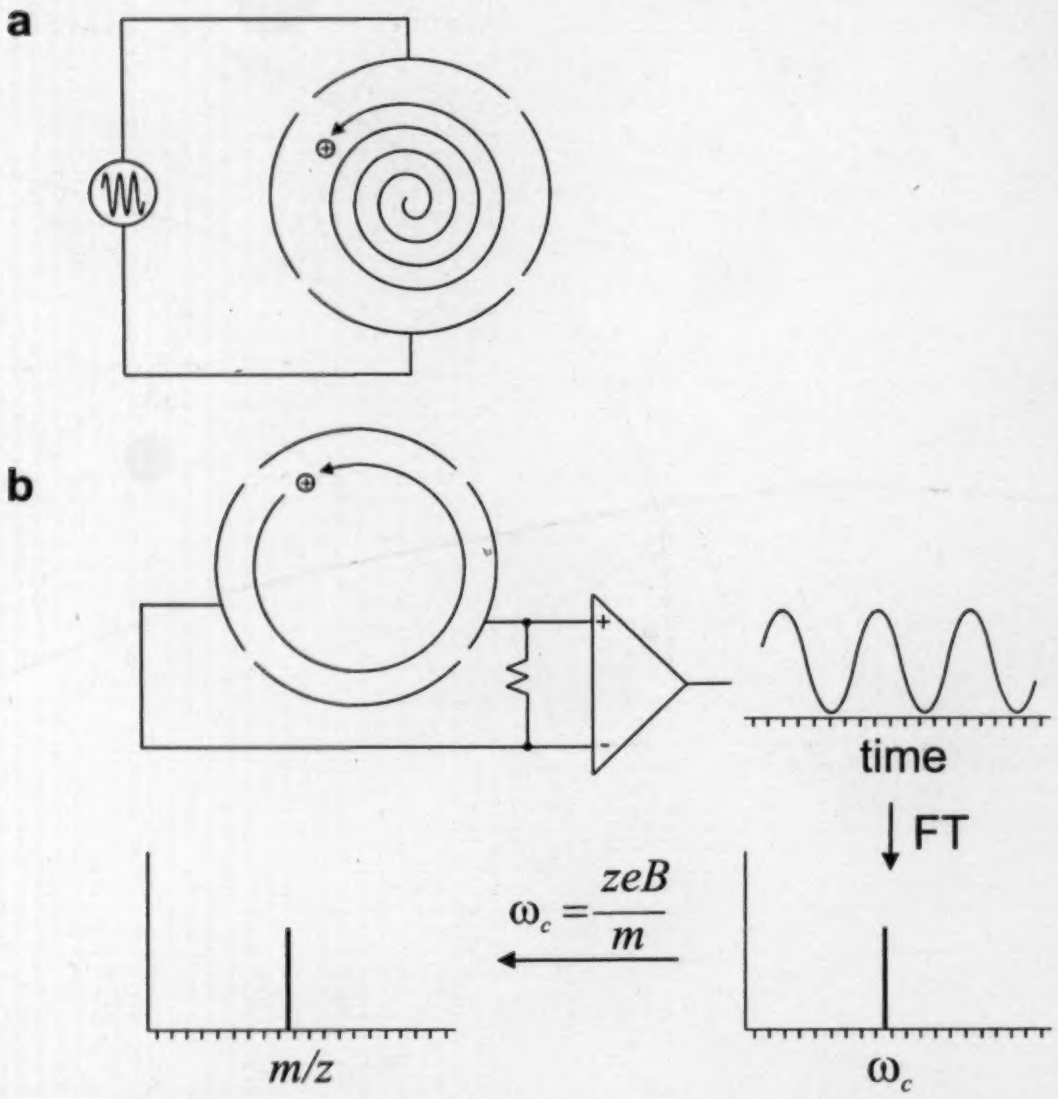

Figure 1.4 Illustration of (a) ion excitation and (b) the generation of a mass spectrum from the measured image current for ions in an FT-ICR/MS mass analyzer cell.

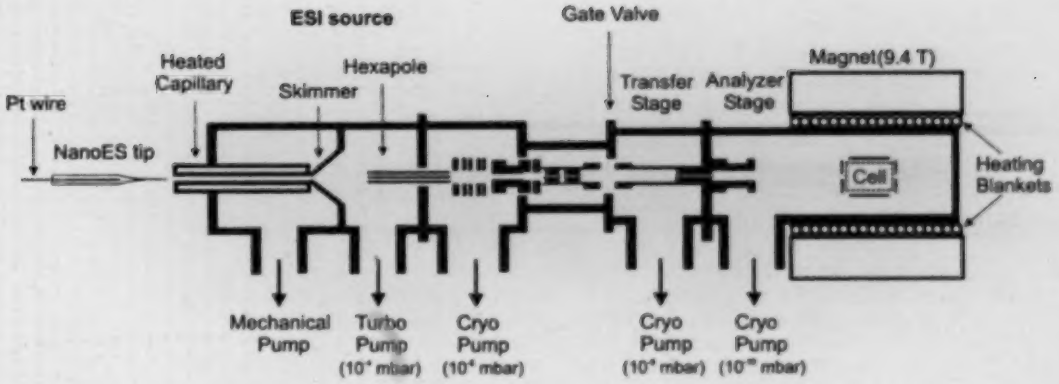

Figure 1.5 Schematic of the nanoES-FT-ICR/MS instrument used in this study.

step mechanism (eq 1.4a-c).[61-64] The first step involves the excitation of AB^+ to activated species, AB^{+*}, by the absorption of infrared photons (eq 1.4b). The activated species can either relax back into AB^+ through the emission of infrared photons, or dissociate into products A^+ and B (eq 1.4c). Under steady state conditions, the observed collisionless unimolecular rate constant, k_{uni}, is expressed in terms of radiative activation and deactivation rate constants, $k_{1,rad}$ and $k_{-1,rad}$, and unimolecular dissociation rate constant, k_d (eq 1.5a). If k_d is much larger than $k_{-1,rad}$, the observed reaction kinetic, k_{uni}, reflects only the rate of photon absorption, $k_{1,rad}$, eq 1.5b. Therefore, no information about the dynamics of the dissociation process is obtained. If k_d is much smaller than $k_{-1,rad}$, k_{uni} is determined by the dissociation kinetics of ions with a Boltzmann distribution of internal energies (eq 1.5c).[63] From the temperature dependence of the unimolecular rate constants for dissociation, k_{uni}, Arrhenius activation energy (E_a) and preexponential factor (A) can be determined. This is the case for large ions such as protein ions which are in the rapid energy exchange limit (REX).[63] In this limit, the unimolecular dissociation rate of the activated ions is slow compared with the rate of energy equilibration of a molecule with the surroundings by photon exchange, and the internal energy of a population of ions is given by a Boltzmann distribution.

$$AB^+ \xrightarrow{k_{uni}} A^+ + B \qquad (1.4a)$$

$$AB^+ + h\nu \underset{k_{-1,rad}}{\overset{k_{1,rad}}{\rightleftarrows}} AB^{+*} \qquad (1.4b)$$

$$AB^{+*} \xrightarrow{k_d} A^+ + B \qquad (1.4c)$$

$$k_{uni} = k_d \left(\frac{k_{1,rad}}{k_{-1,rad} + k_d} \right) \qquad (1.5a)$$

$$k_{uni} = k_{1,rad} \quad \text{if } k_d >> k_{-1,rad} \qquad (1.5b)$$

$$k_{uni} = k_d \left(\frac{k_{1,rad}}{k_{-1,rad}} \right) \quad \text{if } k_d << k_{-1,rad} \qquad (1.5c)$$

The observation of ion-dissociation reactions using BIRD technique is based on two essential requirements. First, BIRD experiments should be performed at a low pressure (below 10^{-6} Torr). At this low pressure, infrared photon absorption and emission exchange between ions and surrounding is the dominant phenomenon compared with negligible collisional energy exchange. Secondly, the time scale of observation of the dissociating molecules should be long enough (on the order of seconds) to give a significant degree of dissociation of the population for this relatively slow mechanism.[61]

1.4 Literature Cited

(1) Pandey, A.; Mann, M. *Nature* **2000**, *405*, 837-846.

(2) Bairoch, A. *Nucleic Acids Research* **2000**, *28*, 304-305.

(3) Miller, B. G.; Wolfenden, R. *Annual Reviews of Biochemistry* **2002**, *71*, 847-885.

(4) Helenius, A.; Aebi, M. *Annual Reviews of Biochemistry* **2004**, *73*, 1019-1049.

(5) Zechel, D. L.; Withers, S. G. *Accounts of Chemical Research* **2000**, *33*, 11-18.

(6) Paulson, J. C.; Colley, K. J. *Journal of Biological Chemistry* **1989**, *264*, 17615-17618.

(7) Feizi, T. *Nature* **1985**, *314*, 53-57.

(8) Dovichi, N. J.; Pinkel, D. *Current Opinion in Biotechnology* **2003**, *14*, 3-4.

(9) Meredith, G. D.; Sims, C. E.; Soughayer, J. S.; Allbritton, N. L. *Nature Biotechnology* **2000**, *18*, 309-312.

(10) Le, X. C.; Zhang, Y.; Dovichi, N. J.; Compston, C. A.; Palcic, M. M.; Beever, R. J.; Hindsgaul, O. *Journal of Chromatography A* **1997**, *781*, 515-522.

(11) Huang, B.; Wu, H. K.; Bhaya, D.; Grossman, A.; Granier, S.; Kobilka, B. K.; Zare, R. N. *Science* **2007**, *315*, 81-84.

(12) Sweedler, J. V.; Arriaga, E. A. *Analytical and Bioanalytical Chemistry* **2007**, *387*, 1-2.

(13) Le, X. C.; Scaman, C.; Zhang, Y. N.; Zhang, J. H.; Dovichi, N. J.; Hindsgaul, O.; Palcic, M. M. *Journal of Chromatography A* **1995**, *716*, 215-220.

(14) Zhao, J. Y.; Dovichi, N. J.; Hindsgaul, O.; Gosselin, S.; Palcic, M. M. *Glycobiology* **1994**, *4*, 239-242.

(15) Jorgenson, J. W.; Lukacs, K. D. *Journal of Chromatography* **1981**, *218*, 209-216.

(16) Landers, J. P. *Handbook of Capillary Electrophoresis*, 2 ed.; CRC Press: New York, 1997.

(17) Chen, D. Y.; Swerdlow, H. P.; Harke, H. R.; Zhang, J. Z.; Dovichi, N. J. *Journal of Chromatography* **1991**, *559*, 237-246.

(18) Wu, S. L.; Dovichi, N. J. *Journal of Chromatography* **1989**, *480*, 141-155.

(19) Colon, L. A.; Dadoo, R.; Zare, R. N. *Analytical Chemistry* **1993**, *65*, 476-481.

(20) Garner, T. W.; Yeung, E. S. *Journal of Chromatography* **1990**, *515*, 639-644.

(21) Vorndran, A. E.; Oefner, P. J.; Scherz, H.; Bonn, G. K. *Chromatographia* **1992**, *33*, 163-168.

(22) Terabe, S.; Otsuka, K.; Ando, T. *Analytical Chemistry* **1985**, *57*, 834-841.

(23) Terabe, S.; Otsuka, K.; Ichikawa, K.; Tsuchiya, A.; Ando, T. *Analytical Chemistry* **1984**, *56*, 111-113.

(24) Hoffstetterkuhn, S.; Paulus, A.; Gassmann, E.; Widmer, H. M. *Analytical Chemistry* **1991**, *63*, 1541-1547.

(25) Weigel, H. *Advances in Carbohydrate Chemistry* **1963**, *18*, 61-97.

(26) Scaman, C. H.; Hindsgaul, O.; Palcic, M. M.; Srivastava, O. P. *Carbohydrate Research* **1996**, *296*, 203-213.

(27) Zhang, Y. N.; Le, X. C.; Dovichi, N. J.; Compston, C. A.; Palcic, M. M.; Diedrich, P.; Hindsgaul, O. *Analytical Biochemistry* **1995**, *227*, 368-376.

(28) Kennedy, R. T.; Oates, M. D.; Cooper, B. R.; Nickerson, B.; Jorgenson, J. W. *Science* **1989**, *246*, 57-63.

(29) Wu, H. K.; Wheeler, A.; Zare, R. N. *Proceedings of the National Academy of Sciences in the United States of America* **2004**, *101*, 12809-12813.

(30) Krylov, S. N.; Zhang, Z. R.; Chan, N. W. C.; Arriaga, E.; Palcic, M. M.; Dovichi, N. J. *Cytometry* **1999**, *37*, 14-20.

(31) Krylov, S. N.; Arriaga, E. A.; Chan, N. W. C.; Dovichi, N. J.; Palcic, M. M. *Analytical Biochemistry* **2000**, *283*, 133-135.

(32) Xue, Q. F.; Yeung, E. S. *Analytical Chemistry* **1994**, *66*, 1175-1178.

(33) Arkhipov, S. N.; Berezovski, M.; Jitkova, J.; Krylov, S. N. *Cytometry Part A* **2005**, *63A*, 41-47.

(34) Luzzi, V.; Lee, C. L.; Allbritton, N. L. *Analytical Chemistry* **1997**, *69*, 4761-4767.

(35) Woods, L. A.; Powell, P. R.; Paxon, T. L.; Ewing, A. G. *Electroanalysis* **2005**, *17*, 1192-1197.

(36) Shoemaker, G. K.; Lorieau, J.; Lau, L. H.; Gillmor, C. S.; Palcic, M. M. *Analytical Chemistry* **2005**, *77*, 3132-3137.

(37) Helenius, A.; Aebi, M. *Science* **2001**, *291*, 2364-2369.

(38) Lis, H.; Sharon, N. *Chemical Reviews* **1998**, *98*, 637-674.

(39) Rudd, P. M.; Elliott, T.; Cresswell, P.; Wilson, I. A.; Dwek, R. A. *Science* **2001**, *291*, 2370-2376.

(40) Fiaux, J.; Bertelsen, E. B.; Horwich, A. L.; Wuthrich, K. *Nature* **2002**, *418*, 207-211.

(41) Aebersold, R.; Mann, M. *Nature* **2003**, *422*, 198-207.

(42) Flory, M. R.; Griffin, T. J.; Martin, D.; Aebersold, R. *Trends in Biotechnology* **2002**, *20*, S23-S29.

(43) Mann, M.; Jensen, O. N. *Nature Biotechnology* **2003**, *21*, 255-261.

(44) Robinson, C. V.; Gross, M.; Eyles, S. J.; Ewbank, J. J.; Mayhew, M.; Hartl, F. U.; Dobson, C. M.; Radford, S. E. *Nature* **1994**, *372*, 646-651.

(45) Zhang, Z. Q.; Smith, D. L. *Protein Science* **1993**, *2*, 522-531.

(46) Zhu, M. M.; Rempel, D. L.; Gross, M. L. *Journal of the American Chemical Society* **2004**, *15*, 388-397.

(47) Hernandez, H.; Robinson, C. V. *Journal of Biological Chemistry* **2001**, *276*, 46685-46688.

(48) Loo, J. A. *International Journal of Mass Spectrometry* **2000**, *200*, 175-186.

(49) Hofstadler, S. A.; Sannes-Lowery, K. A. *Nature Reviews Drug Discovery* **2006**, *5*, 585-595.

(50) Loo, J. A. *Mass Spectrometry Reviews* **1997**, *16*, 1-23.

(51) Wilm, M. S.; Mann, M. *International Journal of Mass Spectrometry and Ion Processes* **1994**, *136*, 167-180.

(52) Wilm, M.; Mann, M. *Analytical Chemistry* **1996**, *68*, 1-8.

(53) Katta, V.; Chait, B. T. *Journal of the American Chemical Society* **1991**, *113*, 8534-8535.

(54) Loo, R. R. O.; Goodlett, D. R.; Smith, R. D.; Loo, J. A. *Journal of the American Chemical Society* **1993**, *115*, 4391-4392.

(55) Cheng, X. H.; Chen, R. D.; Bruce, J. E.; Schwartz, B. L.; Anderson, G. A.; Hofstadler, S. A.; Gale, D. C.; Smith, R. D.; Gao, J. M.; Sigal, G. B.; Mammen, M.; Whitesides, G. M. *Journal of the American Chemical Society* **1995**, *117*, 8859-8860.

(56) Ayed, A.; Krutchinsky, A. N.; Ens, W.; Standing, K. G.; Duckworth, H. W. *Rapid Communications in Mass Spectrometry* **1998**, *12*, 339-344.

(57) Greig, M. J.; Gaus, H.; Cummins, L. L.; Sasmor, H.; Griffey, R. H. *Journal of the American Chemical Society* **1995**, *117*, 10765-10766.

(58) Kitova, E. N.; Kitov, P. I.; Bundle, D. R.; Klassen, J. S. *Glycobiology* **2001**, *11*, 605-611.

(59) Loo, J. A.; Hu, P. F.; McConnell, P.; Mueller, W. T.; Sawyer, T. K.; Thanabal, V. *Journal Of The American Society For Mass Spectrometry* **1997**, *8*, 234-243.

(60) McLuckey, S. A. *Journal of the American Society for Mass Spectrometry* **1992**, *3*, 599-614.

(61) Dunbar, R. C. *Mass Spectrometry Reviews* **2004**, *23*, 127-158.

(62) Price, W. D.; Schnier, P. D.; Jockusch, R. A.; Strittmatter, E. F.; Williams, E. R. *Journal of the American Chemical Society* **1996**, *118*, 10640-10644.

(63) Price, W. D.; Jockusch, R. A.; Williams, E. R. *Journal of Physical Chemistry* **1997**, *119*, 11988-11989.

(64) Tholmann, D.; Tonner, D. S.; McMahon, T. B. *Journal of Physical Chemistry* **1994**, *98*, 2002-2004.

(65) Zubarev, R. A.; Horn, D. M.; Fridriksson, E. K.; Kelleher, N. L.; Kruger, N. A.; Lewis, M. A.; Carpenter, B. K.; McLafferty, F. W. *Analytical Chemistry* **2000**, *72*, 563-573.

(66) Zubarev, R. A.; Kruger, N. A.; Fridriksson, E. K.; Lewis, M. A.; Horn, D. M.; Carpenter, B. K.; McLafferty, F. W. *Journal of the American Chemical Society* **1999**, *121*, 2857-2862.

(67) Zubarev, R. A.; Kelleher, N. L.; McLafferty, F. W. *Journal of the American Chemical Society* **1998**, *120*, 3265-3266.

(68) Little, D. P.; Speir, J. P.; Senko, M. W.; Oconnor, P. B.; McLafferty, F. W. *Analytical Chemistry* **1994**, *66*, 2809-2815.

(69) Xie, Y. M.; Zhang, J.; Yin, S.; Loo, J. A. *Journal of the American Chemical Society* **2006**, *128*, 14432-14433.

(70) Kitova, E. N.; Bundle, D. R.; Klassen, J. S. *Angewandte Chemie - International Edition* **2004**, *43*, 4183-4186.

(71) Kitova, E. N.; Bundle, D. R.; Klassen, J. S. *Journal of the American Chemical Society* **2002**, *124*, 5902-5913.

(72) Mattauch, J.; Herzog, R. *Z. Physik* **1934**, *89*.

(73) Dawson, P. H. *Quadrupole Mass Spectrometry and its Applications*: New York, 1976.

(74) March, R. E. *Mass Spectrometry* **1997**, *32*, 351-369.

(75) Wiley, W. C.; McLaren, I. H. *Review of Scientific Instruments* **1955**, *26*, 1150-1157.

(76) Amster, I. J. *Journal of Mass Spectrometry* **1996**, *31*, 1325-1337.

(77) Hu, Q. Z.; Noll, R. J.; Li, H. Y.; Makarov, A.; Hardman, M.; Cooks, R. G. *Journal of Mass Spectrometry* **2005**, *40*, 430-443.

(78) Kebarle, P.; Tang, L. *Analytical Chemistry* **1993**, *65*, A972-A986.

(79) Tang, L.; Kebarle, P. *Analytical Chemistry* **1993**, *65*, 3654-3668.

(80) Iribarne, J. V.; Thomson, B. A. *Journal of Chemical Physics* **1976**, *64*, 2287-2294.

(81) Thomson, B. A.; Iribarne, J. V. *Journal of Chemical Physics* **1979**, *71*, 4451-4463.

(82) Dole, M.; Mack, L. L.; Hines, R. L. *Journal of Chemical Physics* **1968**, *49*, 2240-&.

(83) Buchanan, M. V.; Hettich, R. L. *Analytical Chemistry* **1993**, *65*, A245-A259.

(84) Marshall, A. G.; Grosshans, P. B. *Analytical Chemistry* **1991**, *63*, A215-A229.

(85) Marshall, A. G.; Hendrickson, C. L. *International Journal of Mass Spectrometry* **2002**, *215*, 59-75.

(86) Perrin, J. *Annals of Physics* **1919**, *11*, 5-108.

Chapter 2

Development of a Quantitative Nanopipettor for Miniaturized Chemical and Biochemical Reaction Sampling[1]

2.1 Introduction

Miniaturization of the scale upon which chemical and biochemical reactions are assayed has been an important goal in chemistry and biochemistry. Smaller chemical reactions are practical in reducing reagent requirements and adapting systems for high-throughput processing. In biological and biochemical studies, small volume enzymatic reactions can reflect activities of single cells or a group of cells which is advantageous in that it reduces sample size requirements and can help eliminate the averaging bias introduced when sampling enzymatic activity from a cell culture.[1-6] Specifically, enzyme activity and expression could be monitored at different stages of cell growth,[2] with multiple detection methods, for a high-throughput detection of single mutant colonies without laborious workup.

Methods based on capillary electrophoresis (CE) are well suited for small scale bioanalytical studies because small sample volumes can be processed (~10 pL). In addition, high sensitivity is achieved by combining capillary electrophoresis with laser induced fluorescence detection (CE-LIF).[7-12] Chemical and biochemical reactions have been performed within the sample injection plug in the capillary and the products are

---

1 A version of this chapter has been published: Lorieau, J; Shoemaker, G.K.; Palcic, M.M. *Anal. Chem.* **2003**, *75*, 6351-6354.

separated by subsequently applying an electric field. These studies have been carried out on single enzymes, single cells, and cellular lysates.[4-6,13-19] Unfortunately the optimal reaction buffer and optimal CE separation buffer can be quite different when performing on-capillary biochemical reactions.[20-23] For biochemical studies, most enzymatic reactions are optimal at pH 6.5-8 while optimal CE running buffers can have pHs that are typically out of this range. Furthermore, other enzymatic buffer components and cofactors may complicate the optimal CE separation conditions.

A method is presented here that combines the high detections levels, separation efficiencies and small injection volumes of CE with the optimal buffer conditions needed for continuous enzyme kinetic reactions. A cost-effective and high precision nanoliter scale pipettor (nanopipettor) was constructed and a reproducible aliquot sampling protocol was developed for the removal of nanoliter volume samples. The nanopipettor's reproducibility in nanoliter-size aliquot sampling is demonstrated, and a standard enzyme reaction is used to validate the nanopipettor as a complementary tool to small scale CE-LIF enzyme kinetics.

2.2 Experimental

2.2.1 Materials and Reagents

To allow fluorescence detection, the carbohydrates were labeled with a tetramethylrhodamine (TMR) tag via synthetic means and were available from previous studies.[24] CE running buffer was a 10 mM sodium phosphate buffer (Sigma) composed of 50 mM sodium dodecyl sulfate (SDS, Caledon), 10 mM phenyl boronic acid (Sigma), and 2.5 mM sodium tetraborate (Fisher) at a pH of 9.3. An organic modifier, 10%

dioxane (Caledon, reagent grade), was added to improve the separation of the carbohydrates. β-galactosidase was purchased from Sigma (Grade VIII).

2.2.2 Nanopipettor Construction

The nanopipettor is based on a hydrodynamic design consisting of an uncoated fused-silica CE capillary (coatings are optional) connected to a 1 mL gas-tight Hamilton syringe (Fisher) with a standard tip needle (Figure 2.1). A PEEK zero dead volume union with an airtight capillary adapter (Upchurch Scientific) connects the syringe tip to the fused-silica polyimide capillary (150 μm O.D and 10 μm I.D, Polymicro Technologies). The total capillary length is 12 cm with approximately 4 cm of the capillary protruding out of the PEEK ZDV union while the remainder is within the union and inserted in the Hamilton syringe needle tip. The nanopipettor aspirates a reproducible volume by changing the pressure within the Hamilton syringe with relation to the atmospheric pressure for a given period of time. The derivation for the volume aspirated, as related to time, is demonstrated in the following hydrodynamic equations.

For a perfect gas, the difference in pressure between two compartments can be related to the change in volume of one of the compartments. In changing the volume inside the syringe (closed environment), the pressure changes from atmospheric pressure (p_0) to a final pressure (p_f) by changing the volume by ΔV.

$$pV = nRT \quad \text{and} \quad p_1V_1 = p_2V_2 \tag{2.1}$$

$$p_oV_o = p_f(V_o + \Delta V) \quad \therefore \quad \frac{V_o}{V_o + \Delta V} = \frac{p_f}{p_o} \tag{2.2}$$

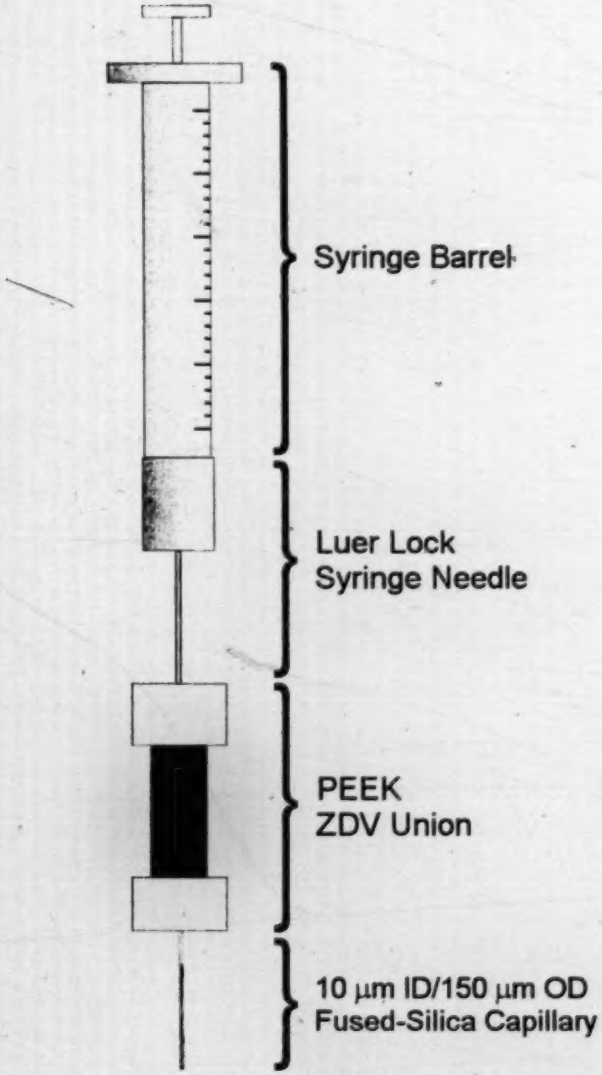

Figure 2.1 Schematic of nanopipettor design and components.

$$\frac{\Delta p}{p_o} = \frac{p_o - p_f}{p_o} = 1 - \frac{p_f}{p_o} \qquad (2.3)$$

$$\Delta p = p_o - p_o \frac{p_f}{p_o} = p_o - p_o\left(\frac{V_o}{V_o + \Delta V}\right) \qquad (2.4)$$

The identity in equation (2.1) assumes the temperature to be constant throughout the sampling process. To achieve this, the glass Hamilton syringe was not handled while aliquoting. The syringe was clamped to a ring stand and only the plunger was in contact with the operator.

The equation for the volume aspirated hydrodynamically from a capillary by applying different pressures to both ends of the capillary is represented in equation (2.5).[25]

$$V_{aspirated} = \frac{\Delta p \pi d^4 t}{128 \eta L} \qquad (2.5)$$

where Δp is the change in pressure, d is the capillary's inner diameter, t is the time the capillary is immersed in the sample vessel (length of hydrodynamic aspiration; called hydrodynamic time), η is the solution viscosity (0.001 $Kgm^{-1}s^{-1}$ for water), and L is the length of the fused silica capillary. When we relate the change in pressure inside the syringe with the atmospheric pressure, the volume aspirated hydrodynamically ($V_{aspirated}$) can be related to the hydrodynamic time using equations (2.4) and (2.5).

$$V_{aspirated} = \frac{p_o\left(1 - \frac{V_o}{V_o + \Delta V}\right)\pi d^4 t}{128 \eta L} = \frac{p_o\left(1 - \frac{V_o}{V_f}\right)\pi d^4 t}{128 \eta L} \qquad (2.6)$$

In the above equation, V_o is the initial volume position of the syringe barrel and V_f is the final position.

2.2.3 Nanopipettor Procedure for Aliquot Transfer

A 12 cm piece of 10 μm fused-silica capillary was rinsed for 8-10 minutes with the wash buffer (100mM sodium phosphate buffer, pH 7.0) before use. Immediately before sampling, the capillary tip was rinsed by inserting the sampling end in a reservoir of Milli-Q water. The tip was then inserted into the sample and the plunger on the Hamilton syringe withdrawn from 200 μL to 600 μL for 38 s (the change in pressure and the hydrodynamic times can both be varied). Using eq 2.6 the calculated volume using these conditions for a 12 cm capillary is 5 nL. With the syringe plunger held at 600 μL, the capillary is removed from the sample. The sampling end of the capillary is again inserted into a vial of Milli-Q water to rinse the tip of the capillary. The solution within the capillary is then expelled by depressing the Hamilton syringe plunger to a volume of 100 μL for 20 s. After use, the capillary is rinsed with HPLC grade methanol.

2.2.4 Capillary Electrophoresis with Laser Induced Fluorescence

The CE-LIF instrument was locally constructed and has been described previously.[12,23,26,27] Electrophoretic potentials were achieved with a CZE100R high voltage power supply (Spellman, Plainview, NY) using an applied potential of 400 V/cm. Separations were conducted over a 40.0 cm long capillary with a 10 μm i.d. and a 150 μm o.d. (Polymicro, Phoenix, AZ). Post-capillary detection was achieved by focusing a 5 mW Helium-Neon laser (Melles Griot, Nepean, Canada) with a wavelength of 543.5 nm on the eluting tip of the capillary. CE running buffer (without dioxane) formed a sheath flow in the quartz cuvette which housed the capillary tip. The fluorescent signal was collected at a right angle from excitation, focused with a 60X, 0.7 NA microscope

objective and spectrally filtered with a 580DF27 band-pass filter (Omega Optical, Brattleboro, VT). The fluorescent signal was focused onto an iris and detected with a R1477 photomultiplier tube, operating at 1000V (Hamamatsu, Middlesex, NJ). Data was digitized with a NB-MIO-16x data acquisition board (National Instruments, Austin, TX) and analyzed with a Macintosh Computer using LabView software (National Instruments, Austin, TX) and Igor Pro version 3.15.

2.3 Results and Discussion

2.3.1 Linearity and Precision of Volume Delivery

In order for the nanopipettor to be a useful analytical tool for small-scale reaction sampling, it must be tunable, precise, and reproducible. The reproducibility and accuracy of delivering aliquots with the nanopipettor was tested with TMR-labeled carbohydrates. Using equation 2.6 as a reference, the hydrodynamic time was varied to change the volume of sample withdrawn. The sample volume acquired was determined by removing aliquots from a 300 nL sample of 100 μM N-acetyllactosamine-TMR (β-D-Gal*p*(1→4)-β-D-GlcNAc*p*-TMR; called LacNAc-TMR), and then delivering the aliquots to 3.5 μL of CE running buffer containing a constant concentration (14 μM) of Lewis-Y-TMR (α-D-Fuc*p*(1→2)-β-D-Gal*p*(1→4)[α-D-Fuc*p*-(1→3)]-β-D-GlcNAc*p*-TMR; called Le^Y-TMR). The Le^Y-TMR and LacNAc-TMR were separated by CE-LIF and the relative fluorescence intensity was measured to quantify the amount of LacNAc-TMR delivered. Measurements were made at 15, 30, 40 and 50-second hydrodynamic time intervals after withdrawing the syringe from 200 μL to 320 μL. Using a 12.0 cm capillary with 10.1 μm i.d., the corresponding calculated volumes were 1.2, 2.4, 3.2, 4.0 nL, respectively. All

samples were analyzed in triplicate. Sample electropherograms for the delivery of LacNAc-TMR to CE running buffer containing Le^y-TMR internal standard at various hydrodynamic times are given in Figure 2.2. As can be seen in Figure 2.2e), when the capillary is inserted into the LacNAc solution, some LacNAc is withdrawn even without changing the pressure on the Hamilton syringe. This phenomena, called spontaneous or ubiquitous injection, was observed in other studies involving small volume manipulations.[28] In order to correct for this, blank measurements were conducted by immersing the nanopipettor tip into the LacNAc sample vessel without changing the syringe pressure (without aspiration). This data is summarized in Table 2.1. It was found that the amount of LacNAc withdrawn for the blank measurements did not vary significantly with the length of time the capillary was left in the solution. By comparison to a micropipette it was found that the blank correction was found to vary between different capillaries and ranged from 0.3 nL to 0.7 nL.

Linear regression equations were determined for the sample and blank aliquots for the linear volume delivery experiment. The blank regression line was subtracted from the sample regression line and relative standard deviations were determined from the replicate measurements. After correction with the blank measurements, the amount of LacNAc delivered was linear with the hydrodynamic time as illustrated in Figure 2.3. This is consistent with equation 2.6. Without any correction the linear fit had a non-zero intercept. However, with blank correction the nanopipettor possesses a zero y-intercept, which implied that a constant amount of analyte is introduced when the capillary is submerged in the sample solution.

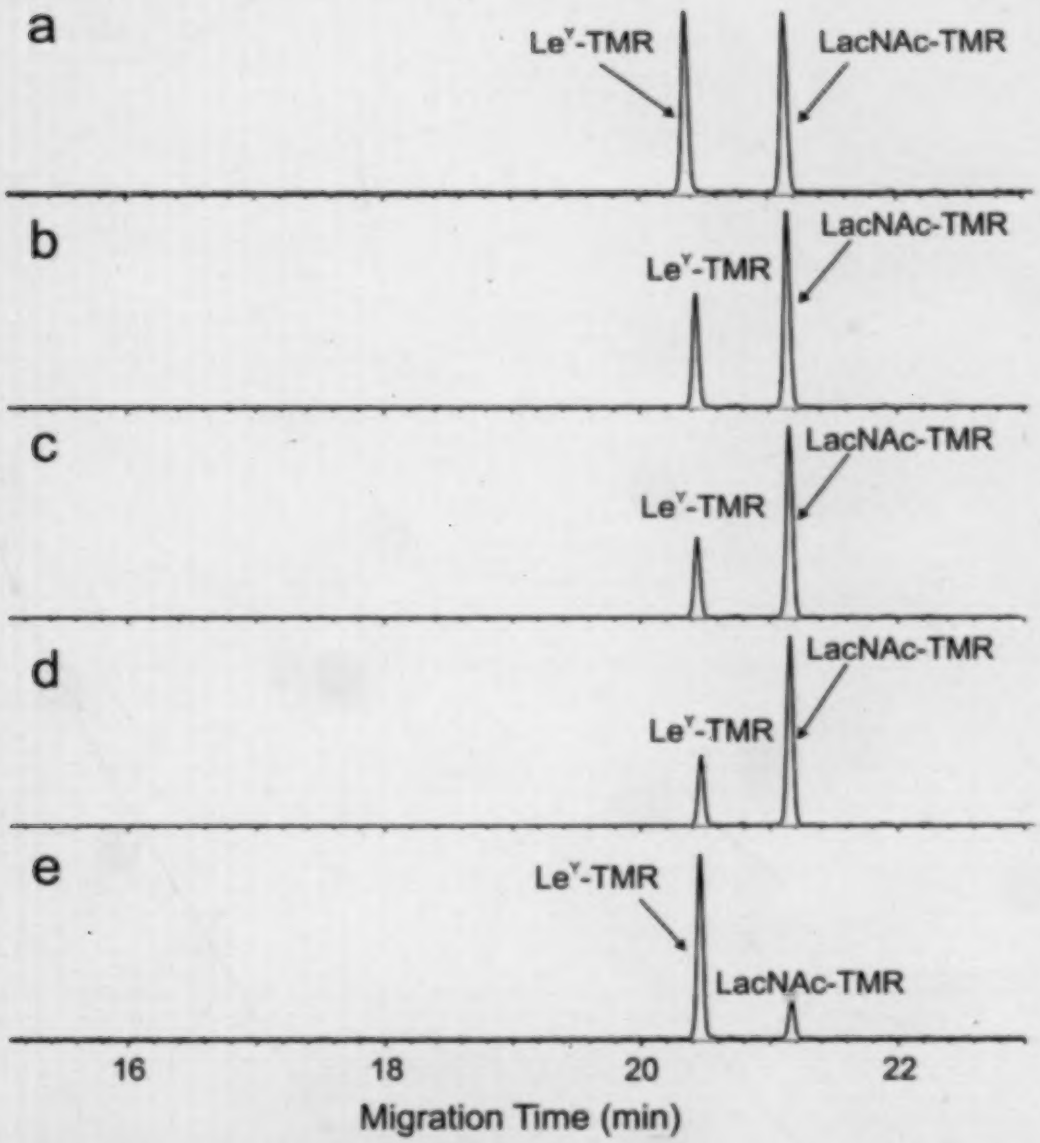

Figure 2.2 Representative electropherograms of solutions containing a Le^{Y}-TMR internal standard in CE running buffer. To each solution LacNAc-TMR was added using the nanopipettor, varying the amount of time the nanopipettor was left in the LacNAc-TMR solutions from (a) 15 s, (b) 30 s, (c) 40 s, and (d) 50 s. (e) Blank measurements, in which no volume was withdrawn on the Hamilton syringe, were also carried out to account for any spontaneous injection.[28]

Table 2.1 Linear Volume Delivery of LacNAc-TMR to Le^Y-TMR using the nanopipettor and the corresponding theoretical value calculated from eq 2.6. The average relative fluorescence intensity represents the ratio in the measured fluorescence intensity of Le^Y-TMR and LacNAc-TMR. The blank relative fluorescence was subtracted from the all measurements.

Hydrodynamic Time (s)	Calculated Delivery Volume (nL)	Average Relative Fluorescence	Relative Standard Deviation of Intensity Ratio
15	1.2	0.7	10%
30	2.4	1.4	5%
40	3.2	1.9	5%
50	4.0	2.33	2%

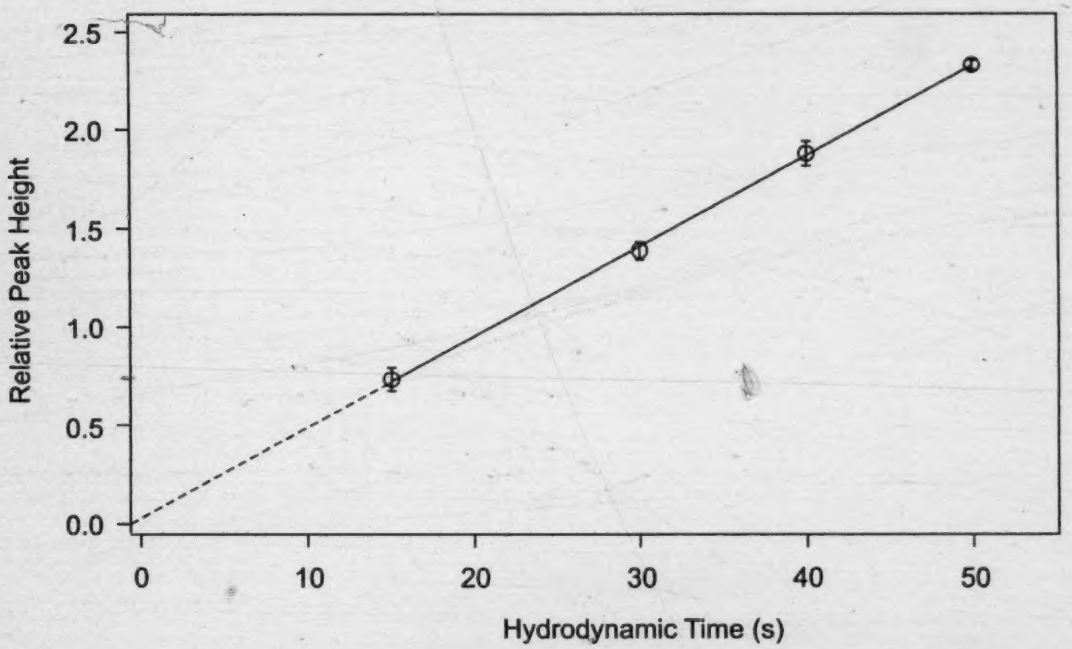

Figure 2.3 Linear volume delivery of LacNAc-TMR to samples containing a constant concentration of Le^Y-TMR using the nanopipettor. Blank measurements were subtracted from each aliquot. Aliquots were collected using a volume displacement of 200 µL to 320 µL on the Hamilton syringe. Samples were analysed in triplicate. Regression analysis yielded a y-intercept of 0.03 ± .03 and a r^2 value of 0.99 ± 0.02.

The linear relationship between hydrodynamic time and aliquot volume allows the nanopipettor to be tuned over a range of nL sized aliquots, thus making it amenable to small scale reaction sampling. The nanopipettor can also be used for quantitative linear volume delivery. The actual volume delivered was calculated by carrying out a study comparing the nanopipettor delivery volume to a dilution using a standard micropipettor. Using a 10 μm i.d. capillary, withdrawing the Hamilton syringe plunger from 300 μL to 600 μL, and a hydrodynamic time of 35 s the theoretical volume predicted form eq 2.6 is 3.6 nL. After blank correction, the experimentally determined volume was 3.4 nL. This suggests that eq 2.6 allows a reasonable estimate of the aliquot volume, within 5.6 % of the actual volume. Thus calibration using a standard micropipette allows quantitative nL sized volume manipulation.

2.3.2 Experimental Challenges: Differential Elution

One of the short-comings that arise from using an uncoated fused silica capillary to aspirate the sample is that sample components with different polarities and charges adsorb to the fused silica walls differentially. As a result, the eluted aliquot may not have the same composition as the source sample. This effect is more problematic at lower substrate concentrations and depends on the nature of the analytes being manipulated.

In order to minimize the problem of differential elution, the substrate concentration and washing solvent were optimized and standardized. For the case of the oligosaccharide used in this study, it was found that a 100 mM phosphate buffer at pH 7.0 was sufficient to minimize differential elution in our system. This was confirmed by using the nanopipettor to transfer a sample from a standard of known composition for all

substrates and products used in these experiments (data not shown). The use of other solvents, salts, mild detergents or capillary coatings can also be optimized to reduce the effect of differential elution.

Substrate concentration is the other factor that can be optimized. If the substrate concentration is too low, most of the substrate and product molecules in an aliquot will adsorb to the fused silica capillary. To avoid this problem, a substrate concentration in the micromolar range was used. Furthermore, very small concentrations of product may not be quantitatively representative of the sample for the same reasons. However, it was found that differential elution was not a significant problem in these experiments.

2.3.3 Monitoring β-galactosidase Activity using the Nanopipettor

The nanopipettor has been shown capable of reproducible and tunable nL sampling, thus making it well suited to small-scale reaction sampling. To demonstrate this, the nanopipettor was used to monitor a small volume enzyme assay of β-galactosidase. This enzyme hydrolyses β-galactosidic bonds in β-linked carbohydrates. It was used to hydrolyse LacNAc-TMR to N-acetylglucosamine-TMR (GlcNAc-TMR) and a free galactose. Reaction mixtures consisted of 490 μU/μL of β-galactosidase, 78.5 mM sodium phosphate buffer pH 7.0, 625 μM LacNAc-TMR, and 1/150 protease inhibitor tablet in a final volume of 7.5 μL. Aliquots were sampled with the nanopipettor and by serial dilution with a 2 μL pipetman (Gilson) at 15-minute intervals. Aliquots of 4.25 nL were sampled with the nanopipettor and delivered to 3.50 μL of CE running buffer – a 1:823 dilution. Using the pipetman, aliquots of 0.50 μL were sampled and serial diluted in two steps to achieved a 1:980 dilution. A concentration of 178.6 nM of Le^Y-TMR was

maintained in the delivery solutions to be used as an internal standard. Samples were analyzed by CE-LIF. The sample aliquot acquired from the nanopipettor had good agreement in composition to the serial diluted standards. In Figure 2.4, the percent conversion over time for the serial dilution method, the nanopipettor and the nanopipettor corrected for differential elution is given. The differential elution correction is a linear correction determined from monitoring the aliquot composition of the nanopipettor as compared to a standard with known composition for the products and reactants – a correction to account for this small differential elution effect.

The nanopipettor aliquot compositions are within quantitative range of the serial dilution standards. Other substrates may have greater deviation between the nanopipettor aliquot composition and the serial diluted standard – this is particularly true for samples that have large differences in polarity or charge between the reactant and product. Precautions can be taken to minimize differential elution or linear corrections can be used to minimize this effect. Regardless, optimization is required to ensure the best quantitative yields from the nanopipettor.

2.4 Conclusions

This work describes the development of a cost-effective and quantitative nanopipettor that is well suited to small-scale reaction sampling. A sampling protocol was developed, and quantitative results were obtained for linear volume delivery with the nanopipettor. It was demonstrated that using eq 2.6, the aliquot volume can be predicted based on the nanopipettor parameters. A standard enzyme reaction, using β-galactosidase, was used to demonstrate the use of the nanopipettor for monitoring small scale reactions.

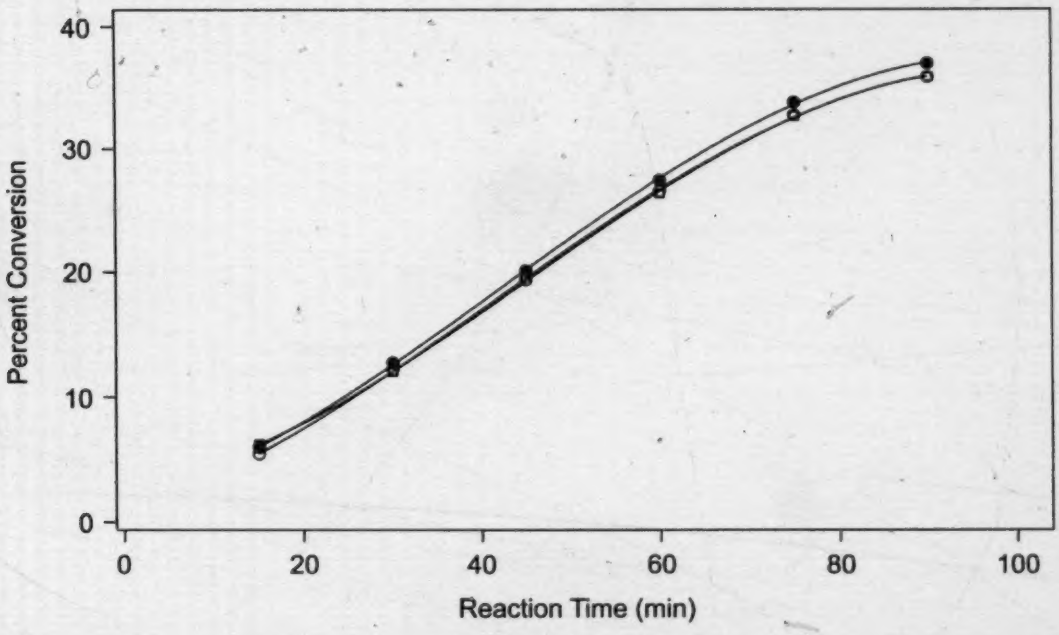

Figure 2.4 Time course of LacNAc hydrolysis by β-galactosidase using a standard serial dilution (▫), the nanopipettor (•), and the nanopipettor after correcting for differential elution (◦).

This can be extended to other small-scale chemical or biochemical reaction sampling. For example, the nanopipettor could be used to monitor lysates from single cells or small tissue samples. This technique will be used in the following chapter in the development of a novel single cell enzyme assay.

2.5 Literature Cited

(1) Tong, W.; Yeung, E. S. *Journal of Chromatography B* **1997**, *689*, 321-325.

(2) Krylov, S. N.; Zhang, Z. R.; Chan, N. W. C.; Arriaga, E.; Palcic, M. M.; Dovichi, N. J. *Cytometry* **1999**, *37*, 14-20.

(3) Krylov, S. N.; Arriaga, E.; Zhang, Z. R.; Chan, N. W. C.; Palcic, M. M.; Dovichi, N. J. *Journal of Chromatography B* **2000**, *741*, 31-35.

(4) Hu, S.; Lee, R.; Zhang, Z.; Krylov, S. N.; Dovichi, N. J. *Journal of Chromatography B-Analytical Technologies in the Biomedical and Life Sciences* **2001**, *752*, 307-310.

(5) Chen, S. J.; Lillard, S. J. *Analytical Chemistry* **2001**, *73*, 111-118.

(6) Anderson, A. B.; Ciriacks, C. M.; Fuller, K. M.; Arriaga, E. A. *Analytical Chemistry* **2003**, *75*, 8-15.

(7) Paegel, B. M.; Yeung, S. H. I.; Mathies, R. A. *Analytical Chemistry* **2002**, *74*, 5092-5098.

(8) Luzzi, V.; Lee, C. L.; Allbritton, N. L. *Analytical Chemistry* **1997**, *69*, 4761-4767.

(9) Huang, Y. P.; Mechref, Y.; Novotny, M. V. *Analytical Chemistry* **2001**, *73*, 6063-6069.

(10) Hu, S.; Dovichi, N. J. *Analytical Chemistry* **2002**, *74*, 2833-2850.

(11) Cheng, Y. F.; Dovichi, N. J. *Science* **1988**, *242*, 562-564.

(12) Chen, D. Y.; Swerdlow, H. P.; Harke, H. R.; Zhang, J. Z.; Dovichi, N. J. *Journal of Chromatography* **1991**, *559*, 237-246.

(13) Zhang, R. Z.; Xu, X. H.; Chen, T. B.; Li, L.; Rao, P. F. *Analytical Biochemistry* **2000**, *280*, 286-290.

(14) Snow, D. M.; Shaper, J. H.; Shaper, N. L.; Hart, G. W. *Analytical Biochemistry* **1999**, *271*, 36-42.

(15) Sims, C. E.; Meredith, G. D.; Krasieva, T. B.; Berns, M. W.; Tromberg, B. J.; Allbritton, N. L. *Analytical Chemistry* **1998**, *70*, 4570-4577.

(16) Ma, L. J.; Gong, X. Y.; Yeung, E. S. *Analytical Chemistry* **2000**, *72*, 3383-3387.

(17) Le, X. C.; Tan, W.; Scaman, C. H.; Szpacenko, A.; Arriaga, E.; Zhang, Y. N.; Dovichi, N. J.; Hindsgaul, O.; Palcic, M. M. *Glycobiology* **1999**, *9*, 219-225.

(18) Krylov, S. N.; Dovichi, N. J. *Electrophoresis* **2000**, *21*, 767-773.

(19) Franklin, K.; Layfield, R.; Landon, M.; Ramage, R.; Brown, A.; Love, S.; Muir, T.; Urquhart, K.; Bownes, M.; Mayer, R. J. *Analytical Biochemistry* **1997**, *247*, 305-309.

(20) Bao, J. M.; Regnier, F. E. *Journal of Chromatography* **1992**, *608*, 217-224.

(21) Yoshimoto, Y.; Shibukawa, A.; Sasagawa, H.; Nitta, S.; Nakagawa, T. *Journal of Pharmaceutical and Biomedical Analysis* **1995**, *13*, 483-488.

(22) Zhang, B. Y.; Chan, N.; Schriemer, D. C.; Palcic, M. M.; Hindsgaul, O. *Glycobiology* **1999**, *9*, 1103-1103.

(23) Zhao, J. Y.; Dovichi, N. J.; Hindsgaul, O.; Gosselin, S.; Palcic, M. M. *Glycobiology* **1994**, *4*, 239-242.

(24) Scaman, C. H.; Hindsgaul, O.; Palcic, M. M.; Srivastava, O. P. *Carbohydrate Research* **1996**, *296*, 203-213.

(25) Landers, J. P. *Handbook of Capillary Electrophoresis*, 2 ed.; CRC Press: New York, 1997.

(26) Chen, D. Y.; Dovichi, N. J. *Journal of Chromatography B-Biomedical Applications* **1994**, *657*, 265-269.

(27) Zhao, J. Y.; Chen, D. Y.; Dovichi, N. J. *Journal of Chromatography* **1992**, *608*, 117-120.

(28) Fishman, H. A.; Amudi, N. M.; Lee, T. T.; Scheller, R. H.; Zare, R. N. *Analytical Chemistry* **1994**, *66*, 2318-2329.

Chapter 3

Multiple Sampling in Single Cell Enzyme Assays using Capillary Electrophoresis with Laser-induced Fluorescence Detection[1]

3.1 Introduction

Improvements in the sensitivity of biochemical methods have resulted in an increase in research devoted to single cell analysis over the past decade. An important aspect of this work is the ability to examine the heterogeneity of complex biological systems. These studies may advance our knowledge of various diseases, including cancer, which manifest themselves in a heterogeneous manner.[1] Furthermore, minimal sample size requirements are well suited to medical research and deleterious gene knockout experiments where tissue or tumor samples may be limited. Analysing biological systems at their most basic level will lead to better understanding of various biological processes such as cellular communication, differentiation and metabolism.

Of the available single cell analytical techniques, flow cytometry is the most established.[2] Although this high-throughput method is capable of analyzing thousands of cells per minute,[3,4] the information available is restricted to a limited number of parameters. While not as rapid, capillary electrophoresis (CE) can be applied to single cell analysis thus permitting a more detailed study of a single cell. Jorgenson and co-workers first employed single cell CE coupled with electrochemical detection to analyse

---

1 A version of this Chapter has been published: Shoemaker, G.K.; Lorieau, J.; Lau, L.H.; Gillmor, C.S.; Palcic, M.M. *Anal. Chem.* **2005**, 77, 3132-3137.

naphthalene-2,3-dicarbaldehyde (NDA)-labeled amino acids from the land snail neuron.[5] The introduction of laser induced fluorescence (LIF) provided another viable detection system for single cell analysis, allowing various analytes to be quantified at the attomolar level.[6,7] This led to a great deal of single cell analysis using CE including determination of the insulin content in pancreatic cells,[8] single cell RNA synthesis,[9] protein mass determination and expression levels in human cancer cells,[10] and the amino acid content of human erythrocytes.[11] Work in this field extends into the subcellular domain, as individual organelles such as mitochondria can be analysed.[12,13]

While the chemical contents of a single cell are an interesting target for analysis, many groups have taken a functional approach by assaying the enzymes from single cells such as lactate dehydrogenase,[14] protein kinases[15-17] and various carbohydrate modifying enzymes.[18,19] Some of these analyses involved incubating cells with fluorescent substrate followed by loading on to a CE capillary where the cell was lysed and its contents analysed. Other studies performed single cell enzyme assays by loading individual cells into a capillary containing substrate for the enzyme of interest. Upon introduction into the capillary the cell was lysed releasing its enzymes which initiated product formation. After a certain amount of time the CE voltage was applied and the amount of product was determined using LIF detection. These methods have high sensitivity since they minimize the dilution of cellular contents, but only represent a snapshot of enzyme activity since the entire single cell lysate is consumed in the analysis. Furthermore, it is often problematic to obtain a balance between the pH and buffer components ideal for enzymatic activity and those required by the CE analysis.

The present study aims to develop new methods that improve the flexibility of small-scale analysis and allow repeated sampling of a single cell enzyme reaction. Currently, repeated sampling of single cells has only been employed to study large cell types such as the *Xenopus Laevis* oocyte which is 1 mm in diameter.[20] In this paper enzyme reactions of smaller cells, such as Sf9 and HT29 cells, with a diameter of approximately 15 μm[21] are lysed and repeatedly sampled. The three main challenges in this study were to avoid extensive dilution of the cellular enzymes, to allow reproducible sampling, and to achieve separation and detection of the reaction products. The development of methodology to address these issues is presented here. This includes the fabrication of a micromanipulator to allow transfer of individual cells to nanoliter scale reaction vessels, removal of 5-10 nL aliquots using a nanopipettor,[22] and ultrasensitive analysis using CE-LIF.

This Chapter describes the work on three carbohydrate-modifying enzymes, α-glucosidase I, α-glucosidase II and α1,3-N-acetylgalactosaminyltransferase (GTA). α-glucosidase I and II are oligosaccharide hydrolyzing enzymes that are a part of the protein folding quality control machinery of the endoplasmic reticulum.[23] The third enzyme, GTA, is a blood group enzyme which synthesizes the specific A antigen that is present on cell surfaces.[24-26] The utility of the method in other small scale analyses is demonstrated in the study of α-glucosidase I activity in single *Arabidopsis* embryos.[27] Mutant and wild type embryos were compared with respect to their α-glucosidase I activity to functionally confirm the deletion of the α-glucosidase I encoding *KNOPF* gene.

3.2 Experimental

3.2.1 Materials and Reagents

To allow fluorescence detection, carbohydrates were linked to a tetramethylrhodamine (TMR) tag as described elsewhere.[28,29] CE Running buffer was a 10 mM sodium phosphate buffer (pH 9.3) (Sigma) composed of 50 mM sodium dodecyl sulfate (Caledon), 10 mM phenyl boronic acid (Sigma), and 2.5 mM sodium tetraborate (Fisher). In the analysis of *Arabidopsis* embryos, 10% dioxane (Caledon, reagent grade) was added to the running buffer to enhance the separation of the four carbohydrates in the reaction aliquots. Fused-silica capillaries were purchased uncoated from Polymicro Technologies.

3.2.2 Cell Culture

Spodoptera frugiperda (Sf9) cells were grown suspended in Sf-900 serum-free media (Invitrogen) at 27°C with shaking at 120 rpm. The cell solution was counted and diluted to a concentration of 1.0×10^6 cells/mL with fresh media every 2-3 days and immediately prior to analysis. From this cell solution, a 1 mL aliquot was removed and washed 5 times in fresh Sf9 media. An aliquot of these cells was placed in a 0.1% trypan blue solution. From this aliquot, cell density and viability were determined using a Bright-line hemocytometer (Hausser Scientific, Horshap, PA) via trypan blue exclusion before and after the washing procedure to ensure cells were not being lysed. The washed cell sample was diluted to a final concentration of 2.5×10^4 cells/mL for single cell manipulation. HT29 cells (human colon adenocarcinoma, American Type Culture Collection) were also used in this experiment and were grown in Dulbecco's Modified

Eagle's Medium (Invitrogen) with 10% fetal calf serum. The culture was passaged twice a week and was grown at 37°C in a 7% CO_2 atmosphere. For analysis the cells were trypsinized and washed in MOPS buffered saline (MBS) prior to manipulation.

3.2.3 Single Cell Manipulation

A micromanipulator was fabricated at the University of Alberta to enable the isolation of a single cell (Figure 3.1). It consisted of three stepping motors (Applied Motor Products Inc., Watsonville, CA) attached to three translational stages (Newport, Irvine, CA). The stepping motors were connected to a control panel which allowed independent adjustment of the three stages in the x, y, and z planes. A capillary holder was mounted onto the translational stages, thus allowing a vertically oriented capillary to be moved in three dimensions. An LED attached to the capillary holder illuminated the viewing area. To withdraw a cell, the distal end of the capillary was connected to a 50 μL Hamilton syringe using a zero dead volume union (Upchurch Scientific). The syringe plunger was attached to a fourth stepping motor with a variable power source allowing the plunger to be withdrawn at different rates. The entire setup was mounted on an inverted microscope to permit visualization of cell manipulation.

To avoid cellular adhesion to the micromanipulator capillary or microscope slide, these surfaces were coated with a hydrophilic polymer, poly(2-hydroxyethyl) methacrylate (PHEMA). It was previously demonstrated that this coating is biocompatible and able to reduce cellular adhesion to the glass surface of the microscope slide.[30] The capillary coating procedure consisted of a 5 minute rinse with 100 mM NaOH, a 10 minute rinse with Milli-Q water, and a 20 minute rinse with a 7.5% PHEMA

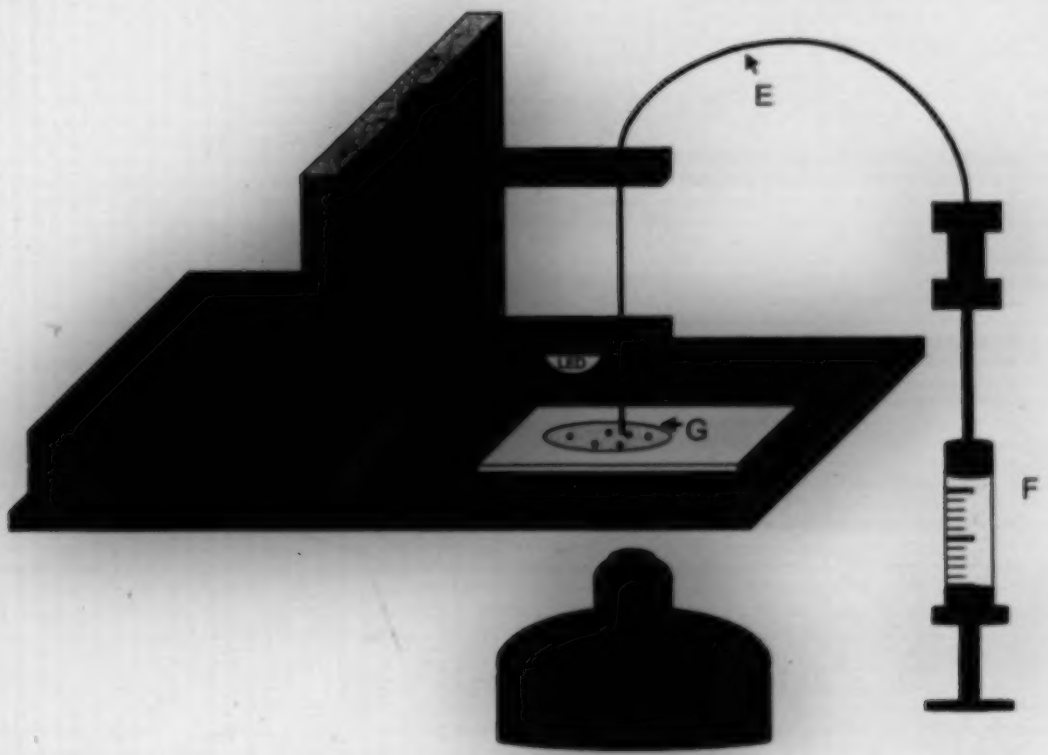

Figure 3.1 Micromanipulator schematic. (A), (B), (C) x,y,z translational stages which are attached to three stepping motors (not shown). A capillary holder (D) holds the vertically oriented capillary (E). One end of the capillary was attached to a 50 μL Hamilton syringe (F) to allow withdrawal of single cells (G) from a PHEMA coated microscope slide.

solution in methoxyethanol. Air was pushed through the capillary for 10 minutes and it was left to dry overnight. Before use, the capillary was rinsed with Dulbecco's modified phosphate buffered saline (PBS) for 15 minutes or with MBS for the GTA assays.

To isolate a single cell, a 7 μL drop of the washed and diluted Sf9 cells was placed on a PHEMA-coated microscope slide using a 10 μL pipetman (Gilson). Figure 3.2 is representative view through the microscope objective of the sampling capillary immersed in solution of Sf9 cells. For single cell isolation, the micromanipulator capillary was positioned above a cell and the syringe was displaced at a rate of 0.24 μL/min until the cell moved into the capillary (typically ≈3-5 seconds). This corresponded to a volume displacement on the Hamilton syringe of 12-20 nL. The capillary was then moved to a fresh 7 μL drop of PBS and the cell was expelled into the drop. The capillary was then moved away from the cell, and the contents were flushed out of the capillary at a rate of 0.94 μL/minute for 5 seconds. This single cell washing step was found to further reduce the contamination of free enzyme from the cell suspension solution.

The cell was redrawn into the capillary along with a 12 nL plug of fresh PBS which was withdrawn to ensure the cell was sufficiently contained within the sampling capillary to prevent cell loss during transfer. The capillary tip was rinsed twice in fresh drops of PBS and then inserted into a vessel containing 200 nL of reaction mixture. The cell was expelled by depressing the syringe plunger at a rate of 0.96 μL/minute for 5 seconds, corresponding to a volume of 80 nL. The capillary was left in the reaction vessel for an additional 10 seconds to ensure cell expulsion. The reaction vessel consisted of a 2-200 μL gel loading tip (Fisher) that was heat sealed at the narrow end of

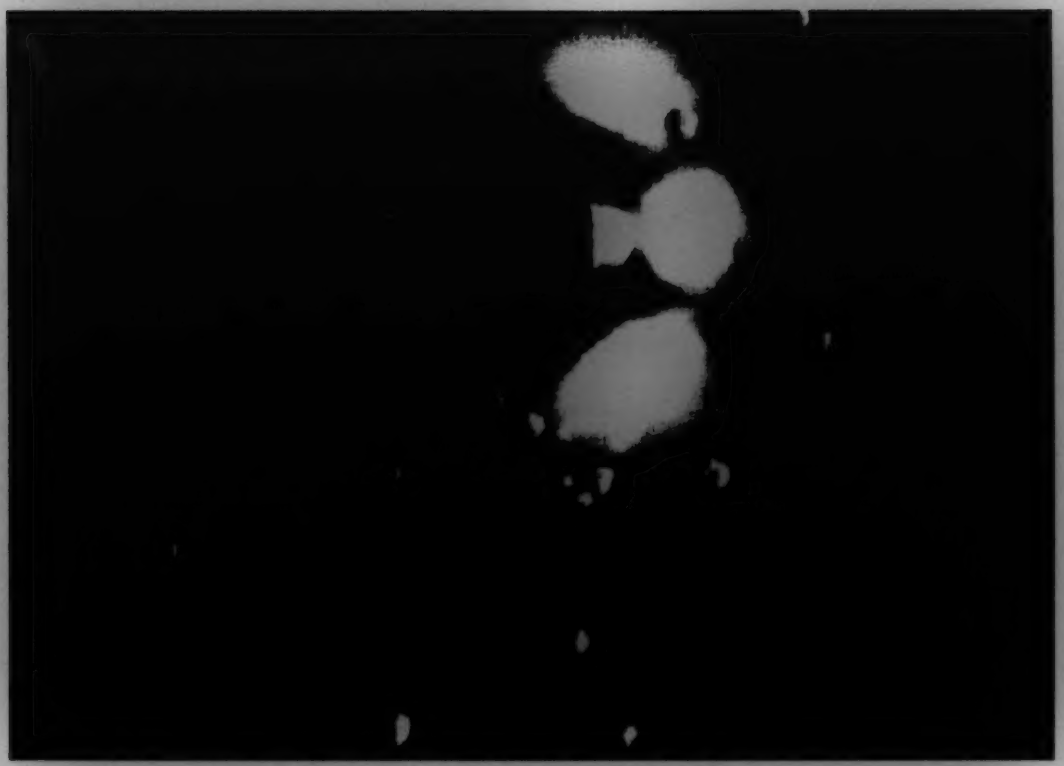

Figure 3.2 View through the microscope objective of the micromanipulator sampling capillary emerged in a solution of Sf9 cells.

the tip. The narrow bore of the gel loading tip was ideal for removing aliquots from this 280 nL reaction. After each manipulation, the capillary was rinsed thoroughly with PBS. Control assays consisted of performing the exact procedure as outlined above in the absence of cells; thus only the solution surrounding the cells was assayed.

3.2.4 Single Cell Enzyme Assays

Quantification of α-glucosidase II activity was determined by measuring the hydrolysis of the synthetic substrate α-D-Glc*p*-(1→3)-α-Glc*p*-O-TMR (DG-TMR) to the monosaccharide α-D-Glc*p*-O-TMR (MG-TMR). The MG-TMR can be further hydrolysed releasing the TMR-linker arm (TMR) by α-glucosidase II but this was not observed on a significant basis in the analysis. The reason for this was due to the fact that DG-TMR is the preferred substrate for α-glucosidase II and it was present at a higher concentration in the early time points of the reaction when the reaction was sampled. The reaction mixture consisted of 50 μM DG-TMR substrate, 0.1% Triton X100 for cell lysis, and protease inhibitors (Roche, 1 tablet/ 20 mL) to avoid enzymatic degradation. The solution was buffered at pH 7.0 using 100 mM sodium phosphate buffer.

To each reaction vessel, 200 nL of the reaction buffer was added. After addition of a cell the vessel was mixed *via* mild agitation and placed in a 37°C incubator. A recently developed nanopipettor, capable of nL sampling,[22] was used to sample the reaction. The nanopipettor consists of a Hamilton syringe connected through a zero dead volume union to a fused silica capillary with a 10 μm inner-diameter. A 5 nL aliquot of the reaction mixture was removed and added to 3.5 μL of CE-running buffer. Micellar Electrokinetic Chromatography (MEKC) was employed to separate the substrate from the

product carbohydrates and they were detected using LIF. The relative fluorescent signals of DG-TMR and MG-TMR were used to quantify α-glucosidase II activity.

In order to test the sensitivity of this approach, the above methods were applied in the analysis of a low abundance enzyme, GTA, from single HT29 adenocarcinoma cells. This enzyme catalyzes the transfer of a monosaccharide, from the nucleotide donor UDP-N-acetylgalactosamine (GalNAc), to the acceptor α-L-Fuc*p*-(1→2)-β-D-Gal*p*-(1→4)-β-GlcNAc*p*-O-TMR forming α-D-GalNAc*p*-(1→3)[α-L-Fuc*p*-(1→2)]-β-D-Gal*p*-(1→4)-β-D-GlcNAc*p*-O-TMR (A antigen). The reaction buffer consisted of 100 μM TMR labeled acceptor, 100 μM UDP-GalNAc donor, 20 mM $MnCl_2$, and protease inhibitor solution (6 X recommended concentration) in a 50 mM MOPS buffer (pH 7.0). Using the micromanipulator, individual cells were added into 100 nL aliquots of the GTA reaction buffer and incubated at 37°C. Aliquots of 20 nL were removed with the nanopipettor after 24 and 52 hours of incubation and analysed by CE-LIF to determine GTA activity.

3.2.5 *Arabidopsis* Embryo Analysis

Single *Arabidopsis* embryos, both wild type and those lacking the α-glucosidase I encoding *KNOPF* gene, were grown as described previously[27] and re-suspended in 0.5 μL of reaction buffer containing 90 μM α-D-Glc*p*-(1→2)-α-D-Glc*p*-(1→3)-α-D-Glc*p*-O-TMR (TG-TMR) substrate, protease inhibitors (1 tablet / 50 mL), and 0.1 % Triton X-100 in 100 mM sodium phosphate buffer at pH 7. The product of the α-glucosidase I reaction is DG-TMR, which is in turn hydrolysed by α-glucosidase II to MG-TMR. Over time α-glucosidase II also hydrolyses the linkage between the TMR label and the remaining monoglucose forming free TMR bound to the linker-arm (TMR). Thus since

α-glucosidase II is present at higher expression levels than α-glucosidase I, any DG-TMR produced by α-glucosidase I was expected to be completely hydrolysed to the TMR-linker arm species.

A second enzyme common to the mutant and wild type embryos, β-galactosidase, was simultaneously assayed to confirm that the mutants were viable. Thus 40 μM of the β-galactosidase substrate, α-D-Gal*p*-(1→4)-β-D-GlcNAc*p*-TMR (LacNAc-TMR, called LN-TMR) was also added to the incubation mixture. The detectable product of the β-galactosidase reaction was β-D-GlcNAc*p*-TMR (GN-TMR). The mixture was incubated at 37°C and after 24 hours a 20 nL aliquot was removed using the nanopipettor. This aliquot was added to 5 μL of CE running buffer and analysed using CE-LIF. The details of the percent conversion calculation for the two enzyme reactions is described elsewhere.[31]

3.2.6 Capillary Electrophoresis with Laser Induced Fluorescence

The CE-LIF instrument was locally constructed and has been described previously.[32-34] Electrophoretic potentials were achieved with a CZE100R high voltage power supply (Spellman, Plainview, NY) using an applied potential of 400 V/cm. Separations were conducted over a 35 cm long capillary with 10 μm i.d. and 150 μm o.d. Post-capillary detection was achieved by focusing a 5 mW Helium-Neon laser (Melles Griot, Nepean, Canada) with a wavelength of 543.5 nm on the eluting tip of the capillary. CE running buffer formed a sheath flow in the quartz cuvette holding the capillary tip. Fluorescence was collected at a right angle from excitation, focused with a 60X, 0.7 NA microscope objective and spectrally filtered with a 580DF27 band-pass filter (Omega

Optical, Brattleboro, VT). The fluorescence was focused onto an iris and detected with a R1477 photomultiplier tube, operating at 1000V (Hamamatsu, Middlesex, NJ). Data was digitized with a NB-MIO-16x data acquisition board (National Instruments, Austin, TX) and analyzed with a Macintosh Computer using LabView software (National Instruments, Austin, TX) and Igor Pro version 2.04.

3.3 Results and Discussion

3.3.1 Optimization of Sf9 Cell Manipulation

Cell lysis represents a potential problem in single cell analysis since it leads to increased contamination of cellular components in the surrounding solution, thus skewing the single cell signal[35] and, in the case of α-glucosidase II assays, leading to an elevated background activity. The combination of gentle centrifugation (800 rpm for 5 min) and the use of Sf-900 II SFM media as the wash solution was found to be optimal in reducing cell lysis during cell washing. The cell population was counted before and after washing. With the use of this gentle washing procedure, it was found that there was only a minimal change in cell density and no change in cell viability. Cells were also found to be more susceptible to lysis with age, therefore cells of a consistent passage window (15-20 passages) were used for analysis.

Prior to injection of a single cell into the reaction vessel, a final individual cell washing was carried out by expelling the cell into a fresh drop of PBS. Control experiments were carried out to determine the amount of cell suspension solution that is added along with a single cell to the reaction chamber and to examine the effectiveness of the individual cell washing step. The total volume of solution added during the injection

of a cell into the reaction vessel was also determined by using a standard solution of LN-TMR. The capillary was filled with LN-TMR and then expelled into CE running buffer using the same conditions as for cell injection. By comparison to a calibration curve it was found that the total volume added was 80 ± 10 nL. It is also important to quantify what volume of the original cell suspension solution is included in this 80 nL total volume. To determine this volume, a standard spike of LN-TMR was added to the cell suspension just prior to cell manipulation. A cell was withdrawn, washed, and expelled exactly as before. Again by comparing the LN-TMR peak to a calibration curve the amount of cell suspension solution was determined to be 3.9 ± 0.8 nL. This demonstrates that the individual cell washing step is quite effective at reducing the amount of cell suspension solution that is added to the reaction vessels since it makes up only 1.4% of the final reaction volume.

3.3.2 Single Cell α-glucosidase II Assay

Twenty individual Sf9 cells were examined for α-glucosidase II activity. After 4.5 hours the reaction vessels were frozen at -20°C to quench the reaction. Each cell was analysed in triplicate by removing three aliquots of 5 nL with the nanopipettor followed by CE-LIF analysis. Figure 3.3 is a sample electropherogram of an α-glucosidase II single cell reaction aliquot and a control assay consisting of the solution surrounding the cells only. The results for the twenty cells and two control assays are presented in Figure 3.4. All cells exhibited enzyme activity significantly larger than the control assays, illustrating the reproducibility of the cell injection method and the effectiveness of the washing techniques. The Sf9 cells exhibited a large degree of heterogeneity with an

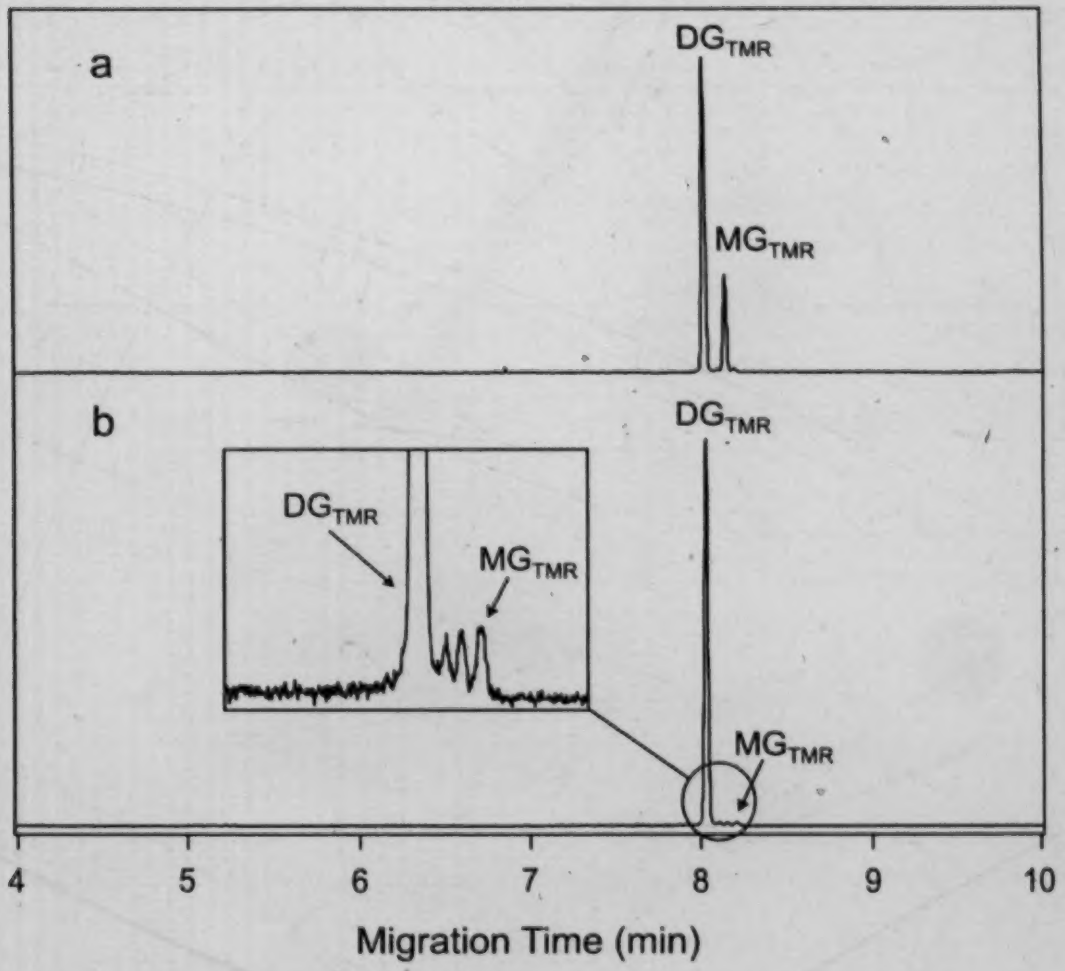

Figure 3.3 Representative electropherograms obtained from the CE-LIF analysis of 5 nL aliquots removed from (a) a single Sf9 cell lysate and (b) a control α-glucosidase II assay after 4.5 h of incubation at 37°C. The inset demonstrates the level of MG product present in the control assay as well as fluorescent impurities in the substrate.

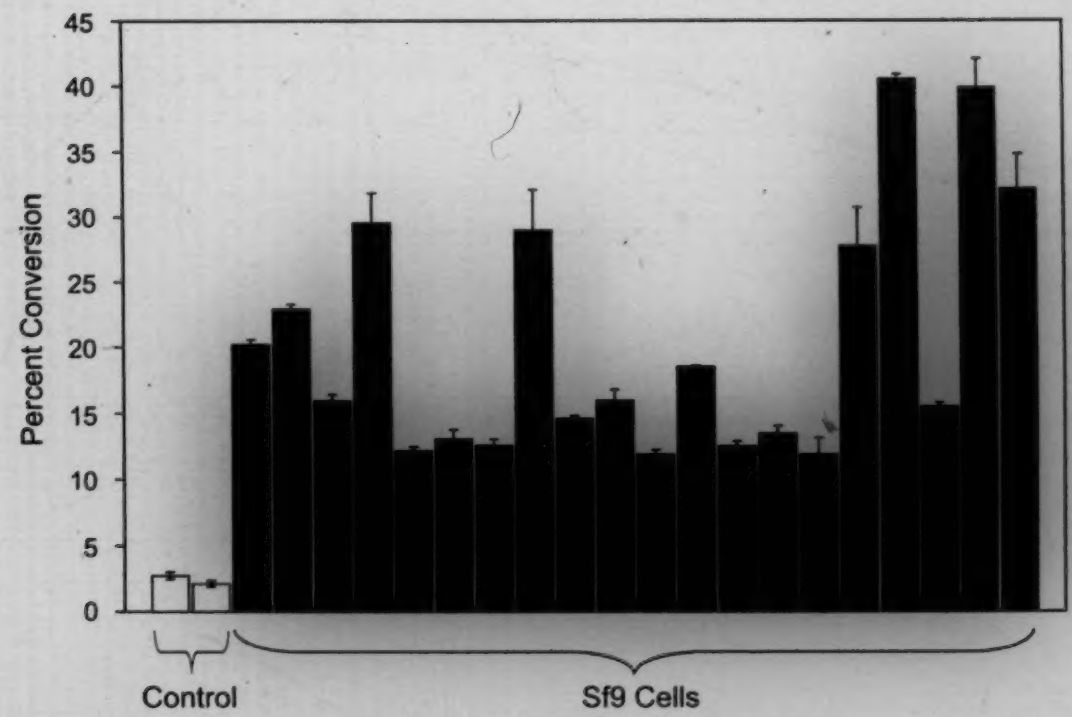

Figure 3.4 Calculated percent conversion of the DG-TMR substrate for 20 individual Sf9 cells and 2 controls after 4.5 h at 37°C. For the 20 Sf9 cells the average activity was found to be 20.9 ± 9.4 %. For each sample, three aliquots were removed and analysed by CE-LIF. The error bars correspond to the standard deviation obtained from this triplicate analysis

average conversion of 20.9 ± 9.4 % after 4.5 hours. Cellular heterogeneity is a common feature of other single cell studies[7,35,36] and has been attributed to differences in cell age[14] and cell cycle.[37] Free enzymes in the surrounding solution could also be a source of heterogeneity. This is unlikely however since it was shown in section 3.3.1 that only 3.9 ± 0.8 nL of the surrounding solution is dispensed into the reaction vessel. Additionally, the control assays displayed minimal activity. This suggests that the surrounding solution was not a significant source of heterogeneity. The possibility of multiple cells being added to the reaction vessels, although unlikely, can also be questioned. In these experiments a cell is visually confirmed to enter the capillary. This cell is expelled into a fresh drop of PBS and is again drawn into the capillary. This double confirmation that only one cell is being manipulated makes it unlikely that multiple cells are being assayed.

It was observed that Sf9 cells are quite variable in size, which is another possible source of this heterogeneity in α-glucosidase II activity. Even if the expression levels, and thus intracellular concentrations, showed little cell to cell variation, larger cells would possess greater activity since they contain a greater quantity of enzyme. Attempts, such as single cell NDA labeling experiments, single-cell PCR and mass spectral analysis (MALDI-TOF), were made to confirm that only one cell was added to each reaction vessel and account for differences in cell size. These methods were unsuccessful, however, due to extensive dilution of cellular contents. Furthermore, the differences in activity may not depend on the quantity of enzyme, but rather the amount of functional enzyme. Further work in this area is needed to gain a better understanding of the basis, and possible effects, of this functional diversity. For example, it would be

interesting to determine whether or not this heterogeneity in α-glucosidase II activity is a general feature by performing single cell assays on other enzymes.

3.3.3 Single Cell α-glucosidase II Reaction Profile

Typically in single cell analysis the sampling process consumes the entire cell. The method described in the present study, however, permits multiple sampling of a single cell lysate and thus more detailed analyses such as the ability to follow a single cell reaction over time. Using the same cell isolation procedure outlined previously, a single Sf9 cell was monitored for α-glucosidase II activity over a period of 24 hours. After 1h, 3h, 5h, and 21h, two aliquots of 5 nL were removed from the single cell reaction using the nanopipettor and analysed by CE-LIF. Sample electropherograms for each time point are given in Figure 3.5. The data is summarized in Figure 3.6, which is a graph of the reaction profile for α-glucosidase II activity from a single Sf9 cell lysate and a control sample. The control consisted of the solution surrounding the cells after washing and thus would reflect the activity of free enzyme in the solution added along with the single cells. After 4.5 hours the conversion for the single cell was 24% and that for the control was 4%. This demonstrates the utility of this technique in metabolic studies of single or small groups of cells.

3.3.4 Analysis of a Low Abundance Enzyme

The methodology has been shown capable of assaying the highly expressed enzyme α-glucosidase II, but analysing a low abundance enzyme like GTA required minimizing cellular dilution to enhance sensitivity. The cell was added to 100 nL of

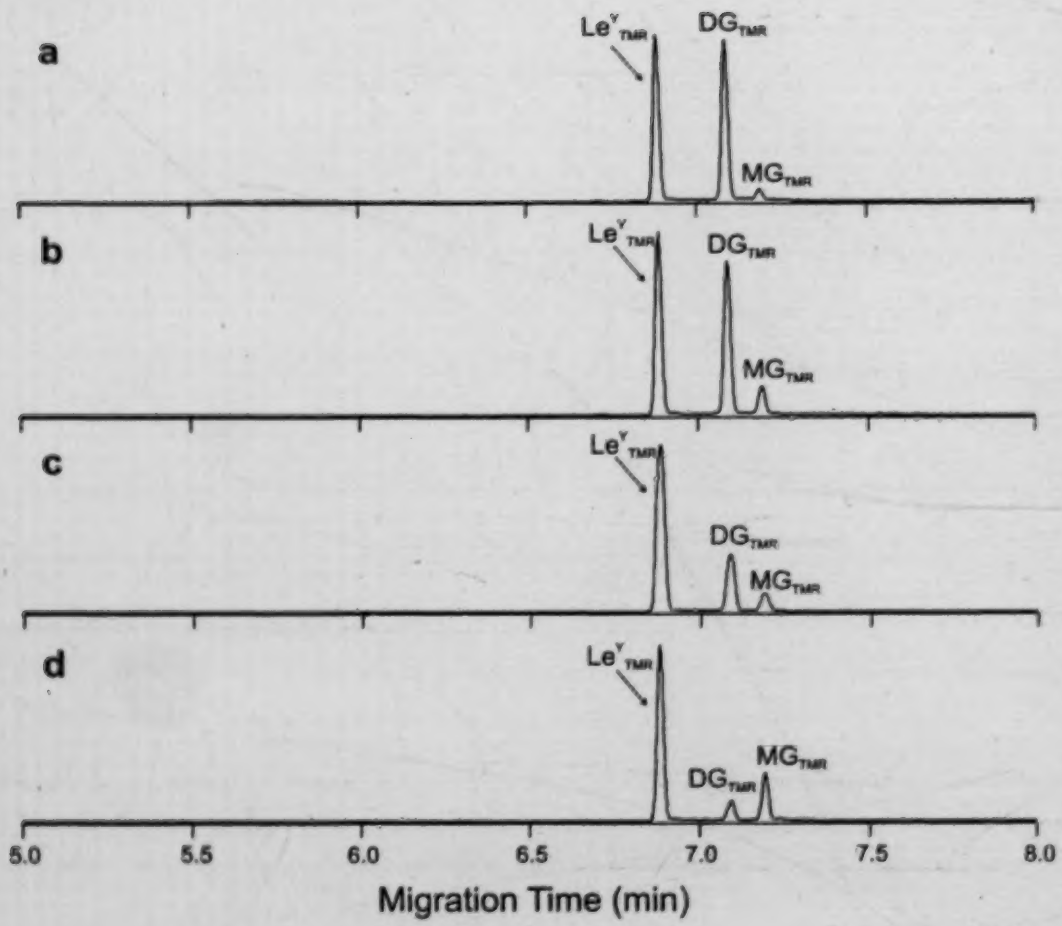

Figure 3.5 Representative electropherograms of aliquots removed from a single Sf9 cell reaction incubated in a 100 mM phosphate buffer (pH 7), 0.1 % Triton X-100, protease inhibitors (Roche, 1 tablet/ 20 mL), and 50 μM DG-TMR substrate. Aliquots were removed after (a) 1h, (b) 3h, (c) 5h, and (d) 21h using the nanipipettor and added to 3.5 μL of CE running buffer containing 0.7 μM Le^Y-TMR internal standard.

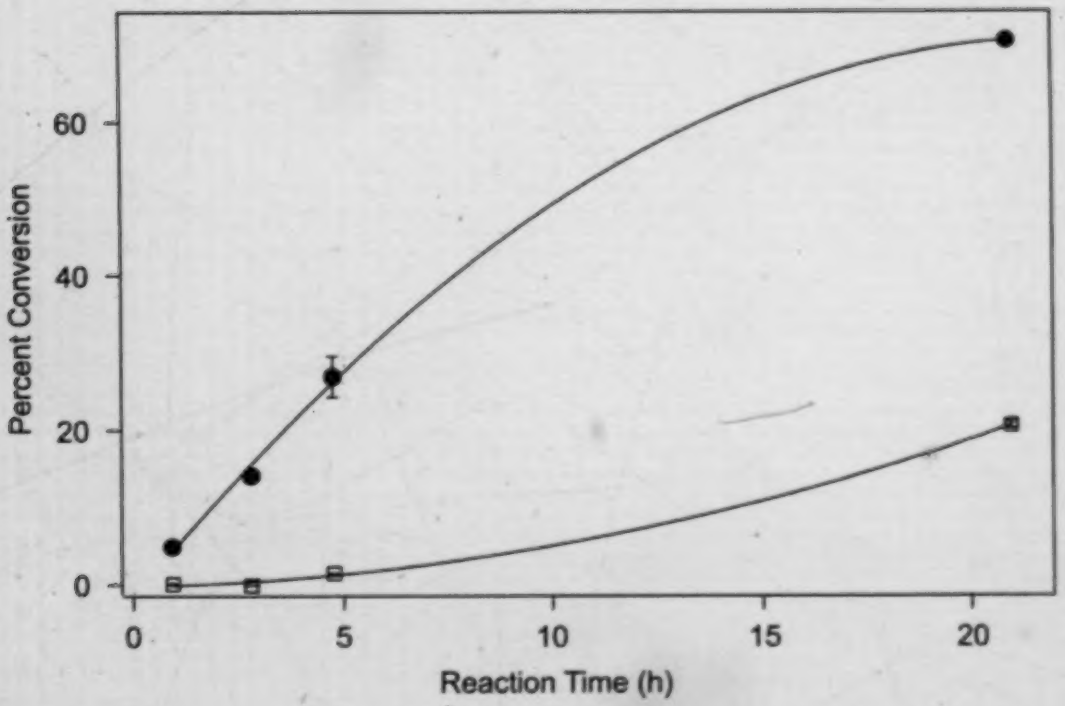

Figure 3.6 Time course illustrating the percent conversion of DG-TMR by α-glucosidase II for a single Sf9 cell (●) and control (□). Each time point was analysed in duplicate by removing two 5 nL aliquots from the reaction mixture.

reaction buffer, instead of 200 nL in the α-glucosidase II assays by using the nanopipettor to dispense 100 nL aliquots. By reducing the extent of cellular dilution by half, it was possible to detect 0.35% conversion of H type II substrate to A antigen product after 24 hours of incubation. Since only part of the single cell reaction was used in the first analysis, another 20 nL sample was removed after 52 hours and was analysed with CE-LIF (Figure 3.7(a)). The enzyme was still active as the percent conversion had increased to 0.81%, demonstrating the robustness of this enzyme. The identity of the A-antigen peak in the electropherograms was confirmed by co-injection of authentic standards. A control assay without cells exhibited no product accumulation (Figure 3.7(b)), confirming that any A-antigen formed is due to GTA activity.

3.3.5 Gene Ablation Verification

In gene knockout experiments functional analysis is often employed to demonstrate that the gene was deleted. The methods developed in this Chapter are well suited to such analyses particularly when the sample size is limiting, such as the case when the deleted gene is crucial for the organism's development. In this study single wild type *Arabidopsis* embryos were compared to mutant embryos lacking the α-glucosidase I encoding *KNOPF* gene. It can be seen in Figure 3.8 that for both wild type (Figure 3.8(a)) and mutant (Figure 3.8(b)) embryos the LN-TMR was converted to GN-TMR by β-galactosidase, indicating that the mutants are viable. However, the mutant electropherograms did not possess significant TMR peaks which arise from the hydrolysis of the trisaccharide TG-TMR by α-glucosidase I and α-glucosidase II. A total of six embryos were analysed, three mutant and three wild type, and after 24 hours the

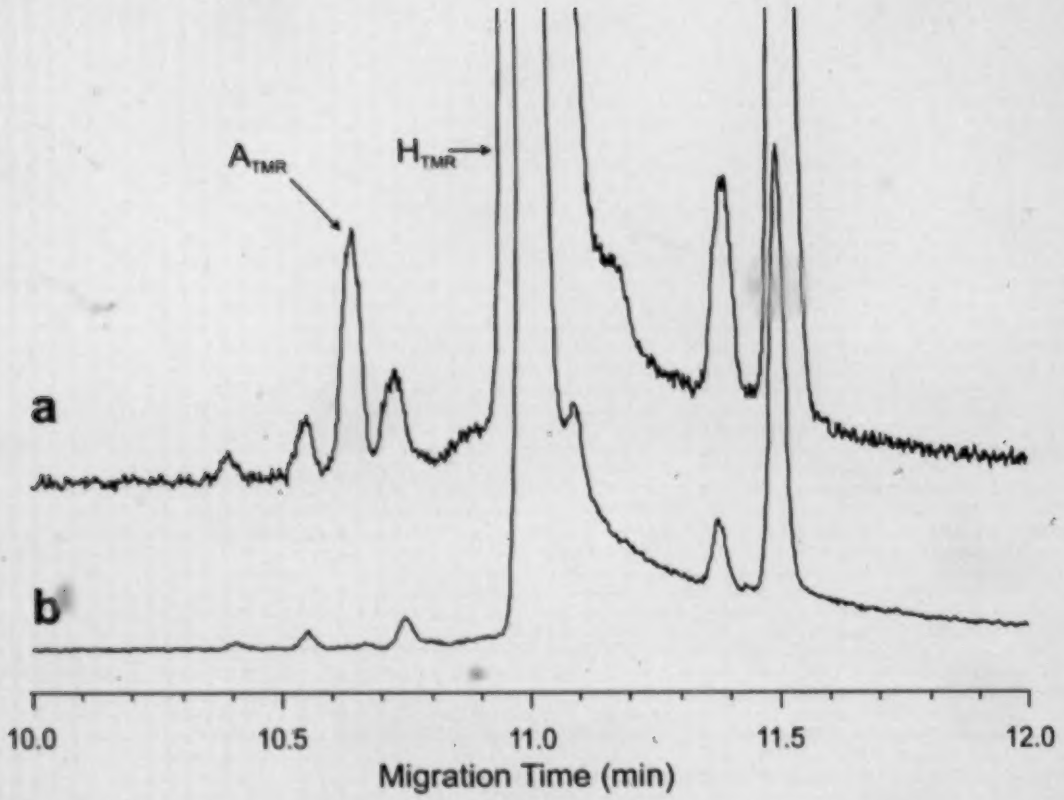

Figure 3.7 Sample electropherograms of the single cell GTA analysis. The blood group enzyme transfers GalNAc from a UDP-GalNAc donor to the H-antigen (H), producing the A-antigen (A). The addition of a (a) single HT29 cell to 100 nL of reaction buffer resulted in 0.81% conversion of the H precursor after 52 hours whereas a (b) control assay without any cells did not exhibit any product formation. Electropherograms have been offset to facilitate visual comparison.

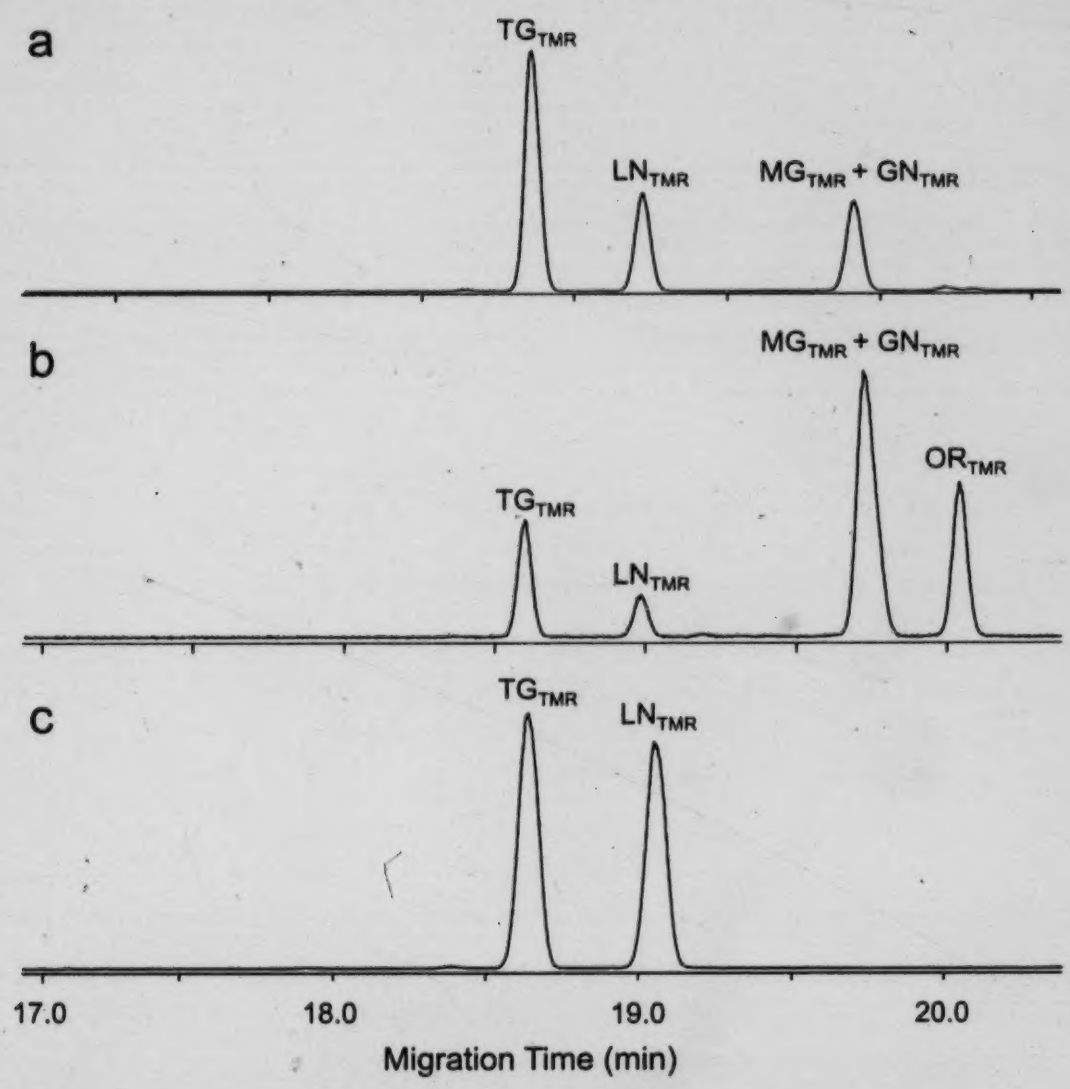

Figure 3.8 Single *Arabidopsis* embryo analysis of (a) mutant and (b) wildtype embryos. Both embryo samples exhibited conversion of the LN-TMR to GN-TMR by β-galactosidase. Mutant embryos, however, were not effective in hydrolyzing the TG-TMR to the TMR linker arm due to deletion of the gene corresponding to α-glucosidase I. The electropherograms have been offset to aid comparison. (c) A blank assay was also performed using reaction buffer in place of embryo lysate and resulted in no conversion of either substrate.

three mutants exhibited an average TG conversion of 1.9%, whereas the wild type embryos had an average activity of 57.1% conversion. Both groups possessed similar LN-TMR conversion to GN-TMR, 61.4% for the mutant and 76.8% for the wild type, suggesting that they both possessed similar levels of β-galactosidase. Therefore, the total cell count in the wild type and mutant embryos must be similar and the lack of significant α-glucosidase I activity in the α-glucosidase I mutants confirms the selective deletion of the gene coding for α-glucosidase I.

3.4 Conclusions

The single cell enzyme assays reported in this study represents another option in the growing field of single cell analysis. This method was shown capable of removing multiple samples from a single cell enzyme reaction derived from small diameter cells (*ca.* 15 μm) such as Sf9 or HT29 cells. The sensitivity of this technique was demonstrated in the analysis of a low abundance carbohydrate synthesizing enzyme, GTA, in single HT29 cells. The methods described here are applicable to other small scale analyses as demonstrated in the functional confirmation of α-glucosidase I deficient mutants at the single embryo level. Improvements will be required to further enhance the sensitivity of the analysis, facilitating the combination of other available single cell techniques. This will involve further miniaturization of the assay to avoid extensive cellular dilution. There is great potential in combining single cell analytical techniques as this will allow new relationships to be probed at the individual cell level. For example, using microdissection techniques[38] with single cell enzyme assays would allow for functional heterogeneity to be compared between tumour and healthy tissue samples.

Performing single cell RT-PCR[39] and enzyme assays in parallel would allow gene expression to be correlated to the corresponding protein's activity. There is an ever-increasing repertoire of techniques available to study biological systems at their most basic level and future studies will benefit greatly through the combination of the available single cell methodologies.

The ability to repeatedly sample a single cell enzyme reaction will find a specific application in single cell metabolic studies where multiple sampling would allow the correlation of an enzyme's expression level to its specific metabolic products. Studying the gene expression and their corresponding proteins within cells does not give a complete picture of what is happening within the cell. Studying metabolites and metabolic pathways is also important in understanding cellular processes.[40,41] The CE-LIF-based assay presented here is well suited to such studies, particularly in situations where sample size is limiting, due to the sensitivity of LIF and ability of CE to separate multiple reaction products.

3.5 Literature Cited

(1) Rubin, M. A. *Science* **2002**, *296*, 1329-1330.

(2) Kruth, H. S. *Analytical Biochemistry* **1982**, *125*, 225-242.

(3) Chitarra, L. G.; van den Bulk, R. W. *European Journal of Plant Pathology* **2003**, *109*, 407-417.

(4) Horan, P. K.; Wheeless, L. L. *Science* **1977**, *198*, 149-157.

(5) Kennedy, R. T.; Oates, M. D.; Cooper, B. R.; Nickerson, B.; Jorgenson, J. W. *Science* **1989**, *246*, 57-63.

(6) Hietpas, P. B.; Ewing, A. G. *Journal of Liquid Chromatography* **1995**, *18*, 3557-3576.

(7) Hogan, B. L.; Yeung, E. S. *Analytical Chemistry* **1992**, *64*, 2841-2845.

(8) Tong, W.; Yeung, E. S. *Journal of Chromatography B-Biomedical Applications* **1996**, *685*, 35-40.

(9) Han, F. T.; Lillard, S. J. *Analytical Biochemistry* **2002**, *302*, 136-143.

(10) Hu, S.; Zhang, L.; Cook, L. M.; Dovichi, N. J. *Electrophoresis* **2001**, *22*, 3677-3682.

(11) Zhang, H.; Jin, W. R. *Electrophoresis* **2004**, *25*, 480-486.

(12) Fuller, K. M.; Arriaga, E. A. *Analytical Chemistry* **2003**, *75*, 2123-2130.

(13) Fuller, K. M.; Arriaga, E. A. *Current Opinion in Biotechnology* **2003**, *14*, 35-41.

(14) Xue, Q. F.; Yeung, E. S. *Analytical Chemistry* **1994**, *66*, 1175-1178.

(15) Huaina, L.; Sims, C. E.; kaluzova, M.; Stanbridge, E. J.; Allbritton, N. L. *Biochemistry* **2004**, *43*, 1599-1608.

(16) Meredith, G. D.; Sims, C. E.; Soughayer, J. S.; Allbritton, N. L. *Nature Biotechnology* **2000**, *18*, 309-312.

(17) Zarrine-Afsar, A.; Krylov, S. N. *Analytical Chemistry* **2003**, *75*, 3720-3724.

(18) Krylov, S. N.; Arriaga, E. A.; Chan, N. W. C.; Dovichi, N. J.; Palcic, M. M. *Analytical Biochemistry* **2000**, *283*, 133-135.

(19) Le, X. C.; Tan, W.; Scaman, C. H.; Szpacenko, A.; Arriaga, E.; Zhang, Y. N.; Dovichi, N. J.; Hindsgaul, O.; Palcic, M. M. *Glycobiology* **1999**, *9*, 219-225.

(20) Luzzi, V.; Lee, C. L.; Allbritton, N. L. *Analytical Chemistry* **1997**, *69*, 4761-4767.

(21) Meneses-Acosta, A.; Mendonca, R. Z.; Merchant, H.; Covarrubias, L.; Ramirez, O. T. *Biotechnology and Bioengineering* **2001**, *72*, 441-457.

(22) Lorieau, J.; Shoemaker, G. K.; Palcic, M. M. *Analytical Chemistry* **2003**, *75*, 6351-6354.

(23) Parodi, A. J. *Annual Review of Biochemistry* **2000**, *69*, 69-93.

(24) Patenaude, S. I.; Seto, N. O. L.; Borisova, S. N.; Szpacenko, A.; Marcus, S. L.; Palcic, M. M.; Evans, S. V. *Nature Structural Biology* **2002**, *9*, 685-690.

(25) Seto, N. O. L.; Palcic, M. M.; Hindsgaul, O.; Bundle, D. R.; Narang, S. A. *European Journal of Biochemistry* **1995**, *234*, 323-328.

(26) Yamamoto, F.; Clausen, H.; White, T.; Marken, J.; Hakomori, S. I. *Nature* **1990**, *345*, 229-233.

(27) Gillmor, C. S.; Poindexter, P.; Lorieau, J.; Palcic, M. M.; Somerville, C. *Journal of Cell Biology* **2002**, *156*, 1003-1013.

(28) Scaman, C. H.; Hindsgaul, O.; Palcic, M. M.; Srivastava, O. P. *Carbohydrate Research* **1996**, *296*, 203-213.

(29) Zhang, Y. N.; Le, X. C.; Dovichi, N. J.; Compston, C. A.; Palcic, M. M.; Diedrich, P.; Hindsgaul, O. *Analytical Biochemistry* **1995**, *227*, 368-376.

(30) Krylov, S. N.; Dovichi, N. J. *Electrophoresis* **2000**, *21*, 767-773.

(31) Shoemaker, G. K.; Lorieau, J.; Lau, L. H.; Gillmor, C. S.; Palcic, M. M. *Analytical Chemistry* **2005**, *77*, 3132-3137.

(32) Chen, D. Y.; Dovichi, N. J. *Journal of Chromatography B-Biomedical Applications* **1994**, *657*, 265-269.

(33) Chen, D. Y.; Swerdlow, H. P.; Harke, H. R.; Zhang, J. Z.; Dovichi, N. J. *Journal of Chromatography* **1991**, *559*, 237-246.

(34) Wu, S. L.; Dovichi, N. J. *Journal of Chromatography* **1989**, *480*, 141-155.

(35) Gilman, S. D.; Ewing, A. G. *Analytical Chemistry* **1995**, *67*, 58-64.

(36) Oates, M. D.; Cooper, B. R.; Jorgenson, J. W. *Analytical Chemistry* **1990**, *62*, 1573-1577.

(37) Krylov, S. N.; Zhang, Z. R.; Chan, N. W. C.; Arriaga, E.; Palcic, M. M.; Dovichi, N. J. *Cytometry* **1999**, *37*, 14-20.

(38) EmmertBuck, M. R.; Bonner, R. F.; Smith, P. D.; Chuaqui, R. F.; Zhuang, Z. P.; Goldstein, S. R.; Weiss, R. A.; Liotta, L. A. *Science* **1996**, *274*, 998-1001.

(39) Zabzdyr, J. L.; Lillard, S. J. *Analytical Chemistry* **2001**, *73*, 5771-5775.

(40) Mashego, M. R.; Rumbold, K.; De Mey, M.; Vandamme, E.; Soetaert, W.; Heijnen, J. J. *Biotechnology Letters* **2007**, *29*, 1-16.

(41) Raamsdonk, L. M.; Teusink, B.; Broadhurst, D.; Zhang, N. S.; Hayes, A.; Walsh, M. C.; Berden, J. A.; Brindle, K. M.; Kell, D. B.; Rowland, J. J.; Westerhoff, H. V.; van Dam, K.; Oliver, S. G. *Nature Biotechnology* **2001**, *19*, 45-50.

Chapter 4

Determination of Protein-Carbohydrate Association Thermochemistry by the Direct NanoES-MS Assay

4.1 Introduction

Protein-carbohydrate binding forms the basis for many important biological processes such as cellular growth and adhesion, bacterial and viral infections, inflammation, as well as various aspects of the immune response.[1-3] The interaction of individual carbohydrate moieties with proteins is generally weak, with binding affinities typically in the 10^3 to 10^5 M^{-1} range. To increase the binding affinity under native conditions, carbohydrate-binding proteins (e.g., lectins, antibodies, enzymes) often form covalently or noncovalently bound oligomers consisting of two or more subunits, with each subunit displaying one or more carbohydrate-binding sites.[2] To understand the nature of protein-carbohydrate recognition processes, detailed information regarding binding stoichiometry, affinity (K_{assoc}), and specificity is required. There are a number of analytical techniques that can be used to quantify protein-carbohydrate binding. Isothermal titration microcalorimetry (ITC) is widely used and is the only technique that provides a direct measure of the enthalpy of association (ΔH_{assoc}).[4] In this technique, a ligand is titrated against its binding partner and the evolved heat is measured as a function of ligand concentration.[5] ITC has several limitations, including the often-prohibitive requirement for milligram quantities of both protein and ligand for each analysis and the inability to provide direct information on binding stoichiometry.

Surface plasmon resonance (SPR) affords high sensitivity and can be used to evaluate the rate constants for the association-dissociation reactions.[6] This technique measures changes in the optical properties of a surface layer, consisting of an immobilized target, upon an increase in mass of this layer (i.e. binding of ligand). Frontal affinity chromatography/mass spectrometry (FAC/MS), which is capable of rapidly screening libraries of carbohydrate ligands against target proteins, is another approach that allows the estimation of protein-ligand K_{assoc} values for strongly bound complexes.[7] In FAC/MS, the retention behaviour of compounds in a column composed of immobilized target protein is used to derive K_{assoc} values. A limitation of both the SPR and FAC/MS techniques is the requirement for the immobilization of one of the analyte (protein or ligand) on a solid surface. In addition to being impractical in certain cases, immobilization may alter the nature of the protein-carbohydrate interactions and, hence, the binding affinity.

Mass spectrometry (MS), combined with electrospray ionization (ES) or nanoflow ES (nanoES), is a powerful tool for evaluating the binding stoichiometry[8-10] and affinity[11,12] for protein-carbohydrate complexes. The key advantages of the direct ES-MS technique are speed of analysis, which can usually be completed within a few seconds, and specificity, which allows for the direct determination of binding stoichiometry for a given protein-carbohydrate system and the ability to study binding between multiple proteins and carbohydrates simultaneously. NanoES also readily allows for the transfer of non-covalent complexes from buffered aqueous solution to the gas phase and facilitates the study of binding at a physiological pH. When combined with nanoES, the MS-based assay also affords high sensitivity, normally consuming

picomoles or less of analyte per analysis. Additionally, the application of a temperature-controlled nanoES-MS device (Figure 4.1) allows for the enthalpy (ΔH_{assoc}) and entropy of association (ΔS_{assoc}) to be estimated from the temperature dependence of K_{assoc}.[13] Here, the direct ES-MS assay is applied to evaluate the binding thermochemistry for two protein – carbohydrate systems.

The first system studied is the monoclonal antibody (mAb) CS-35[14] interacting with a series of synthetic oligosaccharides. The global rise in the incidence of tuberculosis and the emergence of drug-resistant mycobacterial strains has increased the need for novel TB drugs and treatments.[15-17] The CS-35 mAb, originally generated against the cell wall component lipoarabinomannan (LAM) of *Mycobacterium leprae*,[18] has recently been shown to cross react with LAM from other mycobacterium as well, including *M. tuberculosis*.[14] Since humans do not possess arabinofuranose-containing glycoconjugates such as LAM, these cell wall components and the enzymes responsible for their biosynthesis are a promising target for novel therapeutics. In previous studies it was shown that CS-35 recognizes a hexasaccharide (**1**) and a tetrasaccharide (**2**) motif.[14,19] Beyond this, however, nothing is known regarding the fine ligand specificity. Thus various oligosaccharide fragments (**2-6**) of **1**, the structures of which are given in Figure 4.2, were synthesized and their binding affinities determined using the direct nanoES-MS approach to establish which residues are critical for recognition by CS-35. Using temperature-controlled ES, the enthalpies and entropies of binding were also determined.

The second part of this Chapter describes the nanoES-MS study of the human blood group enzyme, α-(1,3)-galactosyltransferase (GTB)[20,21] interacting with donor and

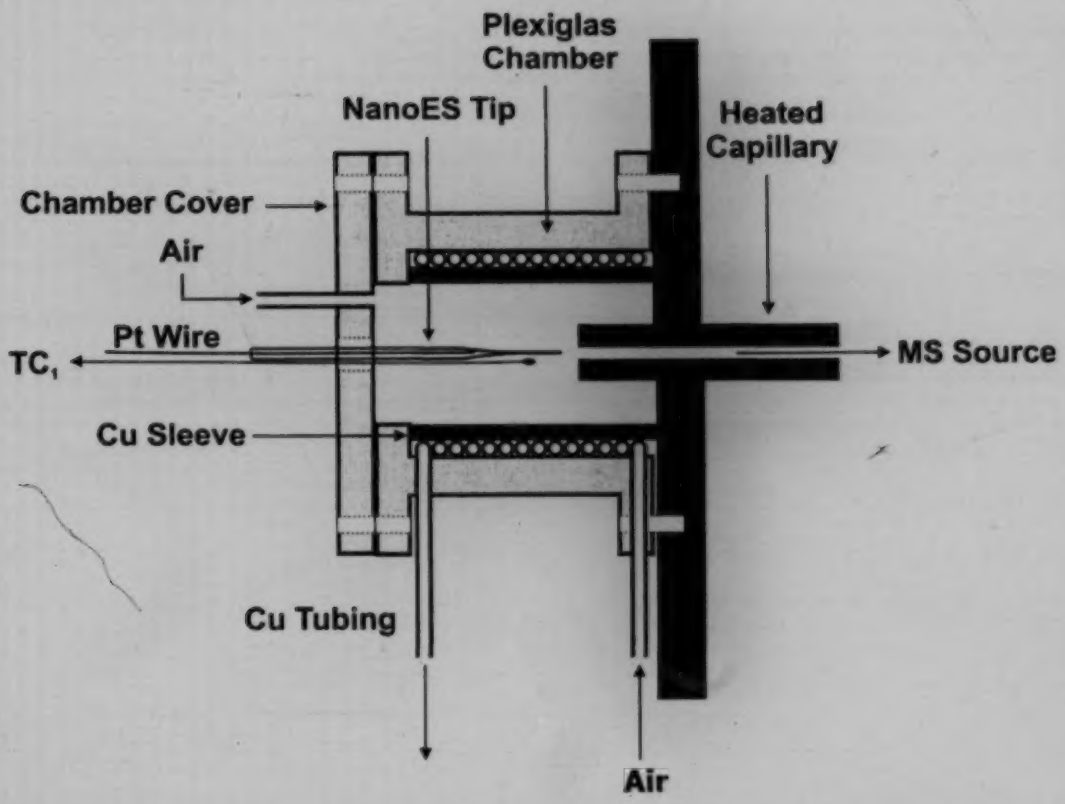

Figure 4.1 Schematic diagram of the temperature-controlled nanoES device. The sample droplets are sprayed using a nanoES tip inserted through a small aperture in the Plexiglas cover of the chamber. The temperature of the nanoES solution is controlled by regulating the air flow through the Cu tubing which is in thermal contact with the Cu sleeve that surrounds the ES chamber. The temperature of the nanoES solution is determined by a thermocouple, TC_1, attached to the nanoES tip and positioned 1-2 mm from the heated sampling inlet capillary. To satisfy the gas intake requirement of the ion source, a portion of the regulated air (~700 mL/min) is introduced into the chamber through the Plexiglas disc. The total volume inside the chamber is approximately 60 mL.

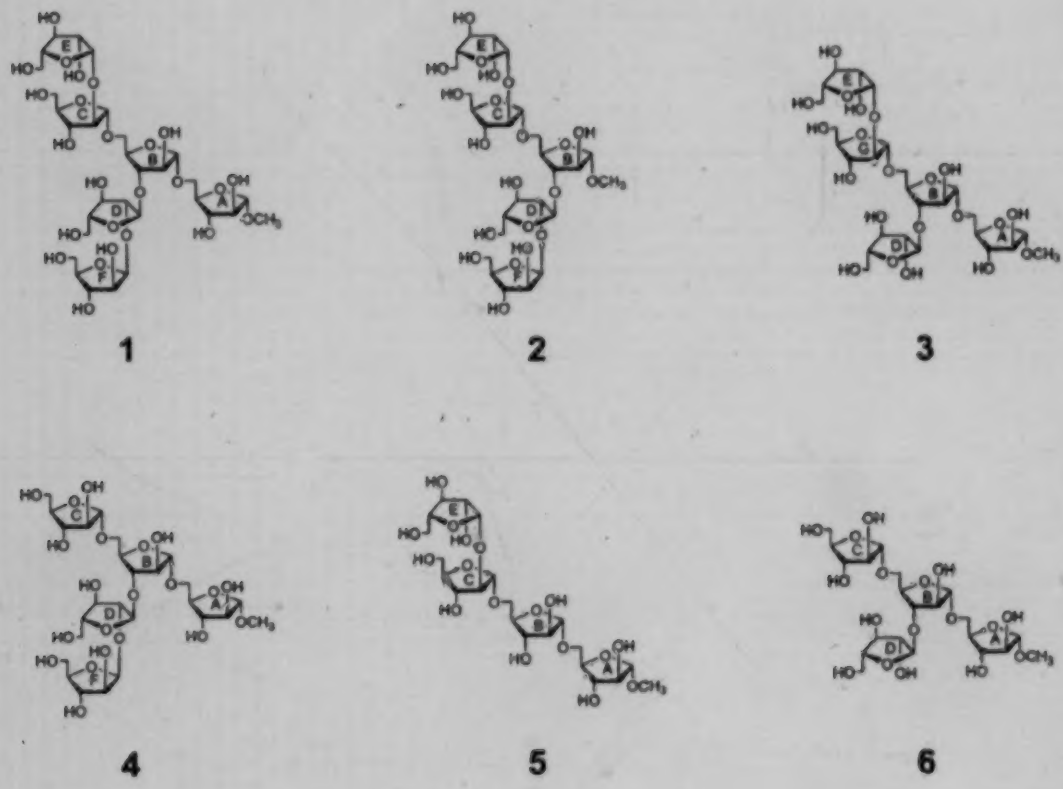

Figure 4.2 Oligosaccharide ligands used in the CS-35 F_{ab} nanoES-MS binding experiments: β-D-Ara*f*-(1→2)-α-D-Ara*f*-(1→5)[β-D-Ara*f*-(1→2)-α-D-Ara*f*-(1→3)]-α-D-Ara*f*-(1→5)-α-D-Ara*f*-OCH_3 (**1**), β-D-Ara*f*-(1→2)-α-D-Ara*f*-(1→5)[β-D-Ara*f*-(1→2)- α-D-Ara*f*-(1→3)]-α-D-Ara*f*-OCH_3 (**2**), β-D-Ara*f*-(1→2)-α-D-Ara*f*-(1→5)[α-D-Ara*f*-(1→3)]-α-D-Ara*f*-(1→5)-α-D-Ara*f*-OCH_3 (**3**), β-D-Ara*f*-(1→2)-α-D-Ara*f*-(1→3)[α-D-Ara*f*-(1→5)]-α-D-Ara*f*-(1→5)-α-D-Ara*f*-OCH_3 (**4**), β-D-Ara*f*-(1→2)-α-D-Ara*f*-(1→5)-α-D-Ara*f*-(1→5)-α-D-Ara*f*-OCH_3 (**5**), α-D-Ara*f*-(1→3)[α-D-Ara*f*-(1→5)]-α-D-Ara*f*-(1→5)-α-D-Ara*f*-OCH_3 (**6**).

acceptor ligands. Glycosyltransferases, a large and diverse group of enzymes of which there is over 200 sequences known in humans,[22] are responsible for the synthesis of the wide array glycoconjugates that are displayed on cell surfaces. Cell surface carbohydrates form the basis of critical cell-cell and cell-matrix interactions and play a role in bacterial, viral, and fungal infections as well as other disorders.[23-27] For these reasons glycosyltransferases have become the focus of a significant body of research in the search for novel therapeutics against various infections and disorders.[28,29] A remarkable feature of glycosyltransferases is the specificity in which they carry out their function, with each glycosyltransferase typically responsible for one specific glycosidic linkage. These enzymes can be classified into two categories, retaining or inverting glycosyltransferases, based on whether the transfer reaction proceeds with net retention or inversion in the configuration of the anomeric centre of the transferred sugar.[30] One common structural motif found in many glycosyltransferases is a DXD motif, which consists of two aspartate residues separated by any other amino acid.[21,31,32] This motif serves to coordinate a divalent metal ion, which has been shown to be essential for catalytic activity in many glycosyltransferases.[33-36]

The reaction catalyzed by GTB, a retaining glycosyltransferase, is given in Figure 4.3. The product of this reaction is the blood group B antigen. GTB, and the homologous blood group A antigen synthesizing enzyme, α-(1,3)-N-acetylgalactosaminyltransferase (GTA), have emerged as model systems to study the mechanism of this important and yet inadequately understood class of enzymes. GTA and GTB both recognize the same acceptor structure, **7**, but they possess different donor specificity. The reaction catalysed by GTA utilizes a uridine 5'-diphosphate – N-

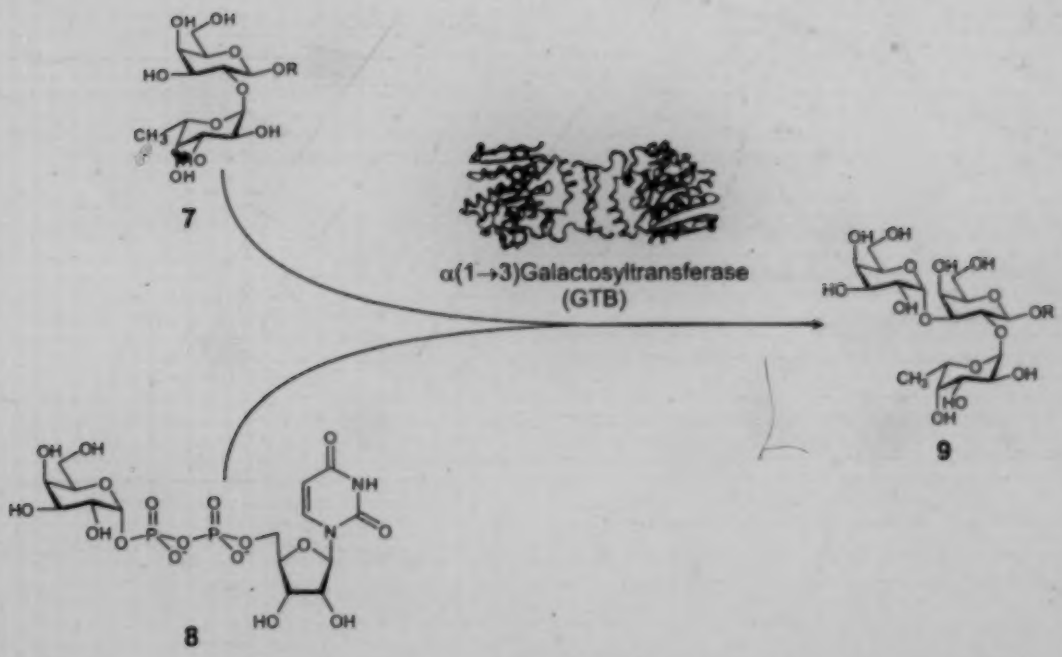

Figure 4.3 The reaction catalysed by the human blood group enzyme α(1→3)galactosyltransferase (GTB). The enzyme recognizes the terminal carbohydrate structure α-L-Fuc*p*-(1→2)-β-D-Gal*p*-O-R (**7**) and transfers a monosaccharide from a nucleotide sugar donor, uridine 5'-diphosphate-Gal (UDP-Gal, **8**), to this acceptor at the 3'-O- position generating the B antigen, α-D-Gal*p*-(1→3)[α-L-Fuc*p*-(1→2)]-β-D-Gal*p*-O-R (**9**). It has been shown previously that a metal ion, possibly Mn^{+2}, is critical for enzyme activity.[33,34,35,36]

acetylgalactosamine (UDP-GalNAc) donor whereas GTB recognizes a uridine 5'-diphosphate – galactose donor (UDP-Gal). Interestingly, this change in donor specificity is the result of only a 4 amino acid difference between the two enzymes (A176G, G235S, L266M, and G288A). This feature makes these enzymes an ideal system in the study of retaining glycosyltransferases. GTA and GTB, and mutants of this enzyme in which these four key amino acids have been interchanged, have been studied using a wide range of techniques such as x-ray crystallography,[20,21,37,38] kinetic analysis,[39,40] and most recently NMR,[41,42] to elucidate the reaction mechanism and the cause of this altered donor specificity. Despite this wealth of data, many questions regarding GTA and GTB remain unanswered. For example, the native oligomeric form of these enzymes in solution is unclear, the role and exact nature the metal cofactor required for activity is not defined, and the precise catalytic mechanism, currently believed to proceed via a double-displacement or possibly an S_Ni mechanism,[43,44] remains vague. A nanoES-MS study of GTB was thus conducted in an attempt to resolve these issues. This work represents the first detailed thermodynamic study of GTB and its interactions with substrate.

4.2 Experimental

4.2.1 Materials and Reagents.

The synthetic oligosaccharides **1** – **6** were synthesized in the laboratory of Dr. Todd Lowary at the University of Alberta.[45] GTB acceptor substrates and analogs (**7**, **9**, **10** - **14**) (Figure 4.4) were provided by Dr. Ole Hindsgaul at the Carlsberg Laboratory. For the GTB acceptor substrate and acceptor analogues, the reducing end of the oligosaccharides is attached to an aliphatic chain, $(CH_2)_7CH_3$ (labeled R), which was

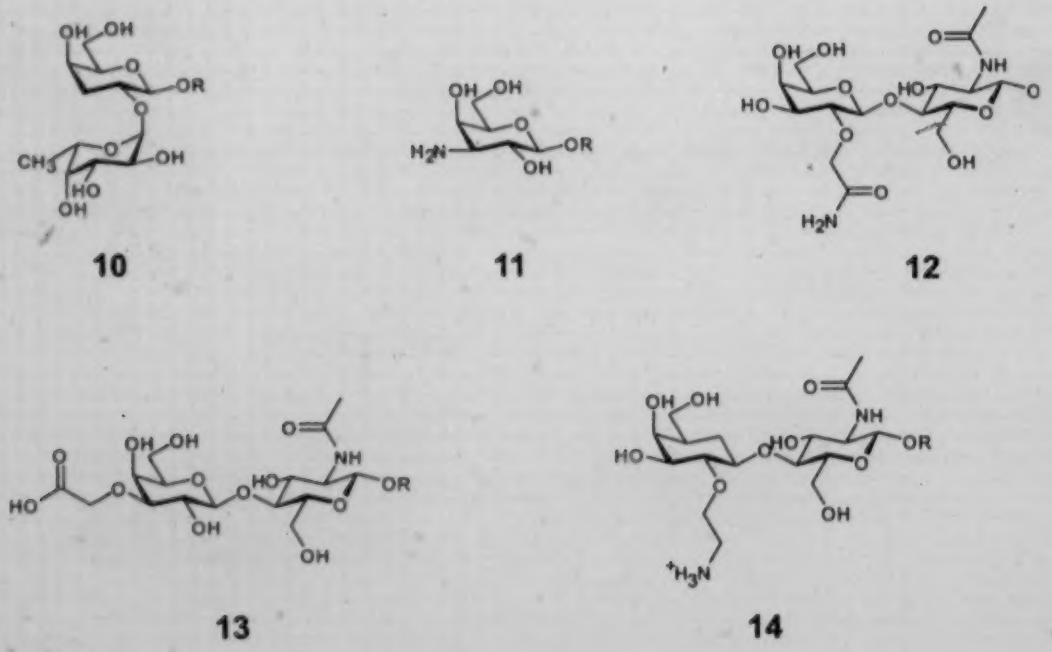

Figure 4.4 Structures of the acceptor analogues used in the nanoES-MS study of GTB: α-L-Fuc*p*-(1→2)-β-D-3-deoxy-Gal*p*-O-R (**10**), 3-Amino-3-deoxy-β-D-Gal*p*-O-R (**11**), 2-O-carbamoylmethyl-β-D-Gal*p*-(1→4)-2-acetamido-2-deoxy-β-D-Glc*p*-O-R (**12**), 3-O-carboxymethyl-β-D-Gal*p*-(1→4)-2-Acetamido-2-deoxy-β-D-Glc*p*-O-R (**13**), 2-O-Aminoethyl-β-D-Gal*p*-(1→4)-2-Acetamido-2-deoxy-β-D-Glc*p*-O-R(**14**).

required for GTB kinetic studies of these ligands[46]. The native GTB donor (**8**) and the donor fragment uridine 5'-diphosphate (UDP, **15**) were purchased from Sigma.

4.2.2 Protein Expression and Purification.

The cell line that produces mAb CS-35 (MW 149 kDa) was obtained from Dr. John S. Spencer of Colorado State University. The cells were placed in a compartment of an artificial mouse bioreactor (CELLine™ CL - 1000 System, BD Bioscience). After one week the cells were centrifuged and the supernatant, which contains the mAb, was collected. The cells were re-suspended in BD media and added back into the bioreactor. This process was repeated until the cell viability, as determined by trypan blue staining, was below 20%. The supernatants were pooled and the mAb was purified as described elsewhere.[47] A portion of the purified mAb solution was then digested with papain to generate the antibody binding fragment (F_{ab}).[47] For MS analysis, the F_{ab} was exchanged into a 50 mM ammonium acetate buffer (pH 7.2) using an Amicon ultracentrifugation filter with a molecular weight cutoff (MWCO) of 10 kDa and then stored at 4°C. The concentration of CS-35 F_{ab} (MW ~ 50 kDa) was determined by lyophilizing an aliquot of this solution and determining the corresponding mass of F_{ab}.

The gene encoding for recombinant GTB enzyme (monomer MW 34 483 Da) was overexpressed in *E. coli* as described previously.[48] The enzyme was purified using established protocols which consisted of anion-exchange chromatography on a SP Sepharose Fast Flow column followed by affinity chromatography using a UDP-hexanolamine column.[48] The purified enzyme was exchanged into a 50 mM ammonium acetate buffer (pH 7) with an Amicon ultracentrifugation filter with a MWCO of 10 kDa

for MS analysis. The enzyme solution was stored at 4°C and its concentration was determined by lyophilizing a known volume of solution and determining the mass of GTB.

The immediate exchange of buffer into ammonium acetate was found to significantly increase the quality of the observed mass spectrum for GTB. This is demonstrated in Figure 4.5 where illustrative nanoES mass spectra are shown for an aqueous solution of GTB purified with (Figure 4.5a) and without (Figure 4.5c) a lengthy dialysis step before exchanging the buffer with ammonium acetate. As can be seen in Figure 4.5a, the dialysis and storage of GTB in the standard purification buffer consisting of 50 mM 3-(N-morpholino)propanesulfonic acid (MOPS), 1 mM dithiothreitol (DTT), 5 mM $MnCl_2$, and 100 mM NaCl leads to GTB ions with extensive adducts. The adduct peaks, which are not fully resolved, likely correspond to the noncovalent attachment of alkali metal ions and, possibly, 2-mercaptoethanol which was also present in the GTB storage buffer. This dialysis step was originally performed because the stability of GTB in ammonium acetate was uncertain. It was found, however, that at 4°C in 50 mM ammonium acetate the enzyme retained binding activity and gave a strong MS signal for up to one month. This demonstrates that in nanoES-MS protein studies, sample preparation is critical and may have to be optimized from standard protein purification methodologies to yield a suitable MS signal.

Recombinant single chain variable fragment (scFv) of the mAb Se155-4 (MW 26 539 Da) was expressed in *E. coli* and purified using procedures described previously.[49]

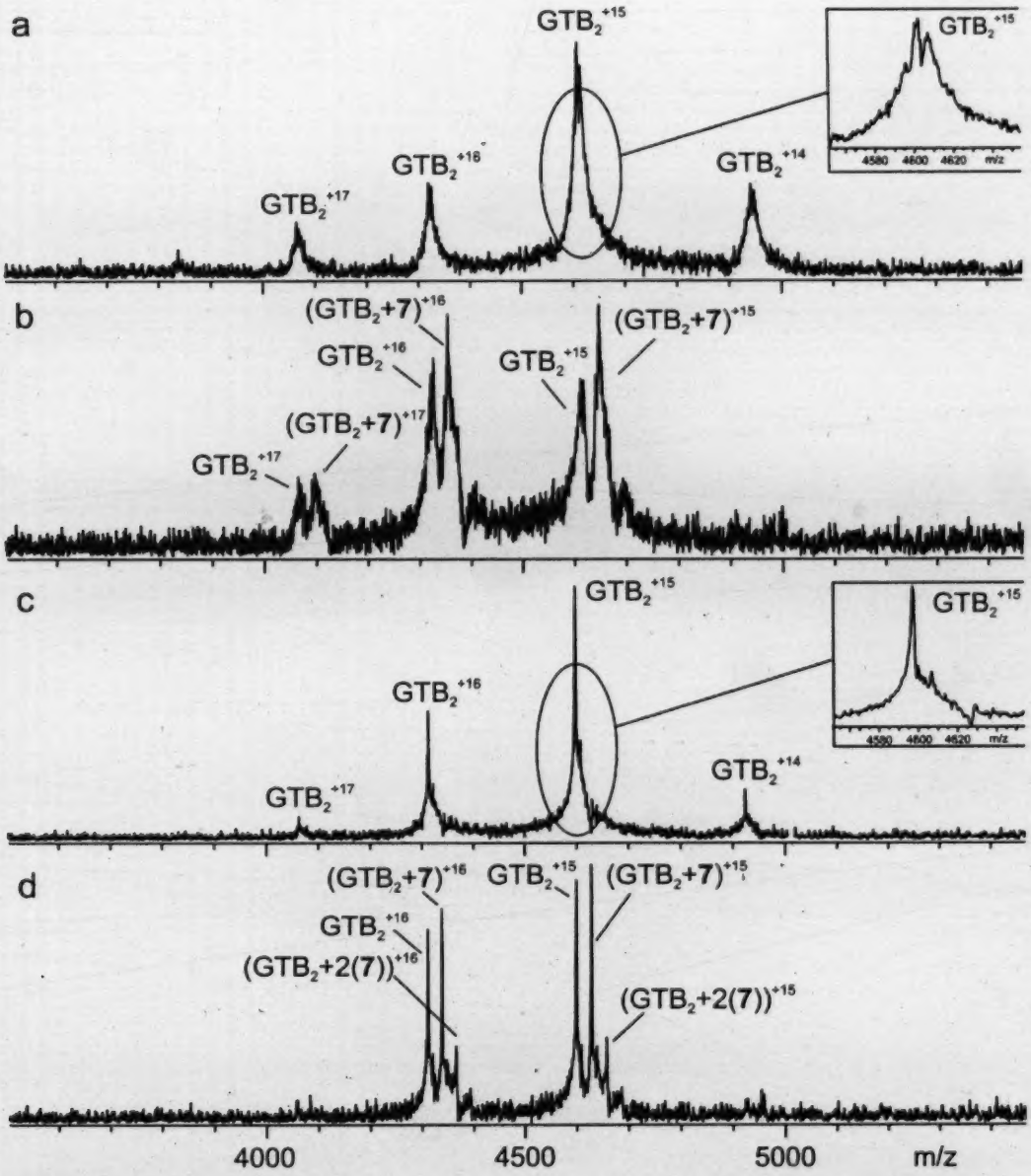

Figure 4.5 NanoES mass spectra obtained in positive ion mode for an aqueous solution of (a) 30-μM GTB and (b) 30-μM GTB with 50-μM **7**. After optimizing the purification of GTB the protein was analysed again using nanoES-MS at a concentration of (c) 17-μM alone and with (d) 40-μM **7**. All solutions contained 10 mM ammonium acetate (pH 7).

4.2.3 Mass Spectrometry

MS measurements were performed using an Apex II 9.4 tesla Fourier transform ion cyclotron resonance (FT-ICR) mass spectrometer (Bruker, Billerica, MA) equipped with a temperature-controlled nanoflow electrospray (nanoES) ion source.[13] A diagram of the instrumental setup is given in Chapter 1 (Figure 1.5). The nanoES solutions were prepared from aqueous stock solutions of protein and ligand with known concentrations. Unless otherwise indicated, aqueous ammonium acetate was added to the nanoES solution to yield a final buffer concentration of 10 mM. NanoES was performed using an aluminosilicate capillary (1.0 mm o.d., 0.68 mm i.d.), pulled to 4 – 7 μm o.d. at one end using a P-2000 micropipette puller (Sutter Instruments, Novato, CA). The electric field required to spray the solution was established by applying a voltage of +800-1000 V to a platinum wire inserted inside the glass tip. The solution flow rate was typically 20 nL/min. The droplets and gaseous ions produced by nanoES were introduced into the mass spectrometer through a stainless steel capillary (i.d. 0.43 mm) maintained at an external temperature of 66 °C. The ion/gas jet sampled by the capillary (+50 V) was transmitted through a skimmer (-2 V) and stored electrodynamically in an rf hexapole. Unless specified otherwise, a hexapole accumulation time of 2.5s was used for all experiments. Ions were ejected from the hexapole and accelerated to -2700 V into the superconducting magnet, decelerated, and introduced into the ion cell. The trapping plates of the cell were maintained at a constant potential of +1.6 V throughout the experiment. The typical base pressure for the instrument was ~$5x10^{-10}$ mbar. Data acquisition was controlled by an SGI R5000 computer running the Bruker Daltonics XMASS software, version 5.0. Mass spectra were obtained using standard experimental

sequences with chirp broadband excitation. The time domain signal, consisting of the sum of 50-100 transients containing 128 K data points per transient, were subjected to one zero-fill prior to Fourier transformation.

4.2.4 Determination of K_{assoc} Values by NanoES-MS

K_{assoc} values for CS-35 F_{ab} and GTB binding to the various ligands were determined using the direct ES/MS technique.[50] The value of K_{assoc} was calculated using eq 4.1:

$$K_{assoc} = \frac{R}{[L]_o - \frac{R[P]_o}{1+R}} \qquad (4.1)$$

where $[P]_o$ and $[L]_o$ are the initial concentrations of protein and ligand, respectively and R is the ratio of the ion intensity (I) of the bound and unbound protein ions (*i.e.* $I(PL^{n+})/I(P^{n+})$) determined from the mass spectrum. Because ES typically produces P^{n+} and PL^{n+} ions with a distribution of charge states, the R value is obtained from the sum of all signal intensities corresponding to ions of the complex divided by the sum of all the signal intensities corresponding to the protein ions over all the observed charge states.[12] When using FT-ICR/MS, for which the ion signal is proportional to the abundance and charge state of the ions, the measured ion intensities must be normalized for charge state, n, eq 4.2.[11]

$$R = \frac{\sum_n I(PL)^{n+}/n}{\sum_n I(P)^{n+}/n} \qquad (4.2)$$

If the protein (or protein complex) can bind to multiple molecules of L, which is the case when working with antibodies, lectins, as well as many enzymes, there are

additional reactions that must be considered. Shown below are the relevant reactions for P binding to between one and N molecules of L:

$$P + L \rightleftharpoons P{\bullet}L \qquad (4.3a)$$

$$P{\bullet}L + L \rightleftharpoons P{\bullet}L_2 \qquad (4.3b)$$

$$\vdots \qquad \vdots$$

$$P{\bullet}L_{N-1} + L \rightleftharpoons P{\bullet}L_N \qquad (4.3N)$$

The equilibrium concentrations of bound protein can be determined from the relative abundance of the corresponding ions observed in the mass spectrum and eq 4.4a. The equilibrium concentration of L can then be found from eq 4.4b.

$$[P]_o = [P]_{equil} + [PL]_{equil} + [PL_2]_{equil} + \ldots + [PL_N]_{equil} \qquad (4.4a)$$

$$[L]_o = [L]_{equil} + [PL]_{equil} + 2[PL_2]_{equil} + \ldots + N[PL_N]_{equil} \qquad (4.4b)$$

If the binding sites are equivalent, K_{assoc} can be determined for each and any of the ligand binding reactions described by eq 4.3 using the general expression:

$$K_{assoc,p} = K_{assoc}\frac{(N-p+1)}{p} \qquad (4.5)$$

where p is the number of occupied binding sites.[12] The analysis of the experimental data is more difficult in cases where the protein possesses nonequivalent carbohydrate binding sites. A complete treatment of the analysis procedure can be found elsewhere.[51]

4.2.5 Experimental Challenges to the Direct NanoES-MS Binding Assay

There are a number of associated challenges with the application of the direct nanoES-MS assay for determination of protein-ligand binding affinity and stoichiometry.[11] Due to a combination of solution and gas-phase processes the robustness and accuracy of this technique can be quite poor. The successful implementation of the

direct nanoES-MS technique for determination of reliable association constants requires that the equilibrium ratio of bound to unbound protein initially present in solution be preserved both throughout the nanoES process and in the gas phase detection. Any physical or chemical process that alters this ratio will lead to an incorrect determination of binding affinity. Recent work in the Klassen group has focused on identifying these processes and accounting for their effects.[11,52,53]

One potential problem is electrochemical reactions that occur at the electrode in the nanoES tip. These reactions can alter the composition of the nanoES solution.[54] When performing nanoES on aqueous solutions in the positive-ion mode, the dominant electrochemical reaction at chemically inert electrodes, such as platinum, is the oxidation of H_2O leading to the production of H_3O^+ (eq 4.6). Due to the small solution volumes used in nanoES, the electrochemical production of H_3O^+ can lead to a significant decrease in pH.[54,55]

$$2H_2O \rightarrow O_2 + 4H^+ + 4e^- \qquad (4.6)$$

These pH changes can be quite large, one or more pH units. Given that binding affinities of protein-carbohydrate complexes (and protein-ligand complexes in general) are sensitive to pH, such changes can introduce error into the affinity measurements. Thus to minimize the effect of pH changes on the binding affinity measurements, the duration of the spray was restricted to < 10 min,[11] and a 10 mM ammonium acetate buffer was used.

Collision-induced dissociation (CID) of the gaseous noncovalent complex ions in the ion source of the mass spectrometer can also lead to erroneous K_{assoc} values due to a decrease in the abundance of the PL^{n+} ions. The influence of in-source dissociation on

the relative abundance of P^{n+} and PL^{n+} ions depends on the configuration of the ion source and on the gas-phase stability of the complex being investigated. In the case of protein-carbohydrate complexes, the gas-phase stability of the complex increases with the size of ligand. Collisional heating of the gaseous complex ions may occur at various stages during the ion sampling process, such as within the heated metal sampling capillary, in the nozzle-skimmer region, and during accumulation of ions within external rf multipole storage devices (i.e., hexapole). Collisional heating within external multipoles, which tend to operate at pressures in the range of 10^{-5} to 10^{-3} torr, tends to be the most significant cause of in-source dissociation.[11,56] The extent of in-source dissociation caused by collisional heating within the rf hexapole can be determined by measuring the relative abundance of bound and unbound protein ions at various hexapole accumulation times. If the relative abundance of these ions is independent of hexapole accumulation times it can be assumed that the effect of gas-phase dissociation in the rf hexapole is negligible. This effect was minimized by operating at low hexapole accumulation times, 2.5 s, for all protein-carbohydrate binding studies presented in this thesis. Recently, a method for stabilizing protein-ligand complexes in the gas-phase has been developed which allows the determination of K_{assoc} values using ES-MS even for protein-ligand complexes that possess low gas-phase stability.[52]

Any difference in the ionization efficiency between the bound and unbound receptor ions will also lead to incorrect ion abundances in the mass spectrum. The ionization efficiency is dependant on the chemical properties of the analytes, solvents, charge agents, and droplet size. Thus it is impossible to predict and account for differences in ionization efficiency. This effect is minimized, however, by calculating

K_{assoc} values based on the relative ion abundances for species with similar ionization efficiencies. It is assumed that the binding of a small molecule ligand to a large macromolecule does not affect its ionization efficiency appreciably. In the evaluation of the binding affinity of protein-carbohydrate complexes, the binding affinity is determined by measuring the relative abundance of bound and unbound protein ions. This difference in ionization efficiency remains a problem, however, for evaluating the binding constants between two large macromolecules (i.e. protein-protein complexes). Considering that many proteins exist and carry out their function as protein assemblies,[57] solving this problem, which is the focus of current research in the Klassen lab, would be a major advance for the application of ES-MS in the study of multiprotein complexes.

Perhaps one of the greatest challenges to the accurate determination of binding affinities by ES-MS is the non-specific attachment of ligands to a protein during the ES process. Nonspecific binding between protein and carbohydrate, which readily occurs during the nanoES process, will influence the intensities measured for the P^{n+} and PL^{n+} ions.[53] This is particularly problematic when studying weakly binding ligands because relatively high concentrations (> 50 μM) of ligand are required to observe abundant PL complex. Recently, a method to quantitatively account for the contribution of non-specific complexes to the nanoES-MS spectra was reported.[53] Briefly, this method involves the addition of a reference protein, P_{ref}, to the ES solution that exhibits no specific binding activity towards the ligands of interest. Importantly, it was shown in previous work that the efficiency of non-specific binding is independent on the size and structure of the protein, and that the extent of non-specific binding depends on the amount of free ligand molecules present in the nanoES droplet that ultimately leads to the

formation of gaseous ions.[58] Thus the distribution of ligands bound non-specifically to P_{ref} can be used to correct the measured intensities for the P^{n+} and specific PL^{n+} ions for nonspecific ligand binding. The corrected ion intensities lead to more reliable values of K_{assoc}. The protein chosen as a reference protein in this study was the scFv of the mAb Se155-4.

4.2.6 Isothermal Titration Microcalorimetry

All isothermal titration measurements were made using a Microcal VP-ITC titration microcalorimeter.[59,60] Dialyzed CS-35 F_{ab} was equilibrated against MQ water using an Amicon ultracentrifugation filter with a MWCO of 10 kDa. This F_{ab} solution was lyophilized and the mass of protein was determined. The lyophilized F_{ab} was dissolved in a 50 mM Tris buffer (pH 7.2) containing 150 mM NaCl. The final concentration of CS-35 F_{ab} was 1.8 mg mL^{-1}. The ligands, **1** and **3**, were also lyophilized and dissolved in the same buffer used to equilibrate the CS-35 F_{ab} solution. The calorimeter cell, with a volume of 1.3215 mL, was filled with the CS-35 F_{ab} solution. Ligand was titrated in 35 x 8 μL injections with 6 min intervals between injections. The value of *c*, which is defined as the product of the binding constant K_{assoc} and the concentration of CS-35 F_{ab}, was ≈2 for all measurements reported here. This value is within the theoretical range of suggested *c* values and ligand concentrations were at least 10 times the concentration of CS-35 F_{ab}. This is recommended in order to obtain a strong binding isotherm.[61] The results were evaluated with the ORIGIN software package (MicroCal Inc., Northampton, MA) using a single binding site model.

4.3 Results and Discussion –NanoES-MS Study of the mAb CS-35

4.3.1 Determining K_{assoc} Values for CS-35-Ligand Binding

Initial nanoES-MS studies were carried out on the mAb CS-35. However, there are several challenges associated with binding studies performed on IgG monoclonal antibodies (~ 150 kDa). First, standard purification protocols generally do not yield protein in sufficient purity, leading to extensive adduct formation in the nanoES-MS analysis. Furthermore, IgG antibodies are glycoproteins and exist in multiple glycoforms, which increases the complexity of the nanoES mass spectra. Shown in Figures 4.6a,b are nanoES mass spectra of a mAb CS-35 solution with and without **1**. The peaks corresponding to the mAb ions are quite broad, presumably due to the presence of adducts and differences in glycosylation, and thus the $(CS\text{-}35)^{n+}$ and $(CS\text{-}35 + \mathbf{1})^{n+}$ ions are not fully resolved.

Antibody-carbohydrate binding studies can be greatly simplified by working with the corresponding F_{ab} (MW ~ 50 kDa), which can be generated by digestion of the mAb. The F_{ab} possesses the same binding characteristics as the mAb but is easier to study owing to its lower mass. Papain was used for the digestion of CS-35 mAb in this study. One feature of papain digestion is that it tends to give a heterogeneous mixture of F_{ab} species.[62] In the case of CS-35, digestion lead to the formation of four distinct F_{ab} species **a**, **b**, **c**, and **d** with masses of 48.25 (**a**), 47.90 (**b**), 48.92 (**c**), and 49.23 kDa (**d**), respectively (Figure 4.6c). In the presence of **1**, the $(F_{ab})^{n+}$ and $(F_{ab} + \mathbf{1})^{n+}$ ions are clearly resolved in the mass spectrum (Figure 4.6d). Notably, only unbound P_{ref} ions are detected, indicating that non-specific ligand binding did not contribute to the mass spectrum. In calculating the K_{assoc} values, the measured ion intensities of all the observed

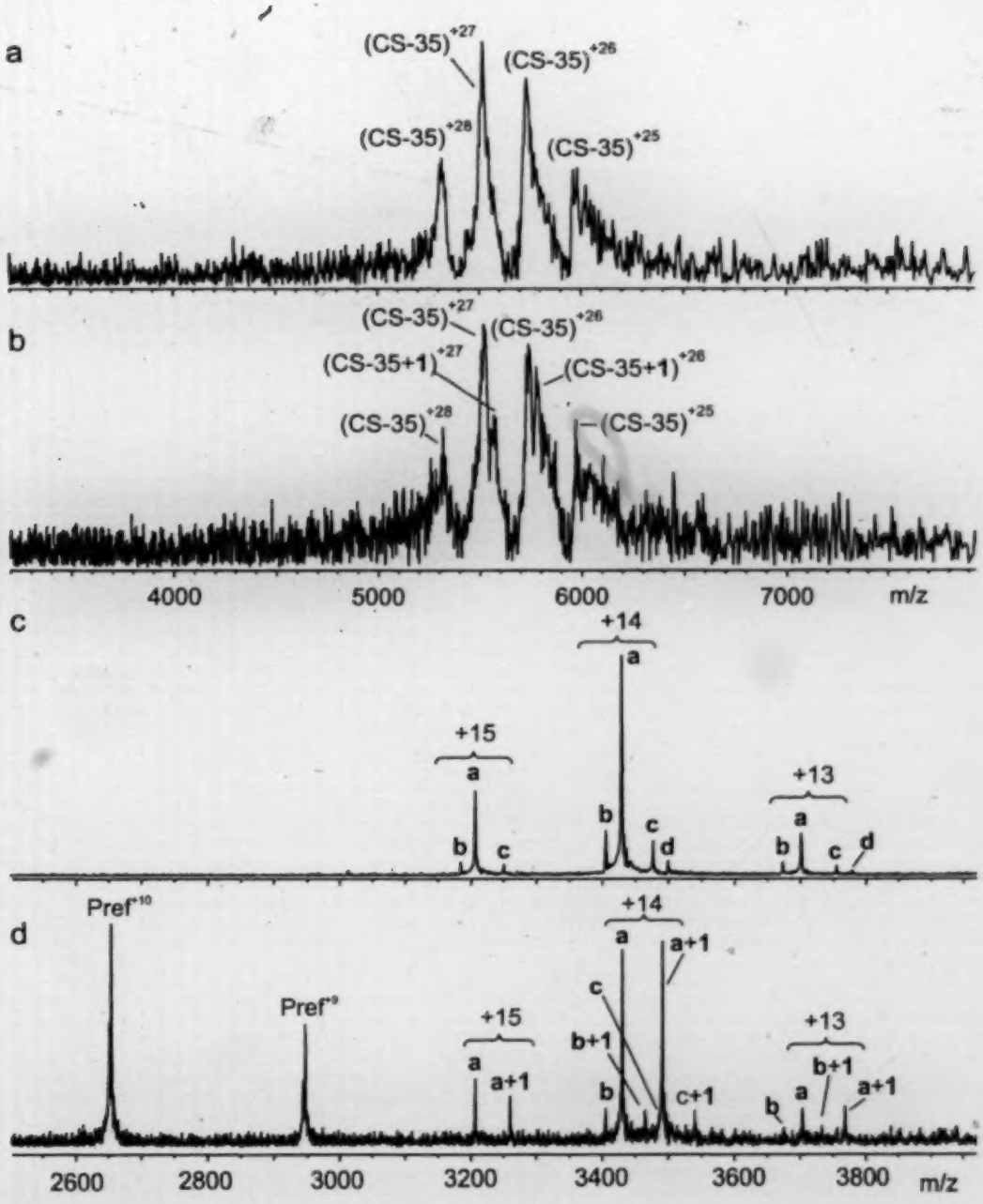

Figure 4.6 Illustrative nanoES mass spectra obtained for aqueous solution of (a) 5 μM mAb CS-35, (b) 5 μM mAb CS-35 mixed with 5 μM **1**, (c) 6.2 μM CS-35 F_{ab}, and (d) 6.2 μM CS-35 F_{AB} with 9.4 μM **1** and 5 μM Pref. Digestion of the mAb CS-35 resulted in four distinct F_{ab} species which are labeled **a**, **b**, **c**, and **d**.

Table 4.1 Binding affinities of oligosaccharides **1 – 6** for CS-35 F_{ab} determined by nanoES-MS, FAC-MS, and ITC at 25°C.[a] K_{assoc} values obtained from FAC-MS[b] measurements have been corrected to take into account the effect of the extra binding site possessed by the mAb compared to the F_{ab}.

Oligosaccharide	Apparent K_{assoc} (M^{-1}) (ES-MS)	Corrected K_{assoc} (M^{-1}) (ES-MS)	K_{assoc} (M^{-1}) (ITC)	K_{assoc} (M^{-1}) (FAC-MS)
1	$1.6 \pm 0.2 \times 10^5$	$1.6 \pm 0.2 \times 10^5$	$1.7 \pm 0.2 \times 10^5$	1×10^5
2	$3 \pm 1 \times 10^3$	$3.4 \pm 0.6 \times 10^2$	Not Tested	Not tested
3	$1.0 \pm 0.6 \times 10^5$	$9.9 \pm 0.5 \times 10^4$	$9 \pm 1 \times 10^4$	8×10^4
4	$8.5 \pm 0.2 \times 10^3$	$6.2 \pm 0.7 \times 10^3$	Not tested	NB[c]
5	$2.9 \pm 0.1 \times 10^4$	$2.6 \pm 0.1 \times 10^4$	Not tested	2×10^4
6	$1.6 \pm 0.4 \times 10^3$	NB[c]	Not tested	NB[c]

a. Error corresponds to one standard deviation.

b. For these measurements mAb CS-35 was biotinylated and loaded onto a 2.5 or 5 cm fused silica capillary column with an i.d. of 250 μM containing streptavidin-controlled-pore glass beads (37 - 74 μM in diameter).[63]

c. NB = no binding detected.

F_{ab} species and their complexes with ligand were added together to obtain values for $I(P^{n+})$ and $I(PL^{n+})$, respectively.

The K_{assoc} values obtained for ligands **1-6** at 25°C are given in Table 4.1. Also listed in the table are binding data obtained using ITC and FAC-MS[47] along with ES-MS derived K_{assoc} values calculated without the correction for non-specific binding (apparent K_{assoc}). These values serve to demonstrate the importance of removing non-specific contributions to K_{assoc}. Non-specific binding leads to an overestimation of K_{assoc}, due to an increase in the relative value of PL^{n+} compared to P^{n+} from the equilibrium ratio in solution. As can be seen in Table 4.1, the effect of non-specific contributions becomes more pronounced for the weak binding ligands **2**, **4**, **5**, and **6**. For **2** binding to CS-35 F_{ab}, the result was a 10 fold overestimate in K_{assoc}. Also, without corrections for nonspecific contributions, **6** was found to possess an apparent K_{assoc} of $1.6 \pm 0.4 \times 10^3\ M^{-1}$ but in fact possesses no specific binding affinity for CS-35.

Comparing the binding affinities of CS-35 F_{ab} for **1–6** allows an estimate of the relative significance of residues A-F to the interaction of F_{ab} to **1**. The low K_{assoc} of **2** and **4** suggests that residue A and E are critical in the binding to CS-35 F_{ab}. The loss of A and E leads to a 500 and 30 fold loss in binding affinity, respectively. The pentasaccharide **3**, which is lacking residue F, possesses a K_{assoc} nearly equal to that of **1**, suggesting F is not a key residue in the interaction. The tetrasaccharide **5**, possessing residues A and E but lacking D and F, exhibited a 5 fold decrease in K_{assoc}. This suggests that residues D and F play only a minor role in the binding of **1** to CS-35 F_{ab}.

This trend in relative binding affinities is consistent with the values obtained from FAC-MS[47,63]. The K_{assoc} values determined for **1**, **3** and **5** at 25 °C are, on average, within

20 % of the estimated values obtained by FAC-MS. The low binding affinity of **4**, as determined by nanoES-MS, explains why no binding was detected for this ligand in the FAC-MS study. Importantly, the K_{assoc} values determined by ITC are in excellent agreement with the values determined by ES-MS.

4.3.2 Determining ΔH_{assoc} for CS-35 Ligand Binding

Temperature-controlled nanoES-MS has recently been used to estimate ΔH_{assoc} and ΔS_{assoc} values for protein-carbohydrate binding.[13] This technique was used in the present study to estimate the thermodynamic parameters for CS-35 binding to **1**, **3**, **4**, and **5**, by measuring their respective K_{assoc} values over a temperature range of 20 to 37°C. The temperature dependence of K_{assoc} was modeled using the linear form of the van't Hoff equation, which assumes a constant heat capacity over the temperature range. The van't Hoff plots for each ligand are given in Figure 4.7. This approach could not be used for **2** due to the absence of detectable (F_{ab} + **2**) complex at elevated temperatures.

The $-\Delta H_{assoc}$ values for CS-35 F_{ab} binding to **1**, **3**, **4**, and **5** were found to be 21.7 ± 0.1, 21.4 ± 0.5, 11.1 ± 0.3, and 19 ± 1 kcal mol^{-1} respectively. The $-\Delta H_{assoc}$ values for **1** and **3** are similar (≈ 21 kcal mol^{-1}), **5** was ~2 kcal mol^{-1} smaller and **4** exhibited the smallest $-\Delta H_{assoc}$, ~10 kcal mol^{-1} lower compared to the value for **1** and **3**. Thus, the trend in $-\Delta H_{assoc}$ follows the trend in K_{assoc} (and $-\Delta G_{assoc}$). The ΔH_{assoc} value for **1** (15.3 ± 0.4 kcal mol^{-1}) and **3** (15.1 ± 0.6 kcal mol^{-1}) interacting with CS-35 F_{ab} were also assessed by ITC. A sample thermogram and corresponding binding isotherm is given in Figure 4.8. Interestingly, the ΔH_{assoc} values obtained from the linear treatment of K_{assoc} values differ significantly with the values obtained from ITC. The difference in the ΔH_{assoc} values

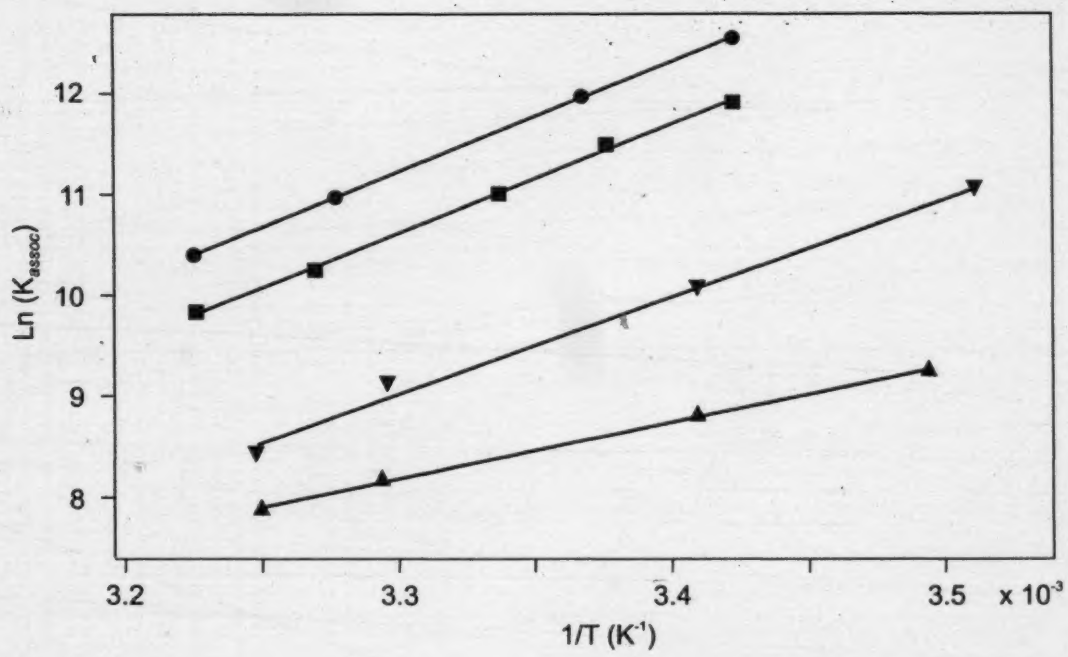

Figure 4.7 Linear van't Hoff plots constructed from nanoES-MS-derived K_{assoc} values obtained at varying temperatures for the association of CS-35 F_{ab} with (●) **1**, (■) **3**, and (▲) **4**, and (▼) **5**.

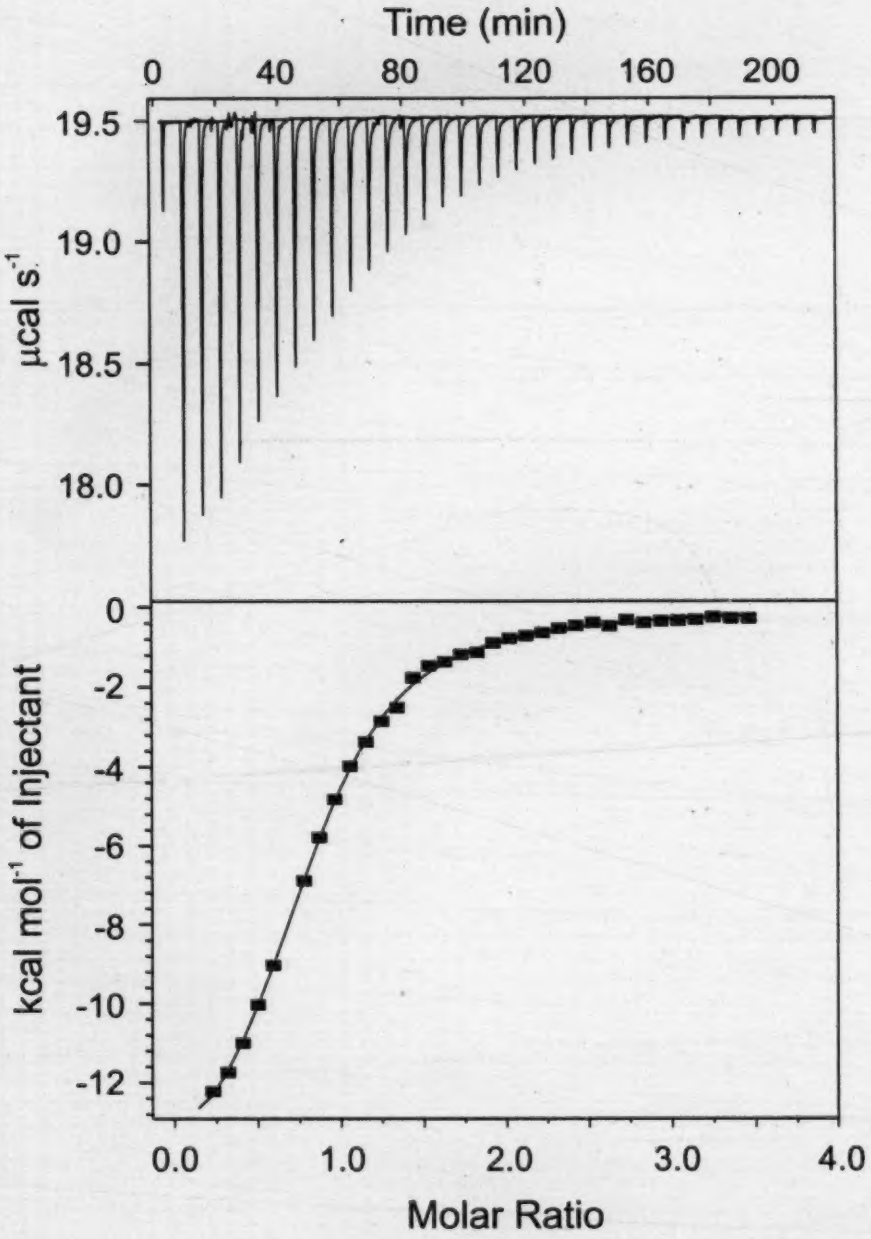

Figure 4.8 Representative (a) thermogram and (b) the corresponding binding isotherm for the titration of 600 µM **1** into a solution of 37.3 µM CS-35 F_{ab} in a 50 mM Tris buffer (pH 7.2) containing 150 mM NaCl. Titrations were carried out on a MicroCal VP-ITC at a temperature of 25°C.

could arise, in part, from the use of the linear form of the van't Hoff equation to analyse the ES-MS derived data. As can be seen in Figure 4, however, the data exhibited excellent linearity for all ligands studied. Alternatively, this discrepancy may arise from the low value of the c constant (≈ 2) in the ITC experiments. Recent theoretical work has suggested that binding isotherms with a low c value (< 10) yield reliable K_{assoc} values but that that ΔH_{assoc} values can be unreliable.[64] Additional support for this explanation is found in the excellent agreement between the K_{assoc} value determined at 30°C by ITC (7.7 ± 0.3 x 10^4 M^{-1}) and the value predicted by the van't Hoff analysis (7.5 ± 0.2 x 10^4 M^{-1}). This suggests that the ES-MS assay provides an accurate measure of the temperature-dependence of the K_{assoc} values and thus yields reliable thermodynamic parameters. It is also worth noting that despite the discrepancies in the absolute values, both methods suggest similar ΔH_{assoc} values for **1** and **3** binding to F_{ab}.

4.4 Results and Discussion –ES-MS Study of a Glycosyltransferase

4.4.1 The Native Oligomeric Form of GTB

Although there exists a great deal of structural information pertaining to GTB,[20,21,37,38] the native oligomeric form of the enzyme under physiological conditions remains unclear. Evidence that GTB forms dimers was obtained in non-denaturing SDS gels and in X-ray crystallographic studies[37]. Recent work, which was based on light scattering data, suggested that the native oligomeric state of GTB is concentration and temperature-dependent.[42] Thus nanoES-MS, which allows a direct measure of protein oligomeric form and ligand binding stoichiometry *in vitro*,[8,9,65] was used to study investigate the native oligomeric form of GTB.

Shown in Figure 4.9a is an illustrative nanoES mass spectrum acquired for an aqueous solution of GTB (10 μM) and ammonium acetate (10 mM, pH 7) in positive ion mode. The protein ions detected by nanoES-MS correspond exclusively to the protonated dimer of GTB, $(GTB_2)^{n+}$, where n = 14 – 16. The measured MW of the GTB dimer, 68 963 ± 4 Da, is consistent with the theoretical value of 68 966 calculated from the amino acid sequence. The complete absence of ions corresponding to monomeric GTB suggests that the enzyme exists exclusively as a homodimer in aqueous solution at neutral pH. To our knowledge, this is the first *direct* experimental determination of the preferred oligomeric state of GTB in aqueous solution. Attempts to thermally dissociate the dimer (into monomer) by increasing the solution temperature were unsuccessful. At temperatures up to 50 °C, only peaks corresponding to the GTB_2^{n+} ions were observed in the mass spectra. Acidification of the solution to pH < 3, however, resulted in the appearance of ions corresponding to both GTB monomer, GTB^{n+}, at n = 11 to 31, and dimer, GTB_2^{n+}, at n 17 = 21 (Figure 4.9b). The crystal structure of the GTB_2 dimer suggests that the dimerization occurs through interactions in the N-terminal region of the protein. Given the presence of a cysteine residue in this region, dimerization could occur via disulfide bond formation. However, the finding that the dimer can be dissociated by decreasing the pH suggests that dimerization of GTB monomers occurs via non-covalent interactions rather than a disulfide bond. The nature of the intersubunit interactions, however, cannot be elucidated from the present measurements.

Using nanoES-MS, the binding affinity and stoichiometry of GTB_2 interacting with substrate molecules was also investigated. It can be seen in Figure 4.10a that the addition of the native disaccharide acceptor (7) for GTB to the nanoES-MS solution leads

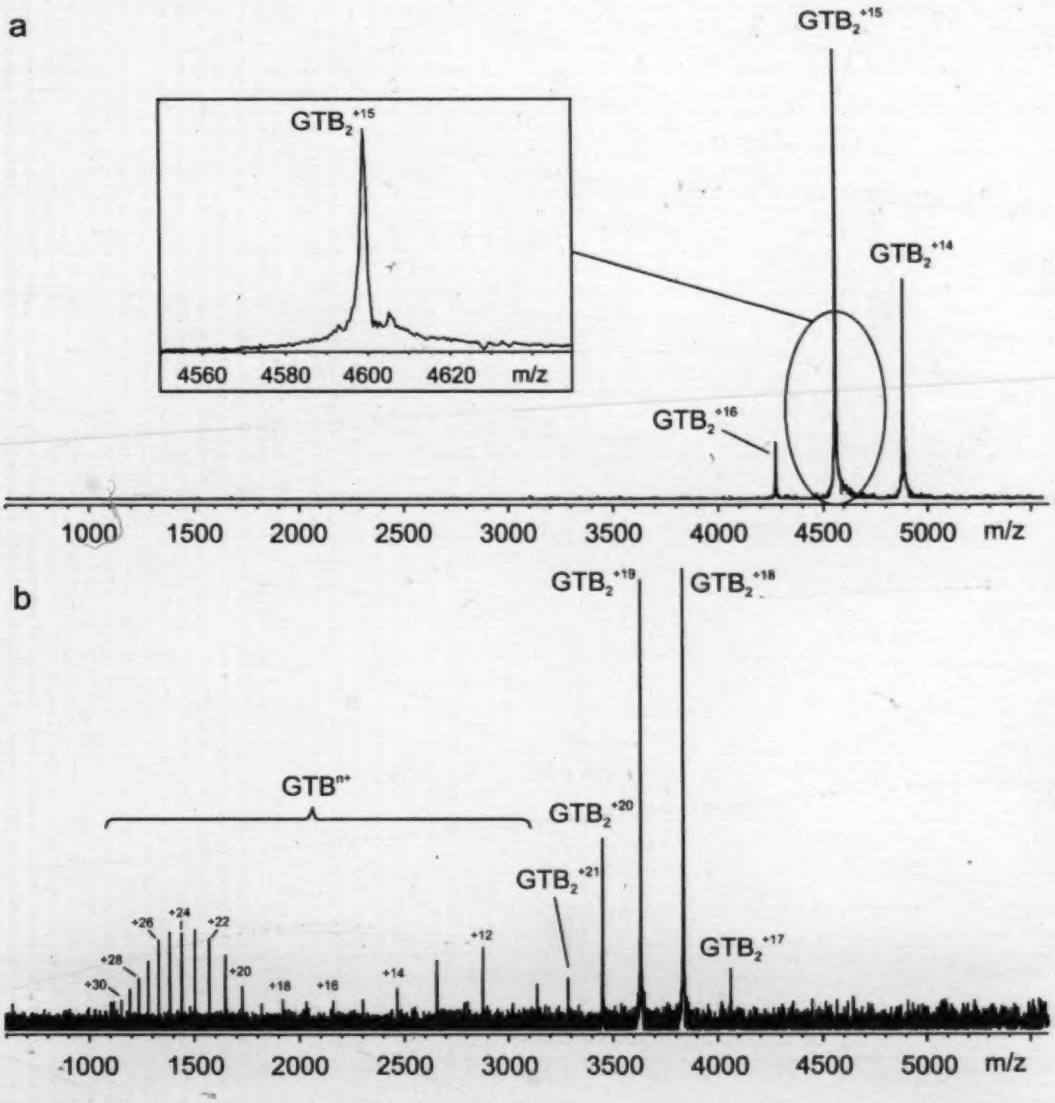

Figure 4.9 Illustrative nanoES mass spectra of an aqueous solution of GTB (12 μM) in a 10 mM ammonium acetate buffer (pH 7) and in a b) 10 mM ammonium acetate buffer containing 10% acetic acid (pH 2.6).

to the formation of $(GTB_2 + 7)^{n+}$ and $(GTB_2 + 2(7))^{n+}$ ions. This suggests that the dimer possesses two acceptor binding sites. It was demonstrated in section 4.3.1 that accounting for non-specific interactions is critical to obtaining reliable K_{assoc} values. It is also important to quantify non-specific interactions in the determination of binding stoichiometry. High concentrations (100 μM) of **7** in the nanoES-MS solution led to the formation of $(GTB_2 + 3(7))^{n+}$ and $(GTB_2 + 4(7))^{n+}$ ions (Figure 4.10b) Based on these measurements, the GTB_2 dimer appears to possess four non-equivalent acceptor binding sites with $K_{assoc,1} = 1.01 \pm 0.03 \times 10^4\ M^{-1}$, $K_{assoc,2} = 8.7 \pm 0.5 \times 10^3\ M^{-1}$, $K_{assoc,3} = 9.9 \pm 0.7 \times 10^3\ M^{-1}$, and $K_{assoc,4} = 3.0 \pm 0.3 \times 10^4\ M^{-1}$. The mass spectrum also revealed extensive binding between **7** and P_{ref}, with $(P_{ref} + 7)^{n+}$ and $(P_{ref} + 2(7))^{n+}$ ions present. Since P_{ref} does not bind **7** specifically, the presence of $(P_{ref} + 7)^{n+}$ and $(P_{ref} + 2(7))^{n+}$ ions must arise from the non-specific attachment of **7** during the ES process. From the observed intensities for the $(P_{ref})^{+n}$, $(P_{ref} + 7)^{n+}$ and $(P_{ref} + 2(7))^{n+}$ ions the non-specific contribution to the observed intensities for the $(GTB_2 + q(7))^{n+}$ ions was quantified. The observed and corrected intensities for each species are given in Figure 4.11. It can be seen from the corrected intensities that the GTB_2 dimer possesses two equivalent acceptor binding sites with $K_{assoc,1} = 1.7 \pm 0.3 \times 10^4\ M^{-1}$ and $K_{assoc,2} = 1.6 \pm 0.4 \times 10^4\ M^{-1}$. This is in good agreement with the apparent K_{dissoc} obtained from kinetic and SPR measurements (40 μM).[39,41] To simplify further discussion, only one K_{assoc} value, an average between $K_{assoc,1}$ and $K_{assoc,2}$, will be reported for the binding of ligands to GTB_2.

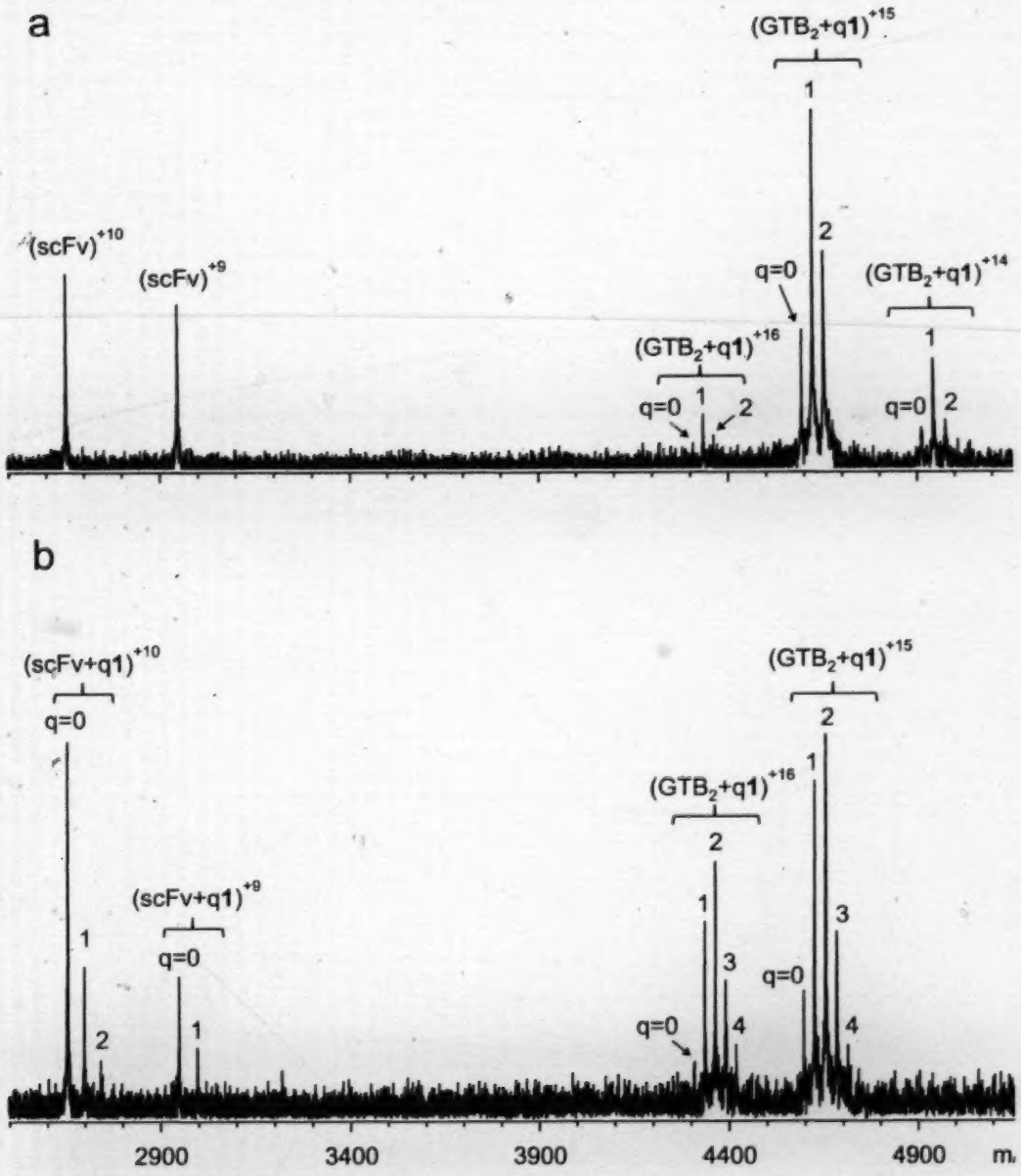

Figure 4.10 Illustrative nanoES mass spectra of solutions consisting of 10 mM ammonium acetate (pH 7), 7 μM GTB_2 and **7** at concentrations of (a) 40 μM and (b) 100 μM. A reference protein, P_{ref} (scFv), was added to both solutions at a concentration of 5 μM to quantify the extent of nonspecific protein-ligand binding during the ES process.

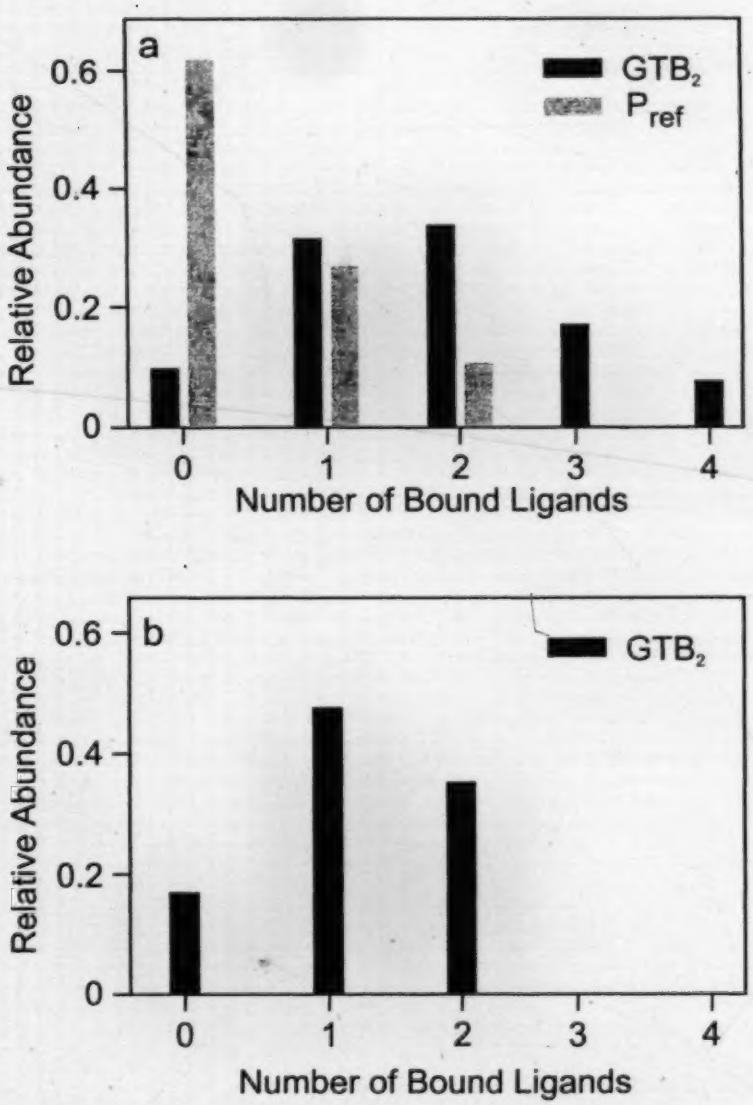

Figure 4.11 (a) Observed intensities for $(GTB_2 + q(7))^{n+}$, q = 0 – 4, ions and for $(P_{ref} + q(7))^{n+}$, q = 0 – 2, ions taken from a nanoES mass spectrum of an aqueous solution consisting of 8.5 μM GTB, 80 μM 7, and 5 μM Pref in a 10 mM ammonium acetate buffer (pH 7). (b) The distribution of nonspecific binding was used to correct the observed intensities by removing the nonspecific contributions to the apparent ion abundances.

4.4.2 NanoES-MS Binding Measurements of GTB_2 with Acceptor Analogues

As mentioned previously, carbohydrates expressed on cell surfaces play critical roles in many life processes. Specifically the ABO(H) antigens have been shown to cause decreased cell motility in human carcinoma cells,[66-68] and thus may play a role in maintaining cellular interactions in benign colorectal tumours. Therefore, inhibitors of glycosyltransferases may provide novel therapeutics and they can also aid in the study of the effects of altered glycosylation. The precise role of the ABO(H) determinants in cellular interactions, as well as the role of other cell surface carbohydrates, are difficult to define. One approach to studying the effects of altered glycosylation is to incubate a cell or tissue sample with a specific inhibitor to a glycosyltransferase of interest.[69] A change in the glycosylation pattern can thus be induced and the affects measured. ES-MS has emerged as a rapid and sensitive technique, requiring no derivitization of ligand or protein, to screen a series of compounds for binding affinity against a target protein.[70] Using nanoES-MS, a series of acceptor analogues for GTB was screened to identify novel GTB inhibitors.

The nanoES-MS binding measurements performed on GTB and ligands **7**, and **9** – **14**, are summarized in Table 4.2. It was expected that **10**, which was previously found to be a competitive inhibitor of GTB,[71] would possess a high K_{assoc} value. Interestingly, the observed binding affinity from nanoES-MS measurements is quite low ($7.1 \pm 3.6 \times 10^2$ M^{-1}). It has been established that gas-phase dissociation of protein-ligand complex in the ES process can occur, especially for small ligands such as mono and disaccharides.[11] This is problematic in the determination of K_{assoc} values since it causes a decrease in the abundance of PL^{n+} ions which leads to an underestimation of the K_{assoc} value. To

Table 4.2 Binding affinities of carbohydrate acceptor analogues **7, 9 – 14** for GTB determined by nanoES-MS.[a,b]

Oligosaccharide	K_{assoc} (M^{-1})
7	$1.7 \pm 0.3 \times 10^4$
9	$2.7 \pm 0.3 \times 10^3$
10	$7.1 \pm 3.6 \times 10^2$
11	$1.7 \pm 0.7 \times 10^4$
12	$5.1 \pm 1.7 \times 10^2$
13	$4.7 \pm 1.8 \times 10^2$
14	$2.9 \pm 1.5 \times 10^2$

a. Error corresponds to one standard deviation.

b. K_{assoc} values represent an average value calculated from the two GTB_2 binding sites

determine whether gas-phase dissociation is occurring for the GTB-ligand complexes, K_{assoc} values were determined for **7** and **11** binding to GTB at different hexapole accumulation times (Figure 4.12). As can be seen in Figure 4.12, even when the ions are stored in the hexapole for extended periods of time (i.e. > 2s), the calculated K_{assoc} values do not change. This suggests that extensive gas-phase dissociation does not occur for the GTB_2 complexes, even for the smallest ligand studied, the monosaccharide **11**. Thus the reason for the observed difference in binding affinity of **10** to GTB obtained from kinetic and ES-MS measurements remains unclear. However, the binding of GTB to **10** was recently investigated using SPR and yielded a value of 7.7×10^2 M^{-1} (unpublished data) which is in excellent agreement with the ES-MS derived value. The monosaccharide **11**, which is a derivative of Gal in which the 3′ hydroxyl group has been replaced with an amino group, exhibited strong binding to GTB_2 with a $K_{assoc} = 1.7 \pm 0.7 \times 10^4$ M^{-1}. This disaccharide acceptor has a binding affinity that is comparable to that of the native disaccharide (**7**), thus making it a potential inhibitor for GTB.

Acceptor analogues **12** – **14** were derivatives of *N*-acetyllactosamine (LacNAc). It is known from previous studies that LacNAc is a poor acceptor in the GTB reaction.[38] The reason for this is believed to be the lack of the fucose moiety, which is present in the native acceptor (**7**). Thus analogues of LacNAc were prepared in which various substitutions were made at the 3′ or 2′ position to compensate for the lack of fucose. The analogues, however, did not possess any significant binding to GTB. From this result, and from the observation that the monosaccharide **11** possesses a high binding affinity for GTB_2, it appears that the fucose moiety does not contribute appreciably to the binding affinity of GTB_2 with **7**, a result that is consistent with recent data from an x-ray

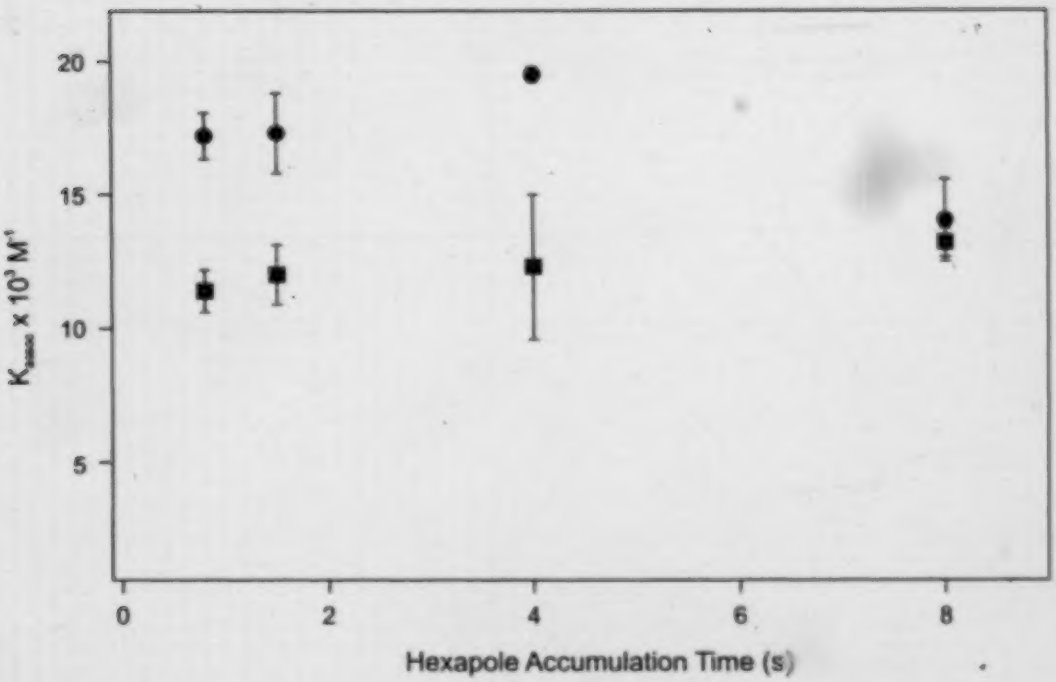

Figure 4.12 Plot of K_{assoc} values obtained at varying hexapole accumulation times for GTB_2 binding to (●) **7** and (■) **11**.

crystallography study of GTB binding to acceptor analogues.[38] Interestingly, the trisaccharide product of the reaction, **9**, also exhibited binding to GTB_2, albeit with a 10 fold decrease in binding affinity compared to the native acceptor (**7**). This is the first report of binding between GTB and its B antigen product.

4.4.3 NanoES-MS Binding Study of GTB_2 to Donor and Donor Fragments

Information regarding the binding of native donor (**8**) to GTB is limited due to a lack of structural information available. Despite much effort, attempts to co-crystallize GTB with **8** have been unsuccessful. Recently, NMR studies have provided fresh insights into the mechanism of donor binding.[41,42] These studies employed a fragment based approach to study donor binding to determine which functionalities are important in donor recognition. The values reported, however, were relative K_{dissoc} values based on an estimated K_{dissoc} from enzyme kinetic measurements.[72] To obtain more precise K_{assoc} values, the direct nanoES-MS approach was employed to study the binding of GTB_2 with native donor (**8**) and the donor fragments **15** and **16** (Figure 4.13). Interestingly, as can be seen in Figure 4.13, the native donor **8** was found to be a weak binder. The galactose moiety, **15**, was also found to bind very weakly to GTB_2. Of the donor species analysed, only UDP (**16**) exhibited strong binding to GTB_2. Thus, in comparing the binding affinity of compounds **8** and **16** to GTB, it appears that the presence of the galactose moiety in **8** destabilizes the (GTB + **8**) complex. This trend in the binding affinity for **8**, **15**, and **16** was also observed in the recent NMR studies.[42] The absolute values, however, obtained for the binding of GTB to **8** and **16** obtained using nanoES-MS differs from those reported from the STD-NMR experiments by a factor of 70 and 10, respectively.

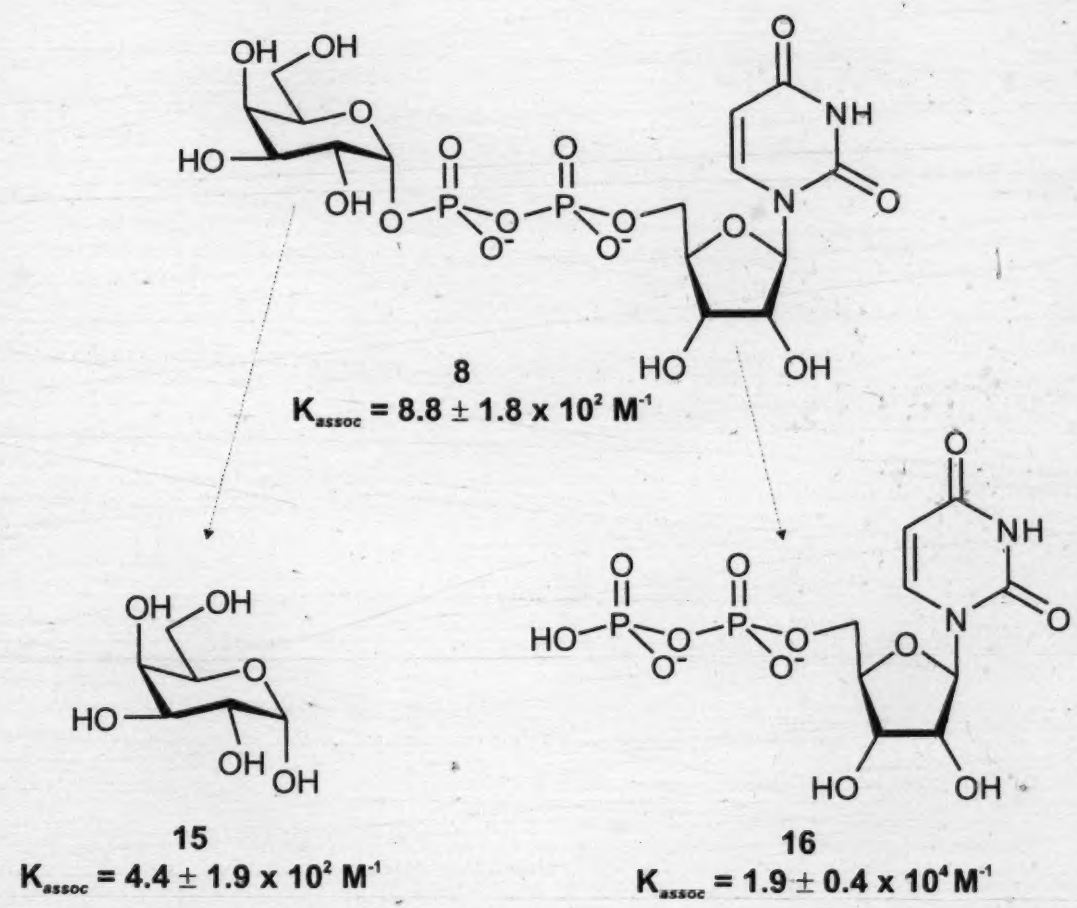

Figure 4.13 Stucture and K_{assoc} values determined by nanoES-MS for GTB donor (**8**) and the donor fragments **15** and **16**.

The reason for this difference is that the relative NMR values are based on a reference K_{dissoc} value of 17 μM for **8** which was obtained from kinetic measurements performed in the presence of Mn^{+2}. The ES-MS derived values, however, were obtained in the absence of any divalent metal ion. It has been previously demonstrated that a divalent metal cofactor has a significant effect on the activity of glycosyltransferases including GTB.[33-36] The role and nature of this cofactor is explored further in the following section.

4.4.4 Role of a Divalent Metal Cofactor in GTB Substrate Binding and Catalysis

The question of which divalent metal ion is the biologically relevant cofactor is currently under debate.[42] To more clearly define the role of the metal cofactor, the binding of GTB_2 with substrate molecules was studied using ES-MS both with and without the addition of a divalent metal ion. As a starting point, the binding of Mn^{+2} and Mg^{+2} to GTB was investigated directly using the ES-MS assay. It has not been established whether ES-MS can be used quantitatively to determine K_{assoc} values for protein-metal binding. This is due to extensive non-specific binding of the charged metal ion to the protein that can occur during the ES process.[73,74] However, the relative binding of different metals to a protein can be estimated using ES-MS.[74] Given in Figure 4.14 are representative nanoES-MS spectra for GTB_2 binding to Mn^{+2} and Mg^{+2}. As can be seen in Figure 4.14a, $(GTB_2 + Mn)^{n+}$ and $(GTB_2 + 2(Mn))^{n+}$ ions were present in the mass spectrum at a Mn^{+2} concentration of 150 μM. The K_{assoc} value, after correcting for non-specific contributions, was found to be $4.1 \pm 2.1 \times 10^2\ M^{-1}$. The $(GTB_2 + Mg)^{n+}$ ions observed in Figure 4.14b, however, appear to be entirely non-specific in nature. Thus it

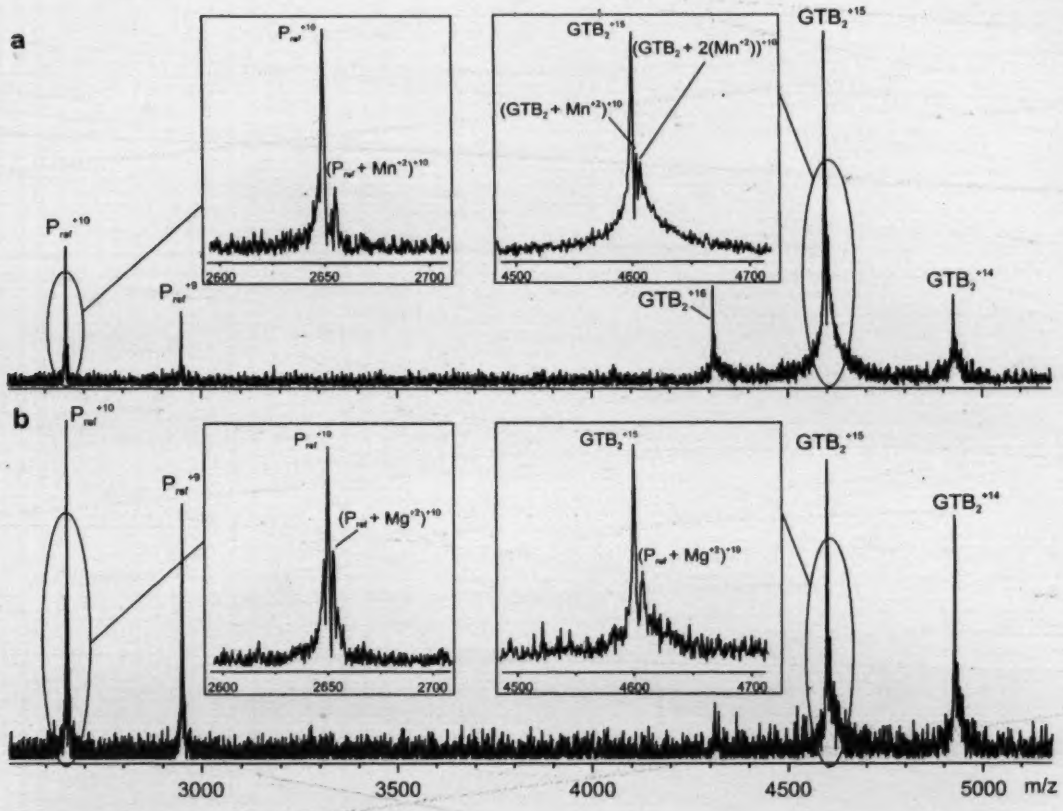

Figure 4.14 Illustrative nanoES mass spectra of solutions consisting of 8 μM GTB_2, 5 μM reference protein (P_{ref}), and either (a) 150 μM Mn^{+2} or (b) 300 μM Mg^{+2} in a 10 mM ammonium acetate buffer (pH 7).

was demonstrated that Mn^{+2} exhibits binding affinity towards GTB whereas Mg^{+2} does not, suggesting that Mn^{+2} is the biologically active cofactor.

To gain a better understanding of the metal cofactor's role, the affect of Mn^{+2} on donor and acceptor binding was studied. The results are summarized in Table 4.3. It was found that the addition of 100 μM Mn^{+2} had no affect on the binding of the native acceptor (**7**) or on the binding of the donor fragment **15** to GTB_2. The K_{assoc} value for UDP (**16**) to GTB_2, however, was enhanced by a factor of 10 in the presence of Mn^{+2}. An even more dramatic effect was found for the binding of **16**. As can be seen in Figure 4.14a, the addition of 150 μM Mn^{+2} to a solution of GTB_2 results in a distribution of $(GTB_2)^{n+}$, $(GTB_2 + Mn)^{n+}$, and $(GTB_2 + 2(Mn))^{n+}$ ions in the mass spectrum with the most dominant species being uncomplexed $(GTB_2)^{n+}$. In the presence of **16**, however, the dominant species was found to be $(GTB_2 + \mathbf{16} + Mn)^{n+}$ and $(GTB_2 + 2(\mathbf{16}) + 2(Mn))^{n+}$ even at low concentrations of Mn^{+2} (10 μM) (Figure 4.15). Thus the binding of **16** to GTB leads to the concomitant binding of a Mn^{+2} ion. The binding of **16** to GTB_2 in the presence of Mn^{+2} is in excellent agreement with the NMR derived value of $2 - 0.7 \times 10^5$ M^{-1}.[42] The affect of Mg^{+2} on the binding of GTB_2 to **16** was also investigated. In the presence of 100 μM Mg^{+2}, a K_{assoc} value of $4.9 \pm 0.8 \times 10^4$ M^{-1} is obtained. This represents a two fold enhancement in the binding of **16** compared to the 10 fold enhancement observed for Mn^{+2}.

Considering the donor specificity of GTB, it is interesting that GTB would exhibit strong binding affinity to **16**. This is a structural element that is common to several other sugar-nucleotide donors, such as UDP-GalNAc and UDP-Glc, which from previous kinetic studies were concluded to be poor substrates of GTB.[72] Thus the galactose

Table 4.3 Binding affinities of the native acceptor (7) and donor fragments **15** and **16** for GTB with and without the addition of 100 μM metal cofactor determined by nanoES-MS.[a,b]

Ligand	K_{assoc} (M^{-1})	K_{assoc} (M^{-1}) (100 μM Mn^{+2})	K_{assoc} (M^{-1}) (100μM Mg^{+2})
7	$1.7 \pm 0.4 \times 10^4$	$1.7 \pm 0.3 \times 10^4$	$1.6 \pm 0.2 \times 10^4$
15	$4 \pm 2 \times 10^2$	$3 \pm 2 \times 10^2$	NB[c]
16	$1.9 \pm 0.4 \times 10^4$	$1.5 \pm 0.2 \times 10^5$	$4.9 \pm 0.8 \times 10^4$

a. Error corresponds to one standard deviation.

b. K_{assoc} values represent an average value calculated from the two GTB_2 binding sites

c. NB = no binding detected.

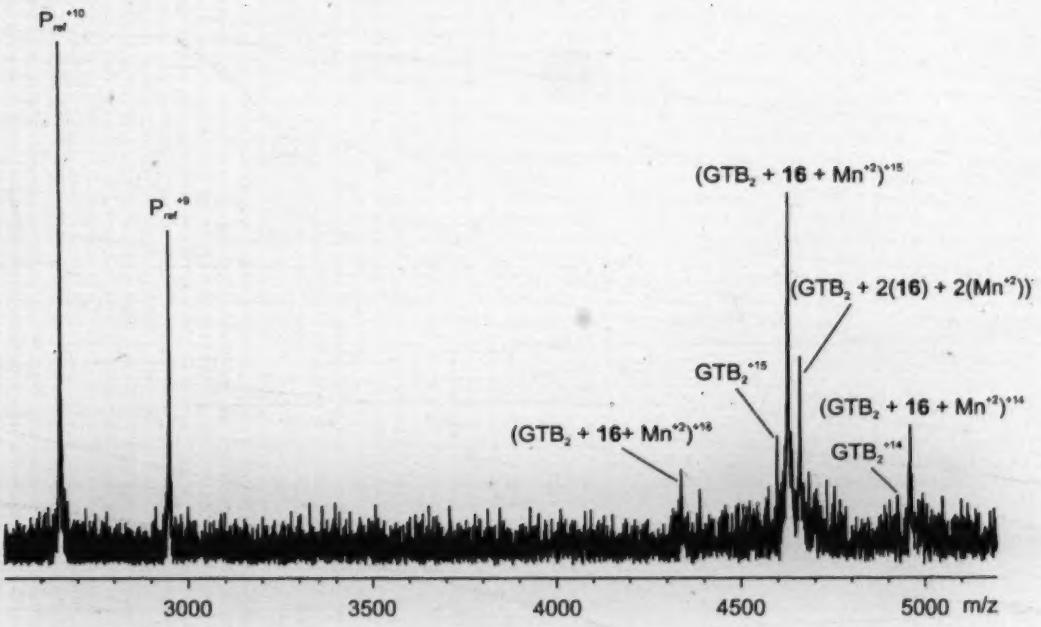

Figure 4.15 Illustrative nanoES mass spectrum of a solution consisting of 8 μM GTB_2, 10 μM **16**, and 10 μM Mn^{+2} in a 10 mM ammonium acetate buffer (pH 7).

residue must play a critical role in determining donor specificity. However, it was found that galactose moiety significantly destabilized the binding of **8**. It was recently suggested from NMR studies of GTB that a metal cofactor is required in order for GTB to form favourable interactions with the galactose moiety of **8**.[41] To investigate this, the effect of Mn^{+2} on the binding of the native donor (**8**) was evaluated. It was not possible to obtain a K_{assoc} value for the binding of **8** to GTB_2 in the presence of Mn^{+2}, however, since the addition of Mn^{+2} to an ES solution containing GTB_2 and **8** led to the rapid hydrolysis of **8** forming the products **15** and **16**. A nanoES mass spectrum of an aqueous solution containing 8 μM GTB_2 and 20 μM **8** in a 10 mM ammonium acetate buffer in the absence of Mn^{+2} is given in Figure 4.16a. Consistent with the previous finding in section 4.4.3 that the native donor (**8**) exhibited weak binding towards GTB there is no detectable $(GTB_2 + \mathbf{8})^{n+}$ ions in the mass spectrum. The addition of 100 μM Mn^{+2} to this solution, however, resulted in a drastic change in the observed mass spectrum (Figure 4.16b). The $(GTB_2 + \mathbf{8} + Mn)^{n+}$ and $(GTB_2 + 2(\mathbf{8}) + 2(Mn))^{n+}$ ions became more abundant compared to Figure 4.16a, suggesting that the binding of **8** was enhanced. This effect could not be quantified, however, since the hydrolysis of **8** was extensive and the appearance of $(GTB_2 + \mathbf{16} + Mn)^{n+}$ and $(GTB_2 + \mathbf{16} + Mn)^{n+}$ ions was observed even 5 minutes after the addition of Mn^{+2}. After 25 minutes, there remained no $(GTB_2 + \mathbf{8})$ complex, suggesting that **8** was completely hydrolysed (Figure 4.16c). It can be deduced from these results that the hydrolysis of the sugar-nucleotide donor occurs rapidly in the presence of Mn^{+2}, which explains why attempts to co-crystallize GTB and **8** were unsuccessful. A possible reason for this, based on structural information from NMR studies of GTB[41] and crystallographic studies of other retaining glycosyltransferases,[44]

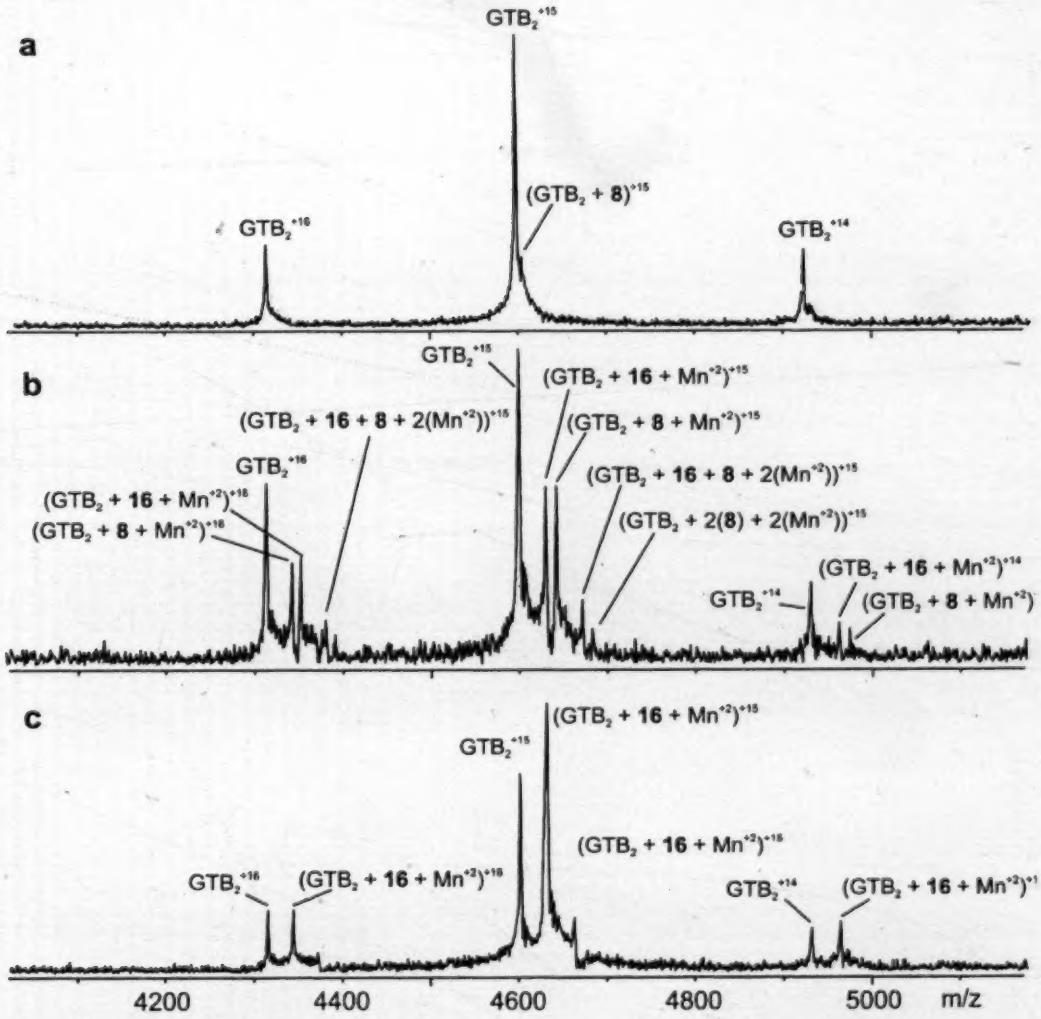

Figure 4.16 Representative nanoES mass spectrum of a solution composed of (a) 8 μM GTB_2 and 20 μM **8**. The addition of 100 μM Mn^{+2} led to the hydrolysis of **8** forming the products **15** and **16** (b) after 5 minutes. After (c) 25 minutes no GTB_2 – **8** complex was detected in the mass spectrum. All solutions were prepared in a 10 mM ammonium acetate buffer (pH 7).

could be that the binding of **8** to GTB in the presence of the metal cofactor leads to a conformational change in **8**, presumably allowing the enzyme to form specific interactions with the galactose residue of **8** and facilitating the transfer reaction. This conformation is sparsely populated in aqueous solutions,[41] which explains why **8** exhibited weak binding affinity to GTB and that no hydrolysis occurred in the absence of Mn^{+2}. To further investigate the question of which metal ion is the biologically relevant cofactor the same experiment was conducted using Mg^{+2} in place of Mn^{+2} (Figure 4.17). As can be seen in the Figure, the addition of 100 μM Mg^{+2} did not lead to the hydrolysis of **8** which was observed for the addition of Mn^{+2}. This is further evidence that Mn^{+2} is the native cofactor.

ES-MS is also well suited to the study of enzyme reactions since it allows the simultaneous detection of substrates, products, reaction intermediates and any non-covalent enzyme substrate complexes.[75] To gain insights into the reaction mechanism of this model glycosyltransferase, the native acceptor (**7**) was added to the reaction mixture containing GTB_2, native donor (**8**) and Mn^{+2}. In Figure 4.18 the nanoES mass spectrum of a solution containing 8 μM GTB_2, 20 μM **7**, 20 μM **8**, and 100 μM Mn^{+2} is given. Again the hydrolysis of **8** appears to be occurring very rapidly, since even 3 minutes after the addition of Mn^{+2}, there was no detectable (GTB_2 + **8**) complex. Using a temperature-controlled ES chamber,[13] the reaction mixture was cooled down to 10°C but still the reaction proceeded to rapidly to obtain information regarding any intermediates. Thus to gain more information regarding intermediates of the GTB transfer reaction, our current instrumental setup needs to be modified. The application of time-resolved ES-MS using a continuous-flow mixing capillary coupled directly in front of the ES source allows

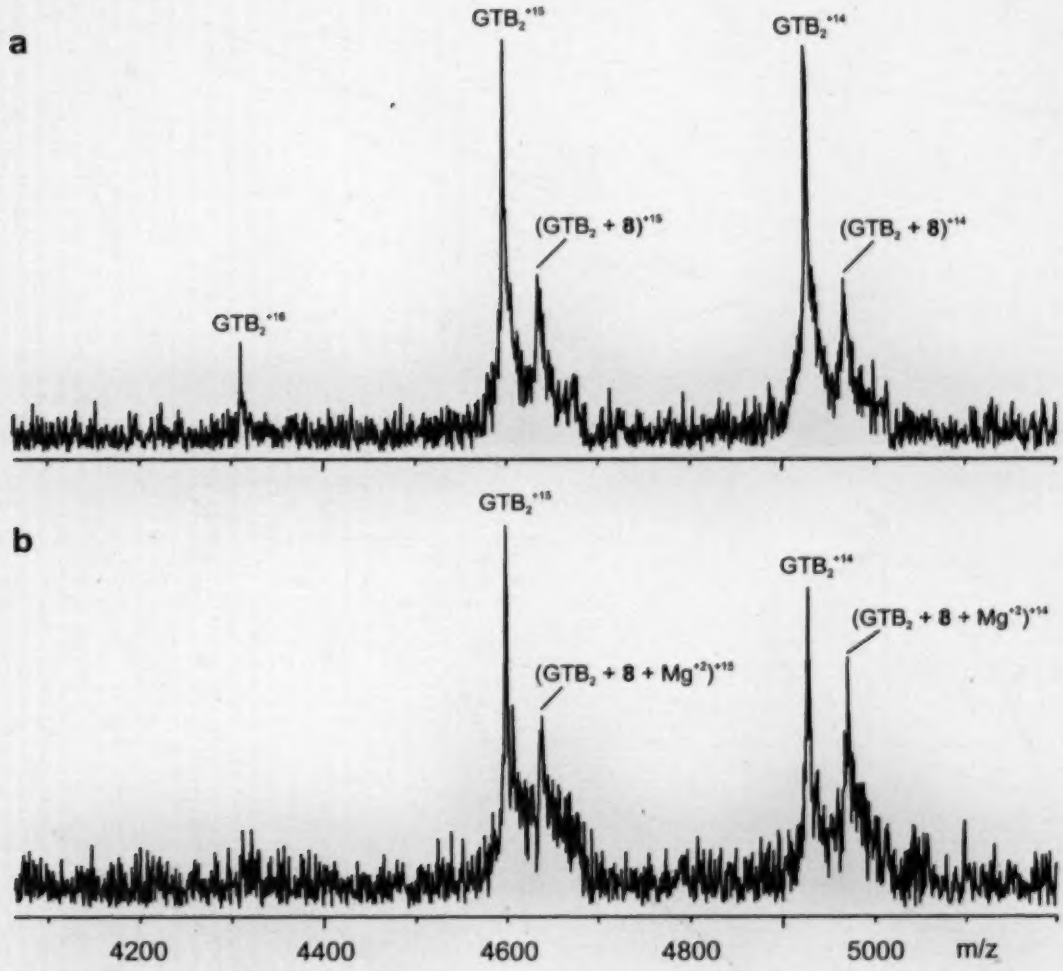

Figure 4.17 Representative nanoES mass spectra of solutions composed of (a) 8 μM GTB_2 and 100 μM **8** alone and (b) in the presence of 100 μM Mg^{+2}. Both solutions were prepared in a 10 mM ammonium acetate buffer (pH 7).

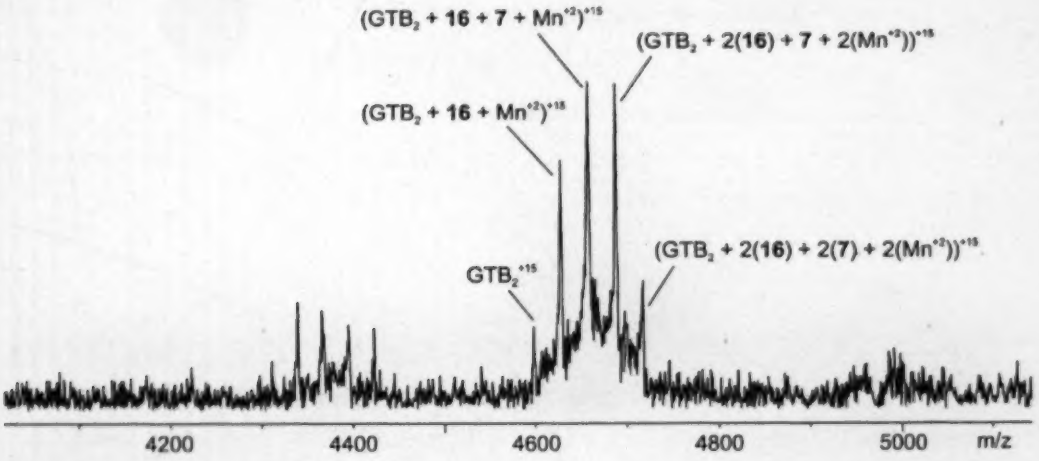

Figure 4.18 Representative nanoES mass spectrum of an aqueous solution composed of 8 μM GTB_2, 20 μM **8**, 20 μM **7**, and 100 μM Mn^{+2} in a 10 mM ammonium acetate buffer (pH 7).

enzyme reactions to be monitored using MS.[75] Using this approach, information pertaining to intermediates and complexes with short lifetimes (≈ 10 ms) for other enzymes, including glycosidases, have been obtained.[76]

These results represent the first application of ES-MS to study a dual substrate reaction and have provided new insights into the role of the metal cofactor in the reaction mechanism of GTB. It was demonstrated that the addition of Mn^{+2} had no affect on acceptor binding, but did enhance the binding of UDP (**16**) by a factor of 10. The largest effect, however, was on catalysis. The addition of Mn^{+2} to a reaction mixture containing GTB_2 and native donor (**8**) led to the rapid donor hydrolysis. Furthermore, in comparing the effects of Mn^{+2} vs. Mg^{+2}, it was found that Mn^{+2} had a greater impact on the binding of **16** to GTB_2 and exhibited a much more significant affect on catalysis. There is an ongoing debate over which metal cation is the biologically relevant cofactor. One of the major arguments against the possibility of Mn^{+2} is that it is present at much lower concentrations in the cell than Mg^{+2} (i.e. 1 μM vs. 500 μM).[42] However, it is very difficult to obtain precise measures of intracellular metal ion concentration and the actual value likely varies significantly between the different intracellular compartments. Also, we have demonstrated that the effect on donor binding and reaction catalysis observed for Mn^{+2} occurs even at low concentrations (10 μM) of Mn^{+2}.

4.5 Conclusions

In the CS-35 F_{ab} ligand binding study, the efficacy of the direct nanoES-MS binding assay to determine the thermodynamic parameters of binding for protein-carbohydrate complexes was demonstrated. The ES-MS derived K_{assoc} values are in

excellent agreement with those obtained using ITC, confirming the accuracy of the direct ES-MS binding assay. Even for weak binding ligands, for which no binding was detected using FAC/MS, accurate K_{assoc} values were obtained. Using this binding data, the key residues in the recognition of **1** by CS-35 F_{ab} were defined. The ΔH_{assoc} of binding was also estimated using temperature-controlled nanoES-MS.[13] One of the greatest benefits of using nanoES-MS to study protein-carbohydrate complexes is the low sample consumption. In ITC, for example, each measurement required ≈6 mg of CS-35 F_{ab} and 0.2 mg of oligosaccharide ligand. Using nanoES-MS, however, quadruplicate analysis of the K_{assoc} value was completed using only 20 μg CS-35 F_{ab} and 1 μg of ligand. This is particularly advantageous in protein-carbohydrate studies such as these, where the synthetic ligand and the antibody can be difficult to obtain in large quantities.

The thermodynamic study of GTB using nanoES-MS provided fresh insights into GTB and its interactions with substrate. It was shown that GTB exists as a dimer in aqueous solution (pH 7) and that the dimerization does not occur via disulfide bond formation. The binding of acceptor and acceptor analogues was investigated using the direct nanoES-MS binding assay. GTB_2 was shown to possess two equivalent acceptor binding sites and a potential inhibitor to GTB was discovered. This monosaccharide (**11**), which is lacking a fucose residue present in the native disaccharide acceptor (**7**), possesses a binding affinity to GTB that is comparable to **7**, suggesting that the fucose residue is not critical in the binding of **7** to GTB.

Interestingly, the native donor substrate (**8**), was found to possess weak binding affinity towards GTB. In fact, the only donor species that exhibited significant binding to GTB in the absence of a divalent metal cofactor was UDP (**16**). The role and nature of

this metal cofactor was also investigated using nanoES-MS. It was found that Mn^{+2} was not critical in the binding of the donor species, **16**, but did yield a 10 fold enhancement in the measured binding affinity. The most dramatic effect, however, was on catalysis. Hydrolysis of **8** occurred very rapidly upon addition of even low concentrations of Mn^{+2}. Our findings are consistent with the NMR studies examining the structure of the GTB-donor complex.[41] Direct binding measurements between GTB and two potential cofactors, Mn^{+2} and Mg^{+2}, demonstrated that Mn^{+2} possesses weak binding affinity towards GTB while no binding was detected between GTB and Mg^{+2}. Also, the hydrolysis of **8** by GTB observed for Mn^{+2} was not observed for Mg^{+2}. Thus we propose that Mn^{+2} is the biologically relevant cofactor.

4.6 Literature Cited

(1) Helenius, A.; Aebi, M. *Science* **2001**, *291*, 2364-2369.

(2) Lis, H.; Sharon, N. *Chemical Reviews* **1998**, *98*, 637-674.

(3) Rudd, P. M.; Elliott, T.; Cresswell, P.; Wilson, I. A.; Dwek, R. A. *Science* **2001**, *291*, 2370-2376.

(4) Bundle, D. R.; Sigurskjold, B. W. In *Neoglycoconjugates, Pt B*, 1994; Vol. 247, pp 288-305.

(5) Wiseman, T.; Williston, S.; Brandts, J. F.; Lin, L. N. *Analytical Biochemistry* **1989**, *179*, 131-137.

(6) Lundquist, J. J.; Toone, E. J. *Chemical Reviews* **2002**, *102*, 555-578.

(7) Schriemer, D. C.; Hindsgaul, O. *Combinatorial Chemistry & High Throughput Screening* **1998**, *1*, 155-170.

(8) Ishigai, M.; Langridge, J. I.; Bordoli, R. S.; Gaskell, S. J. *Journal of the American Society For Mass Spectrometry* **2000**, *11*, 606-614.

(9) Kitova, E. N.; Kitov, P. I.; Bundle, D. R.; Klassen, J. S. *Glycobiology* **2001**, *11*, 605-611.

(10) Siebert, H. C.; Born, K.; Andre, S.; Frank, M.; Kaltner, H.; von der Lieth, C. W.; Heck, A. J. R.; Jimenez-Barbero, J.; Kopitz, J.; Gabius, H. J. *Chemistry-A European Journal* **2005**, *12*, 388-402.

(11) Wang, W. J.; Kitova, E. N.; Klassen, J. S. *Analytical Chemistry* **2003**, *75*, 4945-4955.

(12) Wang, W. J.; Kitova, E. N.; Klassen, J. S. In *Recognition of Carbohydrates in Biological Systems Pt A: General Procedures*, 2003; Vol. 362, pp 376-397.

(13) Daneshfar, R.; Kitova, E. N.; Klassen, J. S. *Journal of the American Chemical Society* **2004**, *126*, 4786-4787.

(14) Kaur, D.; Lowary, T. L.; Vissa, V. D.; Crick, D. C.; Brennan, P. J. *Microbiology-Sgm* **2002**, *148*, 3049-3057.

(15) Dietrich, J.; Lundberg, C. V.; Andersen, P. *Tuberculosis* **2006**, *86*, 163-168.

(16) Orme, I. M. *Vaccine* **2006**, *24*, 2-19.

(17) Skeiky, Y. A. W.; Sadoff, J. C. *Nature Reviews Mircobiology* **2006**, *4*, 469-476.

(18) Hunter, S. W.; Gaylord, H.; Brennan, P. J. *Journal of Biological Chemistry* **1986**, *261*, 2345-2351.

(19) Yamamoto, F.; Clausen, H.; White, T.; Marken, J.; Hakomori, S. I. *Nature* **1990**, *345*, 229-233.

(20) Nguyen, H. P.; Seto, N. O. L.; Cai, Y.; Leinala, E. K.; Borisova, S. N.; Palcic, M. M.; Evans, S. V. *Journal of Biological Chemistry* **2003**, *278*, 49191-49195.

(21) Patenaude, S. I.; Seto, N. O. L.; Borisova, S. N.; Szpacenko, A.; Marcus, S. L.; Palcic, M. M.; Evans, S. V. *Nature Structural Biology* **2002**, *9*, 685-690.

(22) Breton, C.; Mucha, J.; Jeanneau, C. *Biochimie* **2001**, *83*, 713-718.

(23) Hakomori, S.; Kannagi, R. **1983**, *71*, 231-251.

(24) Hounsell, E. F.; Feizi, T. *Medical Biology* **1982**, *60*, 227-236.

(25) Kim, Y. J.; Varki, A. *Glycoconjugate Journal* **1997**, *14*, 569-576.

(26) Laferte, S.; Dennis, J. W. *Cancer Research* **1988**, *48*, 4743-4748.

(27) Saitoh, O.; Wang, W. C.; Lotan, R.; Fukuda, M. *Journal of Biological Chemistry* **1992**, *267*, 5700-5711.

(28) Kleene, R.; Berger, E. G. *Biochimica et Biophysica Acta* **1993**, *1154*, 283-325.

(29) Lazar, K.; Walker, S. *Current Opinion in Chemical Biology* **2002**, *6*, 786-793.

(30) Hancock, S. M.; D Vaughan, M.; Withers, S. G. *Current Opinion in Chemical Biology* **2006**, *10*, 509-519.

(31) Breton, C.; Bettler, E.; Joziasse, D. H.; Geremia, R. A.; Imberty, A. *Journal of Biochemistry* **1998**, *123*, 1000-1009.

(32) Busch, C.; Hofmann, F.; Selzer, J.; Munro, S.; Jeckel, D.; Aktories, K. *Journal of Biological Chemistry* **1998**, *273*, 19566-19572.

(33) Murray, B. W.; Wittmann, V.; Burkart, M. D.; Hung, S. C.; Wong, C. H. *Biochemistry* **1997**, *36*, 823-831.

(34) Tarbouriech, N.; Charnock, S. J.; Davies, G. J. *Journal of Molecular Biology* **2001**, *314*, 655-661.

(35) Vandeneijnden, D. H.; Blanken, W. M.; Winterwerp, H.; Schiphorst, W. *European Journal of Biochemistry* **1983**, *134*, 523-530.

(36) Zhang, Y. N.; Wang, P. G.; Brew, K. *Journal of Biological Chemistry* **2001**, *276*, 11567-11574.

(37) Lee, H. J.; Barry, C. H.; Borisova, S. N.; Seto, N. O. L.; Zheng, R. X. B.; Blancher, A.; Evans, S. V.; Palcic, M. M. *Journal of Biological Chemistry* **2005**, *280*, 525-529.

(38) Letts, J. A.; Rose, N. L.; Fang, Y. R.; Barry, C. H.; Borisova, S. N.; Seto, N. O. L.; Palcic, M. M.; Evans, S. V. *Journal of Biological Chemistry* **2006**, *281*, 3625-3632.

(39) Marcus, S. L.; Polakowski, R.; Seto, N. O. L.; Leinala, E.; Borisova, S.; Blancher, A.; Roubinet, F.; Evans, S. V.; Palcic, M. M. *Journal of Biological Chemistry* **2003**, *278*, 12403-12405.

(40) Seto, N. O. L.; Palcic, M. M.; Compston, C. A.; Li, H.; Bundle, D. R.; Narang, S. A. *Journal of Biological Chemistry* **1997**, *272*, 14133-14138.

(41) Angulo, J.; Langpap, B.; Blume, A.; Biet, T.; Meyer, B.; Krishna, N. R.; Peters, H.; Palcic, M. M.; Peters, T. *Journal of the American Chemical Society* **2006**, *128*, 13529-13538.

(42) Blume, A.; Angulo, J.; Biet, T.; Peters, H.; Benie, A. J.; Palcic, M.; Peters, T. *Journal of Biological Chemistry* **2006**, *281*, 32728-32740.

(43) Kamath, V. P.; Seto, N. O. L.; Compston, C. A.; Hindsgaul, O.; Palcic, M. M. *Glycoconjugate Journal* **1999**, *16*, 599-606.

(44) Persson, K.; Ly, H. D.; Dieckelmann, M.; Wakarchuk, W. W.; Withers, S. G.; Strynadka, N. C. J. *Nature Structural Biology* **2001**, *8*, 166-175.

(45) D'Souza, F. W.; Lowary, T. L. *Organic Letters* **2000**, *2*, 1493-1495.

(46) Palcic, M. M.; Heerze, L. D.; Pierce, M.; Hindsgaul, O. *Glycoconjugate Journal* **1988**, *5*, 49-63.

(47) Rademacher, C.; Shoemaker, G. K.; Kim, H. S.; Zheng, R. B.; Liu, C.; Klassen, J. S.; Peters, T.; Lowary, T. L. *Manuscript in Preparation.*

(48) Seto, N. O. L.; Palcic, M. M.; Hindsgaul, O.; Bundle, D. R.; Narang, S. A. *European Journal of Biochemistry* **1995**, *234*, 323-328.

(49) Zdanov, A.; Li, Y.; Bundle, D. R.; Deng, S. J.; Mackenzie, C. R.; Narang, S. A.; Young, N. M.; Cygler, M. *Proceedings of the National Academy of Sciences of the United States of America* **1994**, *91*, 6423-6427.

(50) Daniel, J. M.; Friess, S. D.; Rajagopalan, S.; Wendt, S.; Zenobi, R. *International Journal of Mass Spectrometry* **2002**, *216*, 1-27.

(51) Tanford, C. *Physical Chemistry of Macromolecules*; John Wiley & Sons: New York, 1961.

(52) Sun, J.; Kitova, E. N.; Klassen, J. S. *Analytical Chemistry* **2007**, *79*, 416-425.

(53) Sun, J. X.; Kitova, E. N.; Wang, W. J.; Klassen, J. S. *Analytical Chemistry* **2006**, *78*, 3010-3018.

(54) Van Berkel, G. J.; Asano, K. G.; Schnier, P. D. *Journal of the American Society for Mass Spectrometry* **2001**, *12*, 853-862.

(55) VanBerkel, G. J.; Zhou, F. M.; Aronson, J. T. *International Journal of Mass Spectrometry and Ion Processes* **1997**, *162*, 55-67.

(56) Sannes-Lowery, K. A.; Hofstadler, S. A. *Journal of the American Society for Mass Spectrometry* **2000**, *11*, 1-9.

(57) Gavin, A. C.; Bosche, M.; Krause, R.; Grandi, P.; Marzioch, M.; Bauer, A.; Schultz, J.; Rick, J. M.; Michon, A. M.; Cruciat, C. M.; Remor, M.; Hofert, C.; Schelder, M.; Brajenovic, M.; Ruffner, H.; Merino, A.; Klein, K.; Hudak, M.; Dickson, D.; Rudi, T.; Gnau, V.; Bauch, A.; Bastuck, S.; Huhse, B.; Leutwein, C.;

Heurtier, M. A.; Copley, R. R.; Edelmann, A.; Querfurth, E.; Rybin, V.; Drewes, G.; Raida, M.; Bouwmeester, T.; Bork, P.; Seraphin, B.; Kuster, B.; Neubauer, G.; Superti-Furga, G. *Nature* **2002**, *415*, 141-147.

(58) Wang, W. J.; Kitova, E. N.; Klassen, J. S. *Analytical Chemistry* **2005**, *77*, 3060-3071.

(59) Bundle, D. R.; Alibes, R.; Nilar, S.; Otter, A.; Warwas, M.; Zhang, P. *Journal of the American Chemical Society* **1998**, *120*, 5317-5318.

(60) Chervenak, M. C.; Toone, E. J. *Journal of the American Chemical Society* **1994**, *116*, 10533-10539.

(61) Christensen, T.; Toone, E. J. In *Recognition of Carbohydrates in Biological Systems Pt A: General Procedures*, 2003; Vol. 362, pp 486-504.

(62) Bennett, K. L.; Smith, S. V.; Truscott, R. J. W.; Sheil, M. M. *Analytical Biochemistry* **1997**, *245*, 17-27.

(63) Kim, H. S., University of Alberta, Edmonton, 2006.

(64) Turnbull, W. B.; Daranas, A. H. *Journal of the American Chemical Society* **2003**, *125*, 14859-14866.

(65) Loo, J. A. *Mass Spectrometry Reviews* **1997**, *16*, 1-23.

(66) Ichikawa, D.; Handa, K.; Hakomori, S. *International Journal of Cancer Research* **1998**, *76*, 284-289.

(67) Ichikawa, D.; Handa, K.; Withers, D. A.; Hakomori, S. *Cancer Research* **1997**, *57*, 3092-3096.

(68) Prokopishyn, N. L.; Puzon-McLaughlin, W.; Takada, Y.; Laferte, S. *Journal of Cellular Biochemistry* **1999**, *72*, 189-209.

(69) Laferte, S.; Chan, N. W. C.; Sujino, K.; Lowary, T. L.; Palcic, M. M. *European Journal of Biochemistry* **2000**, *267*, 4840-4849.

(70) Hofstadler, S. A.; Sannes-Lowery, K. A. *Nature Reviews Drug Discovery* **2006**, *5*, 585-595.

(71) Lowary, T. L.; Hindsgaul, O. *Carbohydrate Research* **1993**, *249*, 163-195.

(72) Seto, N. O. L.; Compston, C. A.; Evans, S. V.; Bundle, D. R.; Narang, S. A.; Palcic, M. M. *European Journal of Biochemistry* **1999**, *259*, 770-775.

(73) Potier, N.; Rogniaux, H.; Chevreux, G.; Van Dorsselaer, A. In *Biological Mass Spectrometry*, 2005; Vol. 402, pp 361-389.

(74) Whittal, R. M.; Ball, H. L.; Cohen, F. E.; Burlingame, A. L.; Prusiner, S. B.; Baldwin, M. A. *Protein Science* **2000**, *9*, 332-343.

(75) Liesener, A.; Karst, U. *Analytical and Bioanalytical Chemistry* **2005**, *382*, 1451-1464.

(76) Tull, D.; Miao, S. C.; Withers, S. G.; Aebersold, R. *Analytical Biochemistry* **1995**, *224*, 509-514.

Chapter 5

Equivalency of Binding Sites in Protein-Ligand Complexes Revealed by Time-Resolved Tandem Mass Spectrometry

5.1 Introduction

The electrospray ionization mass spectrometry (ES-MS) assay is an established method for determining the binding stoichiometry and affinity of protein-ligand interactions, as well as other non-covalent biological complexes, in solution.[1] Tandem MS, which involves the gas-phase dissection of protein-ligand complexes, adds another dimension to the analysis which allows the structure of noncovalent complexes to be studied using MS. While the relationship between the higher order structure of protein complexes in solution and in the gas phase remains hotly debated,[2] there is growing evidence that elements of higher order structure, including the specific intermolecular interactions, are preserved during the ES/desolvation process.[7-9] This raises the exciting possibility of combining ES-MS and gas phase methods, in particular dissociation techniques, to gain insight into the nature of protein-ligand interactions present in solution.

Here, we show for the first time that the number of equivalent ligand binding sites within proteins and multi-subunit protein complexes in solution can be established by time-resolved thermal dissociation experiments performed on the gaseous protein-ligand complexes. The gas phase assay is demonstrated for two model protein complexes: the homodimer of the human ABO(H) blood group B glycosyltransferase (GTB_2) binding with its acceptor substrate, the disaccharide α-L-Fuc*p*-(1→2)-β-D-Gal*p*-O$(CH_2)_7CH_3$ (**1**),

and the homotetramer streptavidin (S_4) binding the small molecule ligand, biotin (**2**). Shown in Figure 5.1 are the intermolecular interaction maps for the two complexes derived from the analysis of the crystal structure.[3-6]

5.2 Experimental

5.2.1 Protein and Ligand Preparation

The human blood group enzyme, GTB (monomer MW 34 483 Da), and the recombinant single chain variable fragment (scFv) of the monoclonal antibody Se155-4 (MW 26 539 Da) were expressed in *E. coli* and purified using procedures described previously.[10-12] Recombinant streptavidin (monomer MW 13 271 Da) was purchased from Roche. All protein solutions were exchanged into a buffer consisting of 50 mM ammonium acetate (pH 7), except for scFv which was exchanged directly into Milli-Q water, using an Amicon microconcentrator with a molecular weight cutoff of 10 kDa. All protein concentrations were determined by lyophilizing a known volume of the protein solutions and measuring the corresponding mass of protein. The protein stock solutions were stored at -4 °C. The synthetic GTB acceptor (**1**) was prepared at the University of Alberta and biotin (**2**) was purchased from Sigma-Aldrich (99% pure). Ligand stock solutions were prepared by dissolving the ligand into Milli-Q water. The ligand stock solutions were stored at -20 °C. NanoES solutions were prepared from these stock solutions and used for MS analysis immediately after preparation.

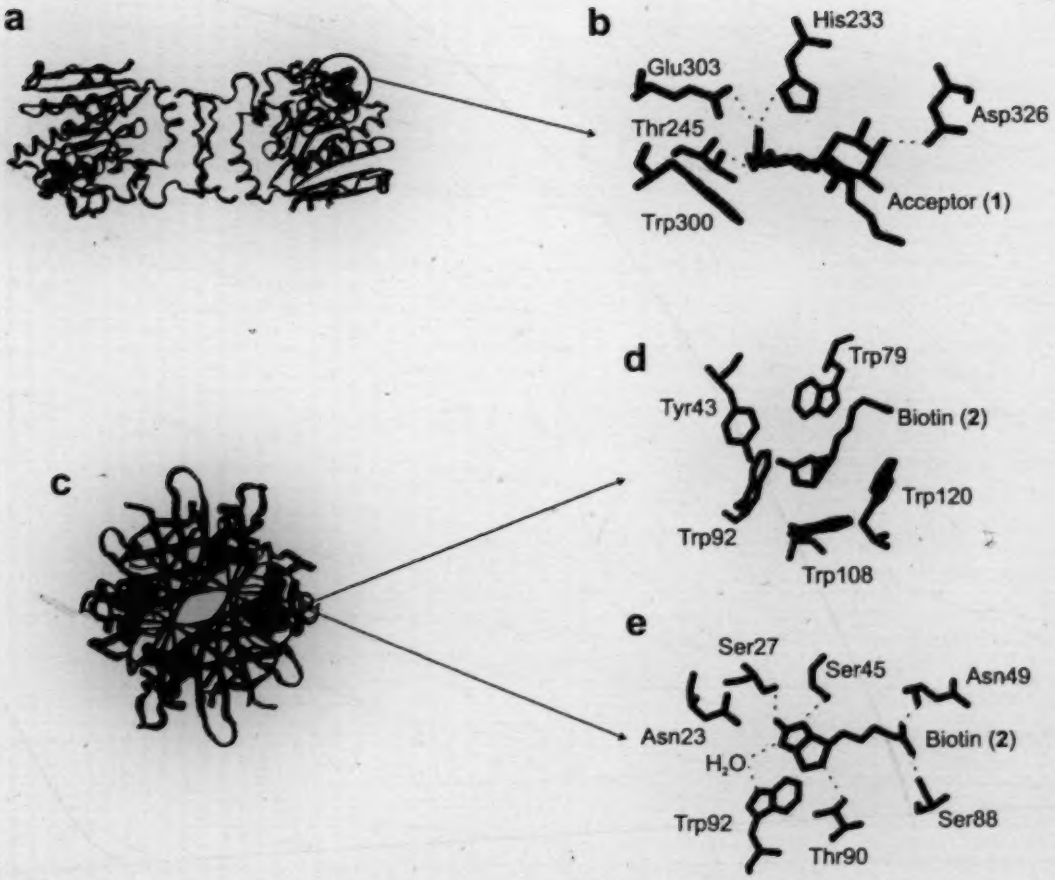

Figure 5.1 (a) Crystal structure of the GTB dimer complexes with acceptor (GTB_2 + 2(**1**)) and (b) the structure of the acceptor binding site based on the published crystal structure.[3-5] (c) Crystal structure of the streptavidin tetramer bound to 4 molecules of biotin (**2**) and the key (d) hydrophobic and (e) hydrogen bonding interactions in the biotin binding pocket.[6]

5.2.2 Mass Spectrometry

All experimental measurements were performed using an Apex II 9.4 T FT-ICR/MS instrument (Bruker, Billerica, MA) equipped with a modified external nanoES ion source. NanoES tips, with an outer diameter of 4 to 7 μm, were pulled from aluminosilicate tubes (1 mm o.d., 0.68 mm i.d.) using a P-2000 micropipette puller (Sutter Instruments, Novato, CA). A platinum wire inserted into one end of the nanoES tip was used to establish electrical contact with the nanoES solution. A potential of +600 to +800 V was applied to the platinum wire in the nanoES tip in order to spray the solution. The tip was positioned 1 - 2 mm from a stainless steel sampling capillary using a microelectrode holder. Typical solution flow rates were 20-50 nL/min, depending on the diameter of the nanoES tip and the voltage used. Charged droplets and solvated ions emitted by the nanoES tip were introduced into the vacuum chamber of the mass spectrometer through a heated stainless steel sampling capillary (0.43 mm i.d.) maintained at an external temperature of 66 °C. The gaseous ions sampled by the capillary (+48 V) were transmitted through a skimmer (+4 V) and accumulated for 5 s in an rf hexapole (+600 V p-p). The ions were subsequently ejected from the hexapole and injected at -2700 V into the bore of the superconducting magnet, decelerated and introduced into the ion cell. Two flexible heating blankets placed around the portion of the vacuum tube that surrounds the ion cell were used to control the temperature of the ion cell for the BIRD experiments. The typical base pressure for the instrument was ~5 x 10^{-10} mbar. Data acquisition was performed using the XMASS software (version 5.0). The time-domain signals, consisting of the sum of 50 transients containing 128 K data points per transient, were subjected to one zero-fill prior to Fourier-transformation.

5.3 Results and Discussion

5.3.1 Probing Equivalency of GTB_2 Binding Sites in the Gas-Phase

In Chapter 4 it was shown by nanoES-MS analysis that GTB exists exclusively as a non-covalent homodimer in aqueous solution at neutral pH and 25 °C. It was also shown that GTB_2 possesses two equivalent binding sites for **1**, each with an intrinsic affinity (K_{assoc}) of 1.2×10^4 M^{-1} at 25 °C. This finding is consistent with results of an analysis of the crystal structure of the GTB dimer bound with two molecules of **1**.[3] NanoES-MS performed on an aqueous solution of GTB_2 (7 μM) and **1** (40 μM) and 50 mM ammonium acetate yields ions corresponding to protonated GTB_2 bound to $q = 0 - 2$ molecules of **1**, i.e. $(GTB_2 + q\mathbf{1})^{n+}$, at n = 14 - 16 (Figure 5.2). Using a newly developed method for identifying nonspecific protein-ligand complexes formed during the ES process,[13] it was confirmed that the $(GTB_2 + \mathbf{1})^{n+}$ and $(GTB_2 + 2(\mathbf{1}))^{n+}$ ions arise exclusively from specific binding in solution. As can be seen in Figure 5.2 the extent of non-specific binding can be quite significant at high concentrations of ligand (i.e. > 80 μM), thus a low concentration, 40 μM, of **1** was used to ensure $(GTB_2 + q\mathbf{1})^{+15}$ complex ions originated exclusively from specific interactions in solution.

After establishing the equivalency of GTB_2 binding sites in solution, time-resolved tandem MS was used to probe binding site equivalency in the gas-phase. Sample BIRD mass spectra for the $(GTB_2 + q\mathbf{1})^{15+}$ ion are given in Figure 5.3. As is demonstrated in the figure, BIRD of the $(GTB_2 + q\mathbf{1})^{15+}$ ions proceeds by the sequential loss of neutral **1** (eq 5.1). From BIRD mass spectra acquired at different reaction times, it is possible to evaluate the reaction kinetics. Shown in Figure 5.4 are kinetic data, plotted as the natural log of the normalized intensity of the reactant ion (I/I_o) versus reaction

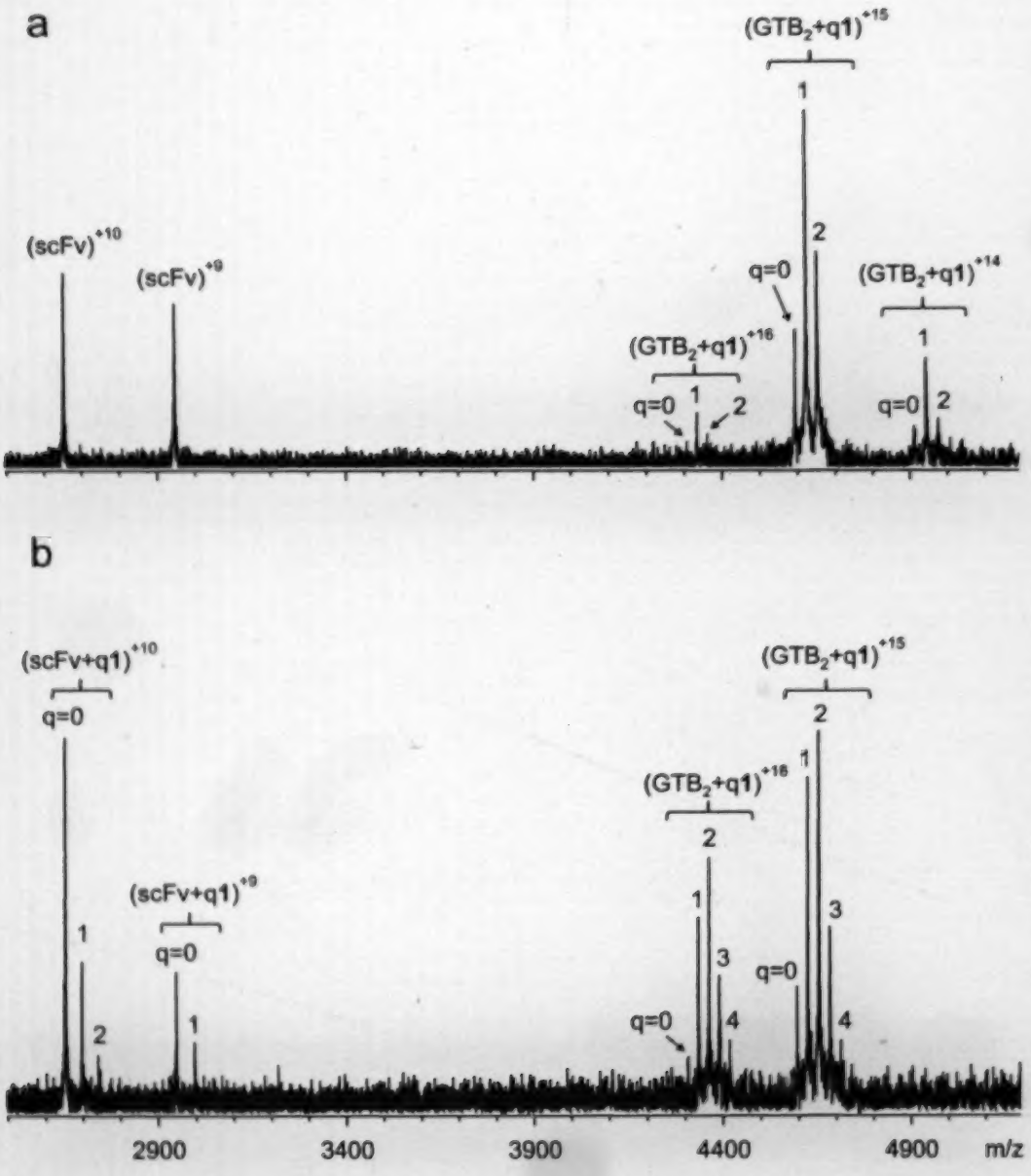

Figure 5.2 NanoES mass spectra of solutions consisting of 10 mM ammonium acetate (pH 7), 7 μM GTB_2 and **1** at concentrations of (a) 40 μM and (b) 100 μM. A reference protein, scFv, was added to both solutions at a concentration of 5 μM to quantify the extent of nonspecific protein-ligand binding during the ES process.

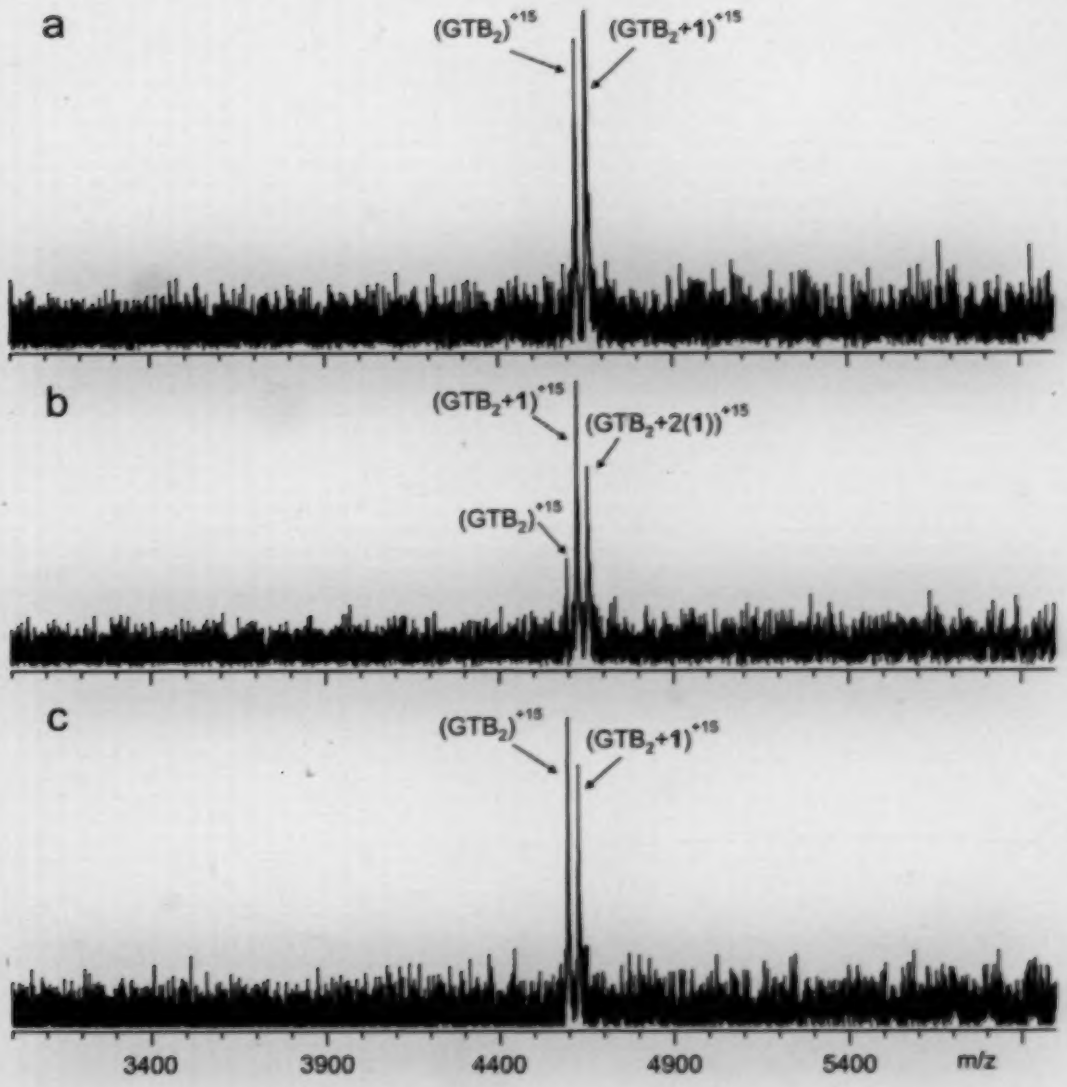

Figure 5.3 Illustrative BIRD mass spectra obtained for (a) $(GTB_2 + \mathbf{1})^{15+}$ ion, originating from specific interaction in solution, at a reaction temperature 145 °C and reaction time of 3 s, (b) $(GTB_2 + 2(\mathbf{1}))^{15+}$ ion, originating from specific interactions, 150 °C and 7 s, (c) $(GTB_2 + \mathbf{1})^{15+}$ ions, originating from specific and nonspecific interactions, 122 °C and 20 s.

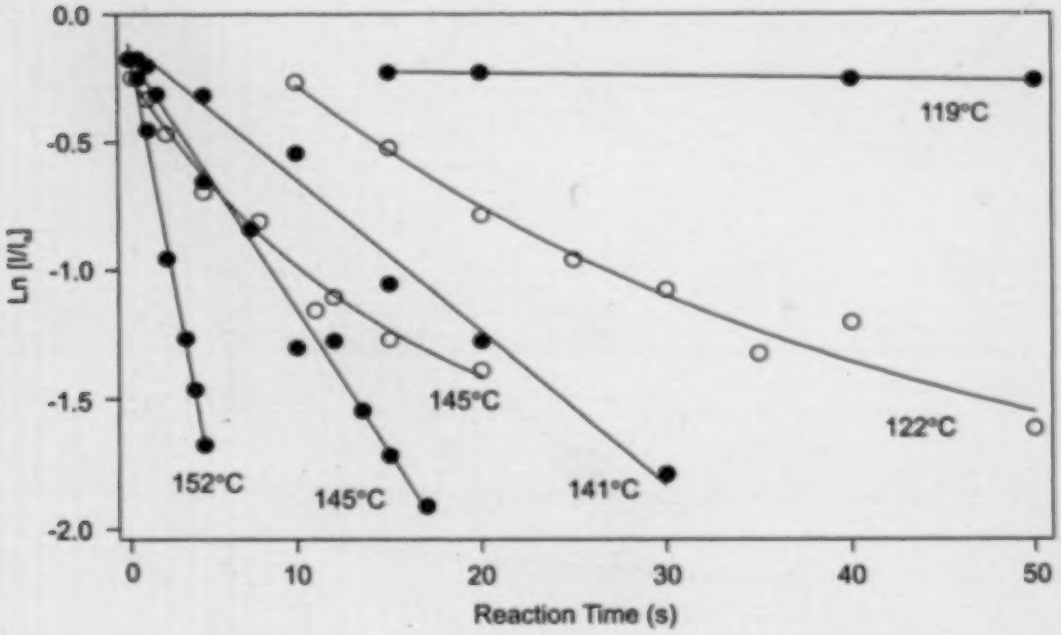

Figure 5.4 Plots of natural logarithm of normalized intensity (I/I_o) of the gaseous $(GTB_2 + 1)^{15+}$ ions, produced from the specific (GTB_2 + 1) complex (•) and from a mixture of specific and nonspecific (GTB_2 + 1) complexes (o), versus reaction time, at the temperatures indicated.

time, measured for the $(GTB_2 + 1)^{15+}$ ion. Notably, the kinetic plots are linear, which is the expected behaviour for the unimolecular dissociation of a single reactant, over the range of temperatures investigated (119 – 153 °C). Since both GTB binding sites are populated with equal probability in solution, the linear kinetic plots indicate that the dissociation rate constants for the loss of **1** from each of the binding sites are equivalent. Linear kinetic plots are also obtained for the loss of **1** from the $(GTB_2 + 2(\mathbf{1}))^{15+}$ ion, a result which is consistent with the operation of parallel dissociation pathways from a single reactant (Figure 5.5).

$$(GTB_2 + q\mathbf{1})^{n+} \rightarrow (GTB_2 + (q\text{-}1)\mathbf{1})^{n+} + \mathbf{1} \qquad (5.1)$$

As previously mentioned, higher concentrations of **1** leads to extensive nonspecific binding of **1** to GTB_2 which in turn gives rise to $(GTB_2 + 3(\mathbf{1}))^{n+}$ and $(GTB_2 + 4(\mathbf{1}))^{n+}$ ions (Figure 5.2). Under these conditions, both specific and nonspecific complexes contribute to the $(GTB_2 + q(\mathbf{1}))^{n+}$ ion signals. In this case, nonlinear kinetic plots were obtained for the $(GTB_2 + q\mathbf{1})^{15+}$ ions (Figure 5.4). The nonlinear kinetic plots can be explained by the presence of multiple, nonequivalent reactant ions, consistent with contribution of both specific and nonspecific interactions to the $(GTB_2 + q\mathbf{1})^{15+}$ ions. It is also interesting to note that, depending on the reaction temperature, the nonspecifically bound ligand can be more or less stable (kinetically) than the specific ligand. This is in contrast with previous work in which the non-specifically bound ligand was found to be more stable than specifically bound ligands.[14]

From the Arrhenius plots constructed for the loss of **1** from the $(GTB_2 + 1)^{15+}$ and $(GTB_2 + 2(\mathbf{1}))^{15+}$ ions originating from specific complexes, it is evident that $(GTB_2 + \mathbf{1})^{15+}$ is kinetically more stable than $(GTB_2 + 2(\mathbf{1}))^{15+}$ (Figure 5.6). The activation

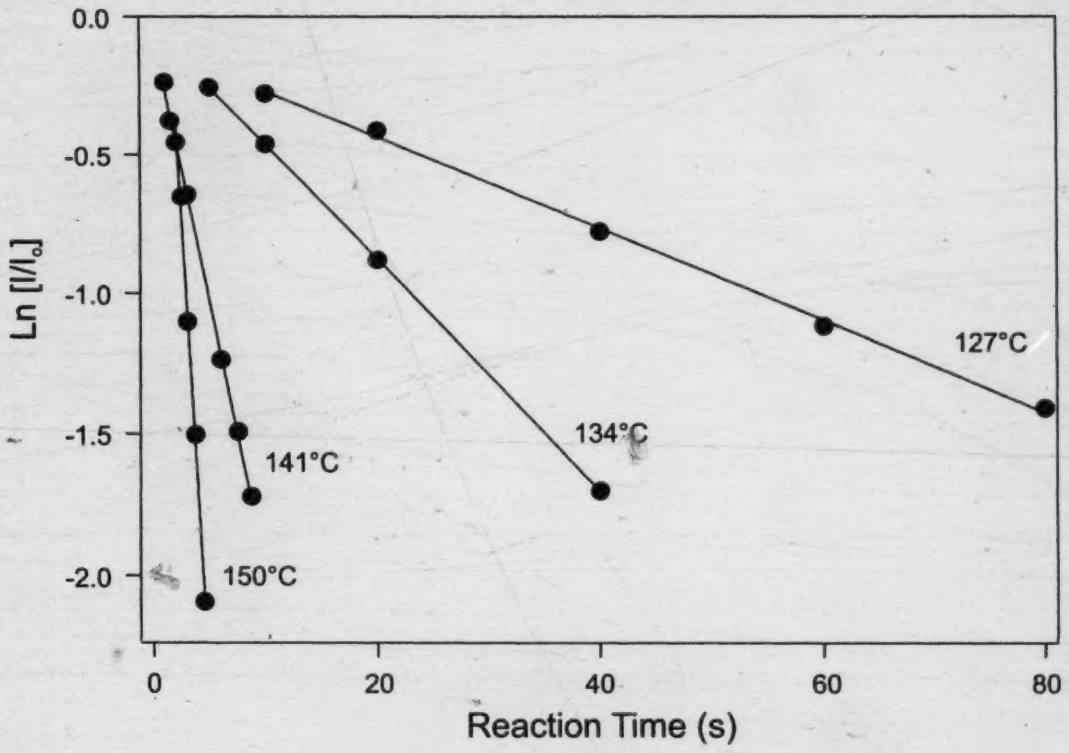

Figure 5.5 BIRD kinetic plots of the natural logarithm of normalized intensity (I/I_o) of the gaseous $(GTB_2 + 2(\mathbf{1}))^{15+}$ ions, originating from the specific $(GTB_2 + 2(\mathbf{1}))$ complex in solution, versus reaction time at the temperatures indicated.

energies, E_a, are indistinguishable within experimental error, 58.3 ± 0.8 kcal mol^{-1} for $(GTB_2 + \mathbf{1})^{15+}$ and 58.0 ± 1.0 kcal mol^{-1} for $(GTB_2 + 2(\mathbf{1}))^{15+}$. Over the temperature range investigated, the average ratio of dissociation rate constants for the loss of **1** from the $(GTB_2 + 2(\mathbf{1}))^{15+}$ and $(GTB_2 + \mathbf{1})^{15+}$ ions was 2.3 ± 0.3. This ratio agrees, within error, with the value of 2.0 expected based on the difference in the number of equivalent bound ligands in the two ions, i.e., the ligand occupancy factor. It is, therefore, concluded that the difference in the kinetic stability of the $(GTB_2 + \mathbf{1})^{15+}$ and $(GTB_2 + 2(\mathbf{1}))^{15+}$ ions is entropic in origin.

5.3.2 NanoES-MS Gas-Phase Assay: S_4-Biotin Dissociation

After demonstrating that this novel gas-phase assay was capable of establishing the equivalency of GTB_2 acceptor binding sites, BIRD was also applied to the complex of S_4 with biotin, **2**. In aqueous solution at pH 7, S_4 binds to four molecules of **2** with a K_{assoc} estimated to be on the order of 10^{13} M^{-1} at 25 °C.[15] Analysis of the crystal structure of the $(S_4 + 4(\mathbf{2}))$ complex reveals four identical ligand binding sites.[16] NanoES-MS performed on an aqueous solution of S_4 (5 μM) and **2** (25 μM) reveals exclusively S_4 ions bound to four molecules of **2**, i.e. $(S_4 + 4(\mathbf{2}))^{n+}$, at n = 14 – 16 (Figure 5.7). At temperatures ≤ 138 °C, BIRD of the $(S_4 + q(\mathbf{2}))^{n+}$ ions proceeds by the loss of both neutral and protonated **2**:

$$(S_4 + q\mathbf{2})^{n+} \rightarrow (S_4 + (q\text{-}1)\mathbf{2})^{n+} + \mathbf{2} \qquad (5.2a)$$

$$\rightarrow (S_4 + (q\text{-}1)\mathbf{2})^{(n-1)+} + \mathbf{2}^{+} \qquad (5.2b)$$

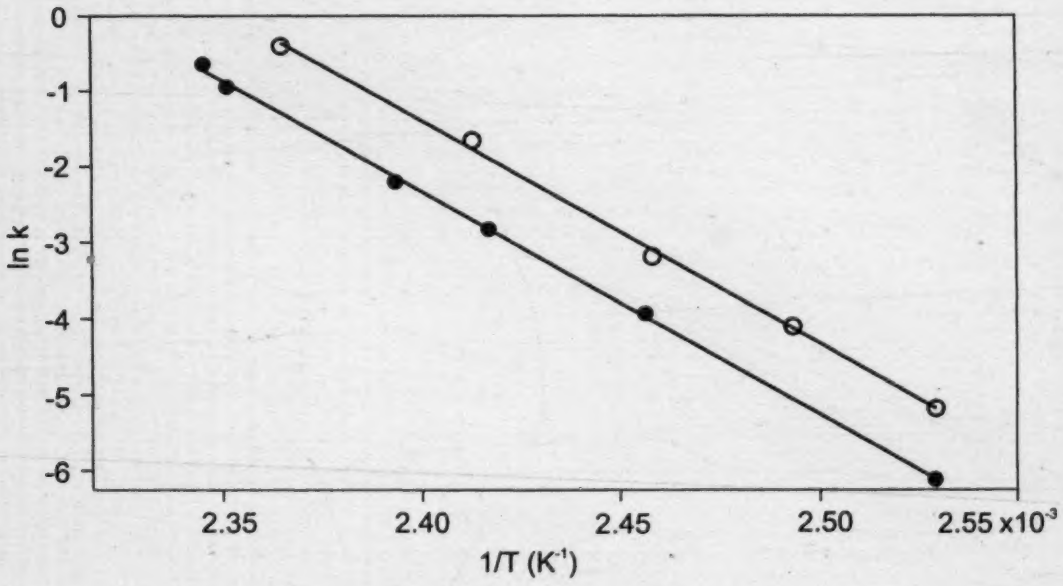

Figure 5.6 Arrhenius plots for the loss of **1** from the $(GTB_2 + q\mathbf{1})^{15+}$ ions, where q = 1 (•) or 2 (o).

Because of the influence of Coulombic repulsion on the dissociation kinetics, the equivalency of the ligand binding sites can not be established from a comparison of the rate constants for the loss of neutral and protonated **2**. However, the charged ligand pathway (eq 5.2b) can be eliminated by reducing the charge states of the $(S_4 + q\mathbf{2})^{n+}$ ions. This in turn can be achieved through the addition of a base, such as imidazole, to the nanoES solution.[17] This effect is demonstrated in Figure 5.7. It is shown in the figure that the addition of 4 mM imidazole lead to the formation of $(S_4 + 4(\mathbf{2}))^{n+}$ ions where n = 12 - 15.

BIRD of the $(S_4 + 4(\mathbf{2}))^{13+}$ ion proceeds exclusively by the sequential loss of neutral **2**. Shown in Figure 5.8 are the breakdown curves for the successive loss of **2** from the $(S_4 + 4(\mathbf{2}))^{13+}$ ion measured by BIRD at 133 °C. Also shown are the theoretical breakdown curves which were calculated from the rate constant (k_1) measured for the loss of one molecule of **2** from $(S_4 + 4(\mathbf{2}))^{13+}$ and assuming that the rate constants for the successive losses of **2** (k_2, k_3, k_4) differ simply by the occupancy factor, i.e. $k_1 = 4/3\ k_3 = 2\ k_2 = 4\ k_4$. Agreement between the experimental and theoretical breakdown curves indicates that the intrinsic dissociation rate constants for the loss of **2** from each of the four binding sites are identical. The equivalency of the rate constants measured for the loss of ligand from multiple, equivalent binding sites within a given protein-ligand complex is compelling evidence that the binding sites are structurally equivalent in the gas phase. This is the first *quantitative* experimental evidence for the preservation of elements of structural equivalency within multi-subunit protein complexes upon transfer from solution to the gas phase. However, from these data alone, it is not possible to establish whether the native structure is preserved in the gas phase or whether each

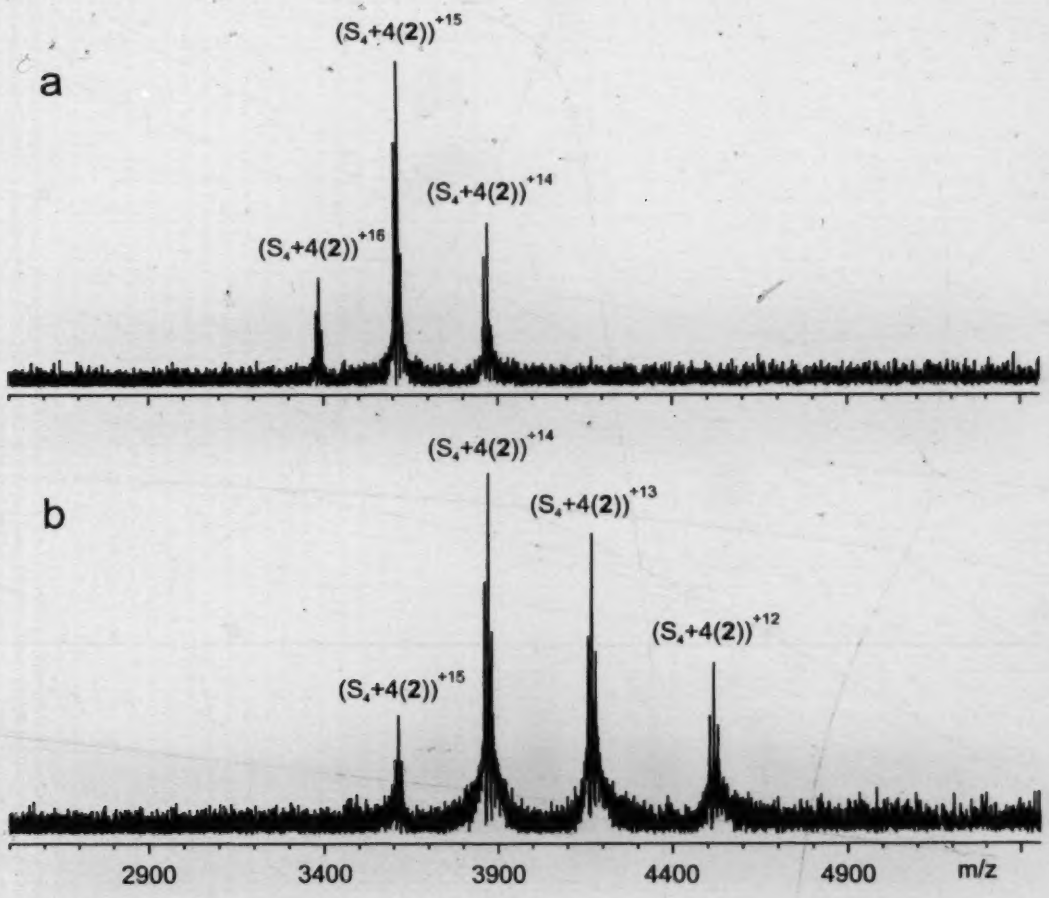

Figure 5.7 (a) NanoES mass spectrum obtained for a solution of 10 mM ammonium acetate (pH 7), 5 μM S_4, and 25 μM **2**. (b) NanoES mass spectrum obtained for a solution of 10 mM ammonium acetate (pH 7), 5 μM S_4, 25 μM **2** and 4 mM imidazole. Three distinct complexes are detected at each charge state: $(S_4 + 4(\mathbf{2}))^{n+}$, $(S_4 + 4(\mathbf{2}) + KH_2PO_4)^{n+}$, and $(S_4 + 4(\mathbf{2}) + 2(KH_2PO_4))^{n+}$.

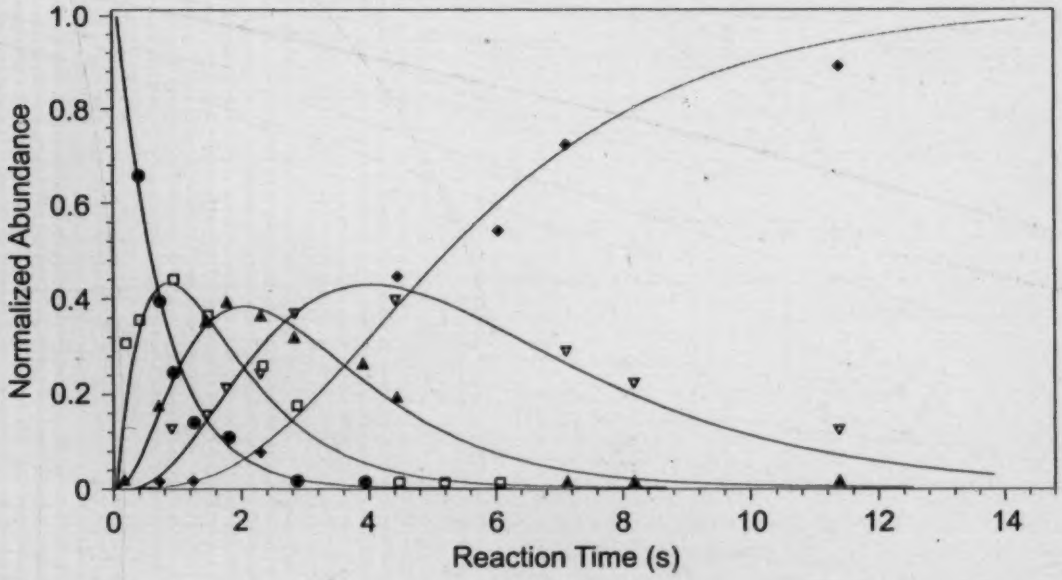

Figure 5.8 Breakdown curves for the sequential loss of **2** from the $(S_4 + 4(\mathbf{2}))^{13+}$ ion at a reaction temperature of 133 °C; The symbols (●= $(S_4 + 4(\mathbf{2}))^{13+}$), □= $(S_4 + 3(\mathbf{2}))^{13+}$), ▲- $(S_4 + 2(\mathbf{2}))^{13+}$), ▽= $(S_4 + 1(\mathbf{2}))^{13+}$), ◆= $(S_4)^{13+}$) represent experimental BIRD data and the solid curves represent the expected breakdown curves based on four equivalent binding sites with an intrinsic dissociation rate constant of 1.4 s^{-1}.

binding site is similarly changed. The present findings are, perhaps, surprising given the overwhelming evidence that heating of multi-subunit protein complexes in the gas phase results in asymmetric unfolding of the subunits.[10] Such asymmetric unfolding, should it occur, would be expected to break the structural homology of the ligand binding sites and result in non-equivalent dissociation rate constants. It is probable that, at the temperatures investigated, the kinetics for ligand loss are significantly faster than the kinetics for subunit unfolding. It is also interesting to note that in comparing the two protein-ligand sytstems, the (GTB_2 + **1**) complex is more stable than the (S_4 + **2**) complex in the gas-phase. This can be seen in Figure 5.8, where it is shown that at a reaction temperature of 133 °C, the majority of the $(S_4 + 4(\mathbf{2}))^{+13}$ species is dissociated in ≈ 2 s. For the $(GTB_2 + 2(\mathbf{1}))^{+15}$ complex, however, it required ≈ 40 s to achieve extensive dissociation at this temperature (Figure 5.5). This observation may seem surprising, given that the binding affinity for S_4 and **2** is ≈ 10^8 fold greater than the binding affinity of GTB_2 for **1** as measured in solution, but highlights the fact that interactions present in solution can be quite different in the gas-phase where solvent affects are absent.

5.4 Conclusions

In summary, we have demonstrated that, upon transfer from solution to the gas phase by ES, thermodynamically equivalent protein-ligand interactions in solution result in equivalent kinetic and energetic stabilities in the gas phase. This important finding serves as the basis for a new assay, which employs time-resolved tandem mass spectrometry, for evaluating the equivalency of ligand binding sites within proteins and multi-protein complexes in solution. Also, although no definitive conclusions on the

absolute preservation of higher order structure can be made, the observation that binding site equivalency was maintained for two protein-ligand complexes contributes more evidence that elements of higher order structure can be studied using ES-MS.

5.5 Literature Cited

(1) Daniel, J. M.; Friess, S. D.; Rajagopalan, S.; Wendt, S.; Zenobi, R. *International Journal of Mass Spectrometry* **2002**, *216*, 1-27.

(2) Heck, A. J. R.; van den Heuvel, R. H. H. *Mass Spectrometry Reviews* **2004**, *23*, 368-389.

(3) Lee, H. J.; Barry, C. H.; Borisova, S. N.; Seto, N. O. L.; Zheng, R. X. B.; Blancher, A.; Evans, S. V.; Palcic, M. M. *Journal of Biological Chemistry* **2005**, *280*, 525-529.

(4) Letts, J. A.; Rose, N. L.; Fang, Y. R.; Barry, C. H.; Borisova, S. N.; Seto, N. O. L.; Palcic, M. M.; Evans, S. V. *Journal of Biological Chemistry* **2006**, *281*, 3625-3632.

(5) Patenaude, S. I.; Seto, N. O. L.; Borisova, S. N.; Szpacenko, A.; Marcus, S. L.; Palcic, M. M.; Evans, S. V. *Nature Structural Biology* **2002**, *9*, 685-690.

(6) Freitag, S.; Chu, V.; Penzotti, J. E.; Klumb, L. A.; To, R.; Hyre, D.; Le Trong, I.; Lybrand, T. P.; Stenkamp, R. E.; Stayton, P. S. *Proceedings of the National Academy of Sciences in the United States of America* **1999**, *96*, 8384-8389.

(7) Kitova, E. N.; Bundle, D. R.; Klassen, J. S. *Journal of the American Chemical Society* **2002**, *124*, 9340-9341.

(8) McCammon, M. G.; Hernandez, H.; Sobott, F.; Robinson, C. V. *Journal Of The American Chemical Society* **2004**, *126*, 5950-5951.

(9) Xie, Y. M.; Zhang, J.; Yin, S.; Loo, J. A. *Journal of the American Chemical Society* **2006**, *128*, 14432-14433.

(10) Marcus, S. L.; Polakowski, R.; Seto, N. O. L.; Leinala, E.; Borisova, S.; Blancher, A.; Roubinet, F.; Evans, S. V.; Palcic, M. M. *Journal of Biological Chemistry* **2003**, *278*, 12403-12405.

(11) Seto, N. O. L.; Palcic, M. M.; Hindsgaul, O.; Bundle, D. R.; Narang, S. A. *European Journal of Biochemistry* **1995**, *234*, 323-328.

(12) Zdanov, A.; Li, Y.; Bundle, D. R.; Deng, S. J.; Mackenzie, C. R.; Narang, S. A.; Young, N. M.; Cygler, M. *Proceedings of the National Academy of Sciences of the United States of America* **1994**, *91*, 6423-6427.

(13) Sun, J. X.; Kitova, E. N.; Wang, W. J.; Klassen, J. S. *Analytical Chemistry* **2006**, *78*, 3010-3018.

(14) Wang, W. J.; Kitova, E. N.; Klassen, J. S. *Journal of the American Chemical Society* **2003**, *125*, 13630-13631.

(15) Chilkoti, A.; Tan, P. H.; Stayton, P. S. *Proceedings of the National Academy of Sciences of the United States of America* **1995**, *92*, 1754-1758.

(16) Weber, P. C.; Ohlendorf, D. H.; Wendoloski, J. J.; Salemme, F. R. *Science* **1989**, *243*, 85-88.

(17) Catalina, M. I.; van den Heuvel, R. H. H.; van Duijn, E.; Heck, A. J. R. *Chemistry-A European Journal* **2005**, *11*, 960-968.

Chapter 6

Conclusions and Future Work

This work described the development and application of analytical techniques to study carbohydrate-modifying and carbohydrate-binding proteins. It can be divided into two general categories; developing novel assays to detect enzyme activity from small samples using CE-LIF and studying protein-ligand and enzyme-substrate interactions using nanoES-MS.

In chapter 2, the development of a novel nanopipettor for small-scale reaction sampling is presented. It was demonstrated that the nanopipettor fulfills the major requirements for its application to monitoring small-scale biochemical reactions; it allows tuneable, reproducible, and accurate nL sampling. The greatest advantage of this nanopipettor is that it is readily constructed using simple, inexpensive, and easily attainable components, requiring only a Hamilton syringe, zero dead volume union, and a short piece of fused-silica capillary. It thus represents an inexpensive, effective, and flexible tool for the removal of nL aliquots that can be applied to any small-scale chemical or biochemical reaction sampling. The volume range could also be extended by using sampling capillaries with various i.d in place of the 10 μm i.d. capillary used in this work. The use of a capillary with an i.d. of 50 μm, for example, would allow the sampling range to be extended as high as 600 nL. Alternatively, the use of capillaries with smaller i.d. than 10 μm would allow removal of aliquots in the pL range. These values were predicted from eq 2.6 and thus need to be confirmed experimentally, but

suggest that the nanopipettor is well suited to a broad range of small-scale sampling applications.

This nanopipettor was then used in the development of a single cell enzyme assay. Of the current single cell techniques, most apply a whole-cell sampling approach. This approach is quite sensitive but only permits a snapshot of the cellular contents. The work described in chapter 3 sought to develop a novel single cell assay by which a single cell reaction could be repeatedly sampled, permitting more detailed studies of a single cell such as monitoring a single cell enzyme reaction over time. There are three main challenges to any single cell enzyme assay; the isolation of individual cells from a cell population, sampling the single cell or single cell lysate, and quantification of reaction progress. The assay presented in chapter 3 overcame these challenges using an in-house built micromanipulator to isolate individual cells in miniaturized reaction vessels, the development of a novel nanopipettor to sample this single cell reaction, and CE-LIF, with its ultrasensitive detection and excellent separation capabilities, to monitor the reaction progress. Using this technique, a single Sf9 cell α-glucosidase II assay was performed and individual Sf9 cells were found to be very heterogeneous with respect to their levels of α-glucosidase II activity. The source of this heterogeneity remains unclear, but it is suggested to arise from either differences in cell size or expression levels of α-glucosidase II. Investigating this heterogeneity is one future direction of the single cell enzyme assay. It could be determined whether this heterogeneity in enzyme activity is a common feature for other enzymes by determining their activity at the single cell level. Additionally, the source of this heterogeneity could be investigated. For example, it could be determined whether cell cycle affects the observed heterogeneity by studying

single cells that are currently in the same growth phase.[1] Attempts were made to investigate this heterogeneity by normalizing activity for amino acid content, which would account for differences in cell size. These attempts were unsuccessful due to the extensive dilution of cellular contents and highlight the future challenges of this technique. For the successful combination of this single cell enzyme assay with other single cell techniques used in chemical cytometry,[2] the assay must be further miniaturized. These technical challenges may be met with the incorporation of microfluidics to the single cell enzyme assay. The dimensions of commonly used fluidic devices (10-100 μm) are well suited to the study of single cells using whole-cell sampling.[3-5] It does not, however, permit multiple sampling. Thus, a technique which would combine a microfluidic platform with a robust sampling method, such as the nanopipettor presented in this work, would yield a sensitive and flexible single cell device.

In chapters 4 and 5, the research focus shifted from monitoring enzyme activity to studying the thermodynamics of enzyme-substrate and protein-carbohydrate binding using nanoES-MS. Although ES-MS has been used since the early 1990's for the detection of noncovalent complexes,[6,7] it is only recent developments to the ES-MS binding assay that have allowed its application to the thermodynamic study of weakly bound complexes.[8] Previously, the study of weakly bound complexes was plagued by the nonspecific binding of ligands to protein during the ES process. This is due to the high ligand concentration that is required to observe protein-ligand complex for weak binding ligands. With a method to account for nonspecific contributions, accurate and reliable K_{assoc} values can be obtained for weakly bound complexes, such as protein-carbohydrate

complexes. The results presented in chapter 4 represent some of the first applications of this modified nanoES-MS binding assay.

In chapter 4, the direct nanoES-MS binding assay was used to evaluate the binding affinity of several oligosaccharides to CS-35 F_{ab}. The oligosaccharides that were examined are analogues of a hexasaccharide motif that is present in the cell wall of various mycobacterium, including *M. tuberculosis*. The nanoES-MS binding affinity data provided insights into which carbohydrate residues were important in the recognition of this hexasaccharide by CS-35 F_{ab}. K_{assoc} values were determined using nanoES-MS even for weak binding ligands, which according to FAC/MS, possessed no binding affinity towards CS-35. The speed, low sample consumption, and ability to evaluate K_{assoc} values for weak complexes make the direct nanoES-MS technique well suited to the study of protein-carbohydrate interactions. The application of temperature-controlled nanoES-MS also allowed the estimation of the ΔH_{assoc} values for the binding of the two ligands with the highest affinity to CS-35 F_{ab}.

In the second part of chapter 4, nanoES-MS was used to study the human blood group galactosyltransferase, GTB, and quantify its interactions with acceptor and donor molecules. This represents the first detailed thermodynamic study of this model glycosyltransferase. The results demonstrate the range of questions that can be addressed using nanoES-MS. For example, it was shown that GTB exists exclusively as a dimer in aqueous solutions (pH 7) and that the dimers possess two equivalent acceptor and donor binding sites. The binding of donor was investigated using a fragment based approach, and UDP was found to be the only donor species that exhibited binding to GTB in the absence of a divalent metal cofactor. The nature and role of the metal cofactor was

investigated by examining GTB-metal binding and the binding of GTB to substrate molecules in the presence of metal. From these experiments it was suggested that Mn^{+2} is the biologically relevant cofactor. While Mn^{+2} enhances the binding of the UDP donor species, its most significant effect is on the catalysis of the native UDP-Gal donor. Based on recent structural information,[9,10] this effect is explained by a conformational change in the donor upon binding to GTB in the presence of a divalent metal cofactor. It appears that only in this bioactive conformation can GTB initiate catalysis. The experiments involving GTB-Mn^{+2} binding have raised questions regarding the accuracy ES-MS derived K_{assoc} values for protein-metal binding, and this issue is presently being investigated in the Klassen lab.

Future work will focus on the thermodynamics of substrate binding for the corresponding blood group A enzyme, GTA. As mentioned previously, GTA and GTB differ in only 4 critical amino acids out of their total 354 amino acids,[11] and yet this confers a change in their specificity for donor. Also, from kinetic measurements[12] and recent studies using x-ray crystallography,[13] it appears that GTA and GTB possess different binding affinity to their common native dissacharide acceptor as well. Thus a comparative thermodynamic study of these two enzymes would allow the differences in how these two enzymes interact with substrate molecules to be quantified and may provide fresh insights into how these four critical amino acids can cause the observed change in function.

The gas-phase dissociation of protein-ligand complexes was explored in chapter 5. It was demonstrated in chapter 4 that, in solution, GTB possesses two equivalent acceptor binding sites. Using time-resolved tandem MS these binding sites were found to

be thermodynamically equivalent in the gas-phase as well. Currently, it is debated whether elements of higher order structural elements of protein-ligand complexes are preserved in the gas-phase.[14-17] In the case of GTB, it can not be concluded that the structure of the acceptor binding site is preserved in the gas-phase. It does, however, suggest that equivalency is maintained. Thus any structural changes that may occur in the GTB dimer when it is transferred to the gas-phase affect both binding sites equally. Using this assay, it was confirmed that streptavidin possesses four equivalent biotin binding sites, which was expected from the crystal structure. The present findings suggest that time-resolved tandem MS can be used to probe binding site equivalency in protein-ligand complexes in solution.

Literature Cited

(1) Krylov, S. N.; Zhang, Z. R.; Chan, N. W. C.; Arriaga, E.; Palcic, M. M.; Dovichi, N. J. *Cytometry* **1999**, *37*, 14-20.

(2) Dovichi, N. J.; Pinkel, D. *Current Opinion in Biotechnology* **2003**, *14*, 3-4.

(3) Andersson, H.; van den Berg, A. *Current Opinion in Biotechnology* **2004**, *15*, 44-49.

(4) Andersson, H.; van den Berg, A. *Sensors and Actuators B-Chemical* **2003**, *92*, 315-325.

(5) Huang, B.; Wu, H. K.; Bhaya, D.; Grossman, A.; Granier, S.; Kobilka, B. K.; Zare, R. N. *Science* **2007**, *315*, 81-84.

(6) Ganem, B.; Li, Y. T.; Henion, J. D. *Journal of the American Chemical Society* **1991**, *113*, 7818-7819.

(7) Ganem, B.; Li, Y. T.; Henion, J. D. *Journal of the American Chemical Society* **1991**, *113*, 6294-6296.

(8) Sun, J. X.; Kitova, E. N.; Wang, W. J.; Klassen, J. S. *Analytical Chemistry* **2006**, *78*, 3010-3018.

(9) Angulo, J.; Langpap, B.; Blume, A.; Biet, T.; Meyer, B.; Krishna, N. R.; Peters, H.; Palcic, M. M.; Peters, T. *Journal of the American Chemical Society* **2006**, *128*, 13529-13538.

(10) Persson, K.; Ly, H. D.; Dieckelmann, M.; Wakarchuk, W. W.; Withers, S. G.; Strynadka, N. C. J. *Nature Structural Biology* **2001**, *8*, 166-175.

(11) Yamamoto, F.; Clausen, H.; White, T.; Marken, J.; Hakomori, S. I. *Nature* **1990**, *345*, 229-233.

(12) Seto, N. O. L.; Palcic, M. M.; Compston, C. A.; Li, H.; Bundle, D. R.; Narang, S. A. *Journal of Biological Chemistry* **1997**, *272*, 14133-14138.

(13) Letts, J. A.; Rose, N. L.; Fang, Y. R.; Barry, C. H.; Borisova, S. N.; Seto, N. O. L.; Palcic, M. M.; Evans, S. V. *Journal of Biological Chemistry* **2006**, *281*, 3625-3632.

(14) Benesch, J. L. P.; Aquilina, J. A.; Ruotolo, B. T.; Sobott, F.; Robinson, C. V. *Chemistry & Biology* **2006**, *13*, 597-605.

(15) Heck, A. J. R.; van den Heuvel, R. H. H. *Mass Spectrometry Reviews* **2004**, *23*, 368-389.

(16) Ruotolo, B. T.; Robinson, C. V. *Current Opinion in Chemical Biology* **2006**, *10*, 402-408.

(17) Xie, Y. M.; Zhang, J.; Yin, S.; Loo, J. A. *Journal of the American Chemical Society* **2006**, *128*, 14432-14433.